UNIVERSITY OF SOUTHAMPTON

FACULTY OF NATURAL AND ENVIRONMENTAL SCIENCES

Chemistry

The fabrication of nanoporous template thin films for supercritical fluid electrodeposition

by

Calum Robertson

Thesis for the degree of Doctor of Philosophy

December 2015

ABSTRACT

This work investigates the fabrication of nanoporous templates as a part of the supercritical fluid electrodeposition (SCFED) project. The goals set for this investigation was to produce films with pore channels (diameter < 5 nm) orientated perpendicularly on top of an electrode. During the course of this work, two techniques were investigated, Stöber-derived method and electrochemical-assisted self-assembly (EASA).

The Stöber films produced perpendicularly orientated pore structure through a hydrothermal process. EASA film were generated through electrodeposition, resulting in highly ordered vertically aligned pore channels. Both these techniques were transferred from indium-tin oxide (ITO) onto titanium nitride (TiN), which increased the potential window of the substrate. The pore diameters of the Stöber and EASA films were determined as 2.6 and 1.6 nm respectively. This could be increased with the addition of a swelling agent or decreased by using a surfactant with a shorter tail length. Helium-ion microscopy was shown to provide high-resolution images of silica films. It provided detailed images of the topography and pores structure at the surface of the films.

Tin was deposited into the pores of an EASA film using SCFED method. The EASA films were also subjected to post-synthesis chemical modification based on grafting functionalised silane molecules. As a result, the pore size and chemical properties were altered using a range of functionalised silane based grafting agents. Trimethylchlorosilane was found to be most successful at coating the pore walls. Other larger grafting agents were shown only to partially coat the surface of the films. This was only possible due to the films being placed on the reflective surface of the TiN substrates, which allowed for changes in porosity to be analysed using ellipsometric porosimetry.

Table of Contents

DECLARATION OF AUTHORSHIP

I, Calum Robertson declare that this thesis and the work presented in it are my own and has been generated by me as the result of my own original research.

"**The fabrication of nanoporous template thin films for supercritical fluid electrodeposition"**

I confirm that:

1. This work was done wholly or mainly while in candidature for a research degree at this University;
2. Where any part of this thesis has previously been submitted for a degree or any other qualification at this University or any other institution, this has been clearly stated;
3. Where I have consulted the published work of others, this is always clearly attributed;
4. Where I have quoted from the work of others, the source is always given. With the exception of such quotations, this thesis is entirely my own work;
5. I have acknowledged all main sources of help;
6. Where the thesis is based on work done by myself jointly with others, I have made clear exactly what was done by others and what I have contributed myself;
7. Parts of this work have been published as:

C. Robertson, R. Beanland, S. A. Boden, A. L. Hector, R. J. Kashtiban, J. Sloan, D. C. Smith, and A. Walcarius, *Phys. Chem. Chem. Phys.*, 2015, **17**, 4763

Signed: .....

Date: .....

Acknowledgements

Due to the size and scope of the SCFED project, I have had the pleasure of working with a wide group of people across a number of different universities during my PhD. However, this would not of been possible for me without the help and guidance of my supervisor, Prof. Andrew Hector. I would like to particularly thank him for keeping me focused on my project and being available to help when possible, regardless of how busy he was. I also like to thank my co-supervisor Dr Robert Raja for his advice and allowing me to present my work during a British Zeolite Association conference at the University of Glasgow.

For hosting me at the LCPME in Nancy, France, I would like to thank Dr Alain Walcarius and Dr Veronica Urbanova for teaching me how to make EASA silica films. Dr Reza Kashtiban and Dr Richard Beanland for expertly imaging my samples using TEM facilitates at University of Warwick. Dr Peter Basa from Semilab for analysing my samples using ellipsometric porosimetry, and Dr Stuart Boden for imaging them using HIM. I would also like to thank Dr Marina Carravetta for running the ^{29}Si NMR analysis of my grafted mesoporous silica powders.

I would like to thank everybody involved in the SCFED project. It has provided me with opportunities and experiences that I wouldn't have thought would normally come with doing a PhD. The Hector Lab group for their help and understanding during the more stressful moments of my PhD. And of course friends and family for patiently listening while I described to them what "super-critical-fluid-electro-deposition" was.

Lastly I would be like to thank the EPSRC for making all this happen by funding my PhD project (EP/I033394/1).

Definitions and Abbreviations

Acac – Acetyl acetone

BJH - Barrett, Joyner and Halenda

BSHe – Backscattered helium

CMC – Critical micelle concentration

CPyB – Cetylpyridinium bromide/ Hexadecylpyridinium bromide

CTAB – Cetrimonium bromide/ Cetyltrimethylammonium bromide/ Hexadecyltrimethylammonium bromide

CV – Cyclic voltammetry

DEA - Diethylamine

DEE – Diethyl ether

DeTAB - Decyltrimethylammonium bromide

DoTAB – Dodecyltrimethylammonium bromide

EASA – Electrochemically-assisted self-assembly

EISA – Evaporation-induced self-assembly

ED - Electrodeposition

EP – Ellipsometric porosimetry

GISAXS – Grazing incidence small angle scattering

HMDS – Hexamethyldisilazane

IPA – Isopropanol

ITO – Indium tin oxide

MAS – Magic angle spinning

MPS – Mesoporous silica

MyTAB – Myristyltrimethylammonium/Tetradecyltrimethylammonium bromide

NMR – Nuclear magnetic resonance

PDCS – Phenyldimethylcholorosilane

posn - Position

PSD – Pore size distribution

PVD – Physical vapor deposition

SAXS – Small angle x-ray scattering

sc - Supercritical

SCF – Supercritical fluid

SCFED – Supercritical fluid electrodeposition

SE – Secondary electrons

tBDCS – tert-Butlydiemthylcholorosilane

TEOS – Tetraethyl orthosilicate

$Ti(O^{i}Pr)_4$ – Titanium isopropoxide

TIPB – 1,3,5-isoproyl benzene

THF - Tetrahydrofuran

TMCS – Trimethylcholorosilane

TMB – 1,3,5-trimethyl benzene

TiN – Titanium nitride

XRD – X-ray diffraction

Units

θ	Angle of incidence	$^{\circ}$
I	Current	amps
n	Number of moles	mol
m	Mass	g
M	Molar concentration	mol/dm^3
n	Refractive index	No unit
E	Potential	V
ppm	Parts per million	ppm
R	Resistence	Ω
λ	Wavelength	nm

Chapter 1 - Introduction

1.1 Aims

This thesis is an investigation into orientated mesoporous template materials to facilitate the production of nanowire-based devices, as a part of the supercritical fluid electrodeposition (SCFED) project. Materials of interest will be deposited from supercritical solvents into high aspect ratio pores using electrodeposition. The role of the template is to define the size of the nanowire and determine the scale at which SCFED is capable of depositing material into pores.

The aim of the thesis focuses on the development of the templates. Mesoporous silica films were chosen with the aim of producing pores with a diameter below 5 nm. A narrow pore size distribution is needed with uniform template thickness for even growth of the nanowires within the pore channels. The template must be chemically inert and electrically insulating to ensure the growth of nanowires from the bottom of the pores channels. Strong adhesion between the template and electrode is required if it is to survive the harsh conditions of a supercritical solvent. Ideally the electrode would have a large potential window to provide suitable surface for the electrodeposition of a wide range of materials. In order to provide good accessibility to the electrode's surface, the orientation of the pore channels would preferably be perpendicular to the substrate.

Post-grafting of chemicals to the pore walls of the template would allow for the control over the pore diameter and its surface properties. In this thesis, an important goal is to find a suitable method for the grafting of molecules and then investigates their effects on the template (e.g. pore diameter and surface properties).

1.2 Supercritical fluid electrodeposition

The fabrication of nanoscale devices using well-established techniques, such as chemical vapour deposition (CVD) and lithography are reaching their limitations. This has been driven by electronics industry producing ever-smaller devices, such as transistors. The benefits of creating ever smaller electronic devices include improvement in processing speed, energy and material efficiency. As a result, new methods of nano-scale fabrication are needed if these limitations are to be overcome. The problem with current fabrication methods, like CVD and photolithography, is that they require flat, planar surfaces for the material to be deposited onto.[1] This requires large amount of space in order to effectively deposit material, therefore increasing the size of the resulting device. As a results these techniques are also based on a top-down approaches and are unable to depositing material into complex, high aspect ratio nano-scale template structures without resulting in blockages.[2]

The wide range of three dimensional nanoscale templates that are possible, varying in size and shape, could be used to mould and guide the structure of material deposited within them. SCFED overcomes the limitations of conventional deposition techniques by applying a bottom-up approach during the deposition process. This is achieved by combining the advantages of both supercritical fluids (SCF) and electrodeposition (ED). The advantages of SCFs are that they have no surface tension, which allows them to enter nanoporous materials that otherwise only gases can. Its density allows it to dissolve a range of precursor materials, which can be carried into the nanopores for deposition. They can also achieve higher rates of mass transport than liquids enabling the deposition of material into higher aspect ratio channels.[3] When combined with ED, controlled deposition can be used to attract the precursor toward an electrode positioned beneath the template. The bottom-upward deposition can be used to control the rate of deposition (see Fig. 1).

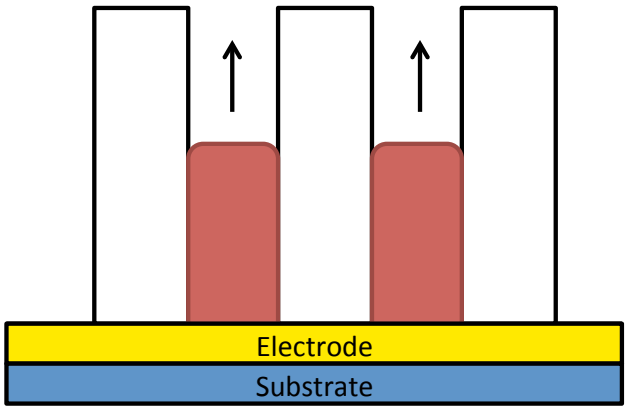

Figure 1 – Diagram demonstrating the bottom-upward growth of nanowires within the pore channels of the template positioned on an electrode

The driving force behind the advancement of SCFED is the formation of nanowires. These nanowires have a wide range of potential applications, which include electronic, optics and piezoelectric devices.[4,5] Controlled growth enables the formation of nanowire allowing for the creation of hetero-junctions, which are vital in the production of transistors. This growth is not restricted to 2D planar surfaces and can increase the density of transistors within a given area.

Prior to SCFED, there has been little investigation in the study of SCFs using electrochemistry. Some of the reasons for this have been highlighted by a comment made by Darr and Poliakoff: "Working with supercritical fluids involves high pressures and sometimes high temperatures. Nearly always, it will be easier to carry out an experiment under conventional conditions than supercritically".[6] Specific problems include achieving sufficient enough conductivity from a lower density medium in order to perform the required electrochemistry. The earliest SCFED reports were based on the electrodeposition of silver from supercritical (sc) ammonia by Williams and Naiditch.[7] Sone and co-workers have demonstrated electroplating nickel films from sc. [8-10] This resulted in the formation of denser film, free of pinholes generated by the release of hydrogen gas when water was present. However, few investigations have been done in this area, most likely due to the nature and complexity of the work.

The first example using SCFED to deposit copper into mesoporous templates was done by current members of the SCFED project, Bartlett and co-workers.[11] This involved utilising $scCO_2$/MeCN or CH_2F_2 as the solvent to dissolve the precursors, which were deposited into 3 nm mesoporous silica films. Subsequent work has focused on refining the deposition method to access of more elements, which now include germanium.[12] Other work has concentrated on understanding of fundamental behaviours of the process, such as the influence that SCFs have on the electrochemistry[13] and alternate solvents/electrolytes.[14, 15]

1.2.1 Supercritical fluids

Supercritical fluids (SCF) occur when a solvent is exposed to temperatures and pressures above their critical point. Consequently, the substance enters a unique phase known as a supercritical fluid (see Fig. 2). Once in this state, the boundaries between the gas and liquid phase do not exist. It becomes diffuse like a gas, whilst being able to achieve densities similar to liquids. These properties allow the SCFs to dissolve salts and carry them into areas that liquids cannot access, (i.e. high aspect ratio nanopores). This can be attributed to the SCF having no surface tension and low solvent viscosity. The physical properties of SCFs can be tuned based on the temperature and pressure that the solvents are exposed to. A wide range of materials are soluble within SCFs, which can be achieved through the choice of solvents and cell conditions.[16]

Supercritical fluids have previously been shown to deposit germanium and silicon in the pores of mesoporous silica by Holmes and co-workers via a process they coined supercritical chemical depositon.[17,18] This was achieved by dissolving the salts in a SCF, which undergoes capillary-condensation within 5 nm pores channels. In order to achieve this, precursors diphenylgermane and diphenylsilane were dissolved in supercritical hexane at 773 K and 375 bar. These precursors decompose within the pores of the template, resulting in deposition of the element from the SCF. In work prior to the SCFED project,

Southampton groups and collaborators used supercritical chemical fluid deposition (SCFD) to deposit CdS, InP and InAs films and nanowires on Si/SiO_2 substrates.[19,20]

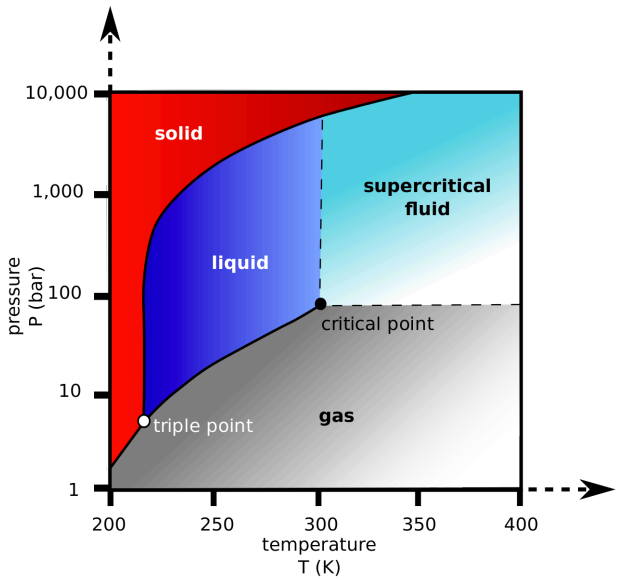

Figure 2 - Phase diagram of carbon dioxide[21]

Watkins *et al* demonstrated that copper and nickel films could be deposited from supercritical carbon dioxide onto both planar and etched silicon substrates.[3] Referred in this case as chemical fluid deposition (CFD) this was achieved by the chemical reduction of soluble organometallic compounds using hydrogen, which is miscible in sc CO_2. They have also demonstrated the use of alcohols in place of H_2 to reduce copper, in order to grow films on SiO_2 and TiN.[22]

1.2.2 Electrodeposition

The principle behind electrodeposition involves applying an electric current to an electrode, for example, the electrodeposition of copper metal from copper sulphate. This is achieved by cathodic reduction at the surface of the electrode (cathode):

$$Cu^{2+} + 2e^{-} \rightarrow Cu^{0}$$

An overpotential (η) is applied to the cell in order reduce the metal and induce the deposition of copper. It can be broken up into different subcategories:

$$\eta_{total} = \eta_{act} + \eta_{conc} + iR$$

Where activation overpotential (η_{act}) describes the charge transfer kinetics of the electrochemical reaction. Concentration overpotential (η_{conc}) defines mass transport limitations of the electrochemical process. iR or ohmic drop accounts for parameters such as electrolyte resistance. The electric field produced by passing a current through the electrode attracts the precursor to its surface. Consequently electrodeposition using liquid solvents has been used to deposit a range of materials into porous templates above 3 nm, which include mesoporous silica and anodic alumina membranes.[23–26] Soft templates (e.g. surfactants) can be used to guide the structure of the resulting films. The use of triblock copolymers as liquid crystals have been utilised during the deposition of platinum films as shown by Attard *et al.*[27]

Three criteria needed to be met if electrodeposition is to effectively deposit material within the pores of the template. Firstly, a conductive substrate is needed in order to reduce the precursor at the template/electrode interface. Ideally the template should be grown directly on to the surface of an electrode to limit post processing to the template. This would decrease the chances of damaging the template causing cracks. Secondly, the only exposure the electrolyte must have of the electrode must be at the bottom of the template via diffusion down the pores channels. A consistent template thickness and pore dimensions are needed in order to achieve uniform nanowire growth throughout the film. Differences in diffusion rate of electrolyte down the pore channels would result in uneven deposition. This is because if one nanowire were to break through to the surface, the electrolyte would not need to travel down the pore channels in order to be deposited. The final criterion is that the

template must be an electrical insulator, chemical resilient and mechanically strong. There are a numerous examples of materials capable of performing the role of a template, which include silica, alumina, metal-organic frameworks, AlPOs, zeolites and polymers.

1.3 Template materials

A mesoporous material is defined as having a pore diameter of between 2 to 50 nm. Below this range (< 2 nm) is defined as microporous and above (> 50 nm) is macroporous.[28] An effective template material needs to be able to be mounted on a conductive surface in order for electrodeposition to be possible. Also, the material must be stable in the SCF and must not react with the precursor. A number of suitable materials have been used as templates before, these include anodic alumina membranes and mesoporous silica films.

1.3.1 Anodic alumina membranes

Anodic alumina membranes (AAM) are able to provide pores with a diameter of 10 to 500 nm.[29] AAMs are fabricated by anodising aluminium sheet/foil in acidic electrolytes, such as sulphuric, oxalic and phosphoric acids. This produces a membrane with hexagonally arranged pore channels running perpendicular to its surface. Alumina (Al_2O_3) has great mechanical strength, high surface area and chemical/thermal stability. Precise control over structure can be achieved over wall thickness and pore length during the anodisation process. Pore diameter can range between 10-400 nm and interpore distances can be varied as far as 50-600 nm by the choice of electrolyte.[30] Lee *et al* summarises the anodisation potentials required for the different acid electrolytes and their effect on interpore distance.[31]

Functionalisation of the surface of alumina membranes is a desirable in order to change the properties of the membrane including polarity to aid solvent

penetration and functional groups to modify nanowire properties. This can be achieved through a number of different reagents. These include using alkoxide and monochloride organosilanes,[32] as well as alkyl phosphoric acids.[33] These grafting agents react with hydroxyl group present at the pore walls. Mutalib *et al* describes a new process of layering different functional grafting agents to the pore walls of AAM. This was achieved through the partial anodisation of aluminum sheet.[34,35] In between each stage of anodisation, grafting was performed on the channels of the AAM. This was repeated a number of times to produce membrane with multiple layers down the walls of the pore channels.

1.3.2 Mesoporous silica

Mechanically strong and chemically resilient, porous silicas have pore diameters ranging approximately between 2 and 500 nm. Mesoporous silica can be produced as films, powders or monoliths and have been intensely investigated for a number of areas including catalysis, filtration and sensors. The most common methods of producing silica follows is the sol-gel process, in which alkoxide silicate precursors ($Si(OR)_4$) are hydrolysed with water. This displaces alkoxides groups through nucleophilic substitution. The hydrolysed molecules are nucleophiles that can condense with neighbouring silica centres, which is catalysed by the addition of acid or base forming polymeric chains or dense particles, respectively.[36]

Hydrolysis:

$$[Si(OR)_3(OR)] + H_2O \rightleftharpoons [Si(OR)_3(OH)] + ROH$$

Alcohol condensation:

$$[Si(OR)_3(OR)] + [Si(OR)_3(OH)] \rightleftharpoons [(RO)_3Si\text{-}O\text{-}Si(OR)_3] + ROH$$

Acid condensation:

$$Si(OR)_3(OH) + [Si(OR)_3(ORH)^+] \rightleftharpoons [(RO)_3Si\text{-}O\text{-}Si(OR)_3] + ROH$$

Base condensation:

$$[Si(OR)_3O^-] + Si(OR)_4 \rightleftharpoons [(OR)_3Si\text{-}O\text{-}Si(OR)_3] + OH^-$$

The pore channels are the result of surfactant or surfactant-like molecules undergoing self-assembly through a soft templating mechanism. This can be explained by two mechanisms: liquid crystal templating or cooperative self-assembly (see Fig. 3). The first example of synthetic ordered mesoporous solids was disclosed by Mobil researchers who developed the M41S family of molecular sieve materials in 1992.[37] They also demonstrated that by varying the tail length of the surfactant, the pore diameter could be altered. The inorganic precursor solidifies around the pre-formed micelles present in solution. The surfactant can be washed or burnt out of the support leaving an inverse framework made of the inorganic support. Attard and co-workers applied the formation of lyotropic liquid-crystalline phases in the formation of non-ionic surfactant ($C_{12}EO_8$ and $C_{16}EO_8$) templated mesoporous silica monoliths.[38] This was achieved by utilising high concentrations of surfactant (e.g. 50 wt%). The non-ionic surfactants only interact with the silica oligomers through hydrogen bonding, where the pore structure is already established for the inorganic precursor to solidify around. The resulting structure produces hexagonally ordered pores under acidic conditions (pH 2). Following work showed that the surfactant ratio had an important impact on the pore arrangement, as did temperature. This altered the liquid crystal phase of the surfactant and the subsequent mesophase of the silica.[39] This method of pore formation has been transferred onto a wide range of other materials including platinum, selenium, tellurium and CdTe.[40–43]

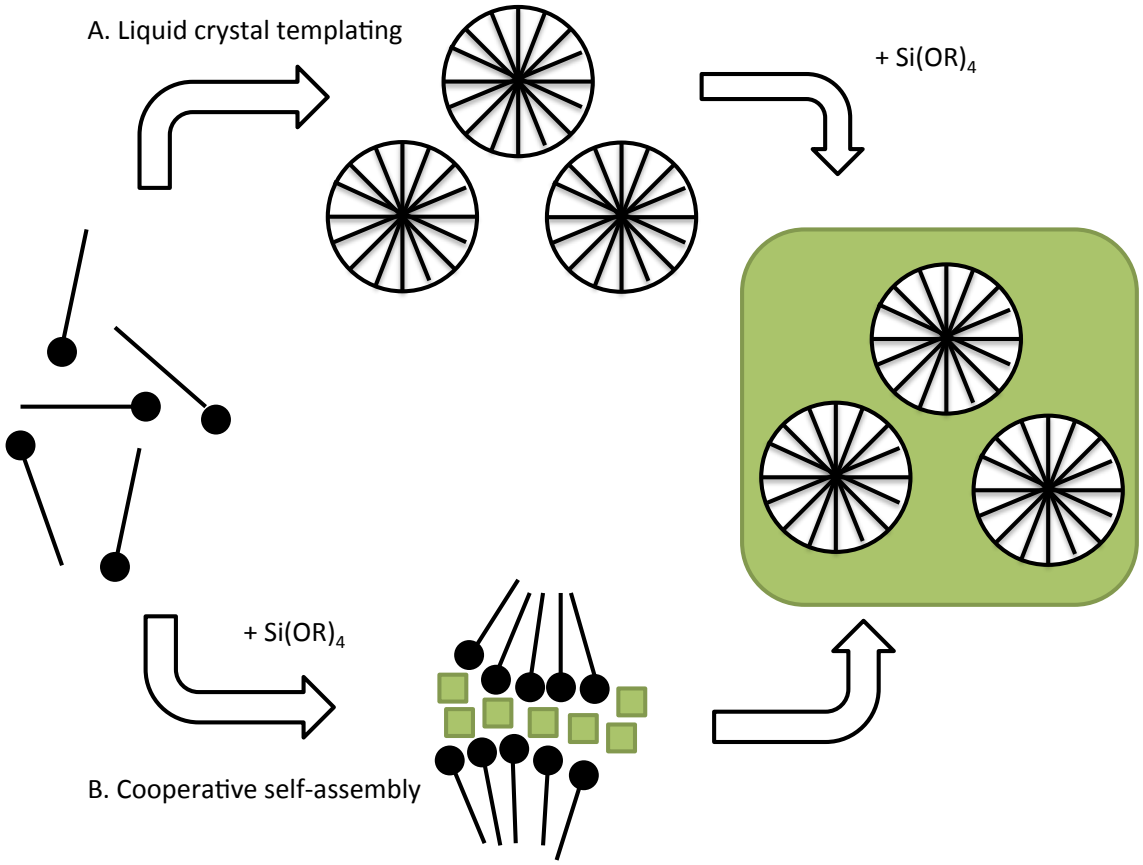

Figure 3 – Schematic of preparing mesopores either by (A) pre-formed liquid crystals (B) or the cooperative self-assembly between surfactant and inorganic. Adapted from ref 44, Copyright (2002) American Chemical Society.[44]

Cooperative self-assembly utilises a lower concentration of a surfactant and the mechanism was originally proposed by Monnier et al.[45] This is based on the ionic interaction between inorganic oligomers and surfactant (S^+I^- or S^-I^+). They explain the three crucial phenomena that control the formation of the mesophase. These are: i) that the silica oligomers form multidenate structures with the CBA^+ surfactants, ii) polymerisation of silica is preferred at the silica-silicate boundary, iii) and this is induced by charge density matching at the interface.

1.3.3 Mesoporous silica films

Various structures are attainable when growing mesoporous silica films. These are affected by surfactant type, concentrations and surface/precursor affinity of the substrate. A wide number of structures based of the self-assembly of surfactants are achievable. The first reported growth of mesoporous silica films was by Yang *et al* on mica substrates using hexadecyltrimethylammonium chloride (CTACl).[46] This was achieved through hydrothermal growth resulting in parallel-aligned pores in the presence of an acid-catalyst.

The most common method of fabricating mesoporous silica films is evaporation-induced self assembly (EISA).[47] This involves using the relatively low concentrations of reagents, acid and surfactant within a sol. The silica precursor is typically hydrolysed in the presence of an acid and ageing the sol by exposing it to a moderate temperature (typically 60 °C). The sol is applied to a substrate through dip or spin-coating. As the solvent begins to evaporate, it triggers self-assembly of surfactant as it reaches critical micelle concentration (cmc). The relative concentrations of precursor and catalyst also rise on the substrate's surface, increasing the rate of gelation. The resulting film can be aged in an oven to remove any remaining solvent and strengthen the resulting structure.

Generally, the self-organisation of surfactant with the surface of the substrate leads to the formation of parallel-aligned pores. Richman and co-workers utilised nanometre-scale epitaxial growth of vertically aligned mesoporous silica on top of cubic mesoporous titania.[48] A Stöber-derived method devised by Teng *et al* lead to the formation of pores orientated perpendicularly on its substrate.[49] This method involves hydrothermally growing films on negatively charged substrates (ITO or silica) instead of monodispersed silica spheres originally established by Stöber and co-workers.[50] The thickness of the film can be controlled the length of the reaction. The mechanism for the vertical aligned films is based on the attraction of cationic micelle (CTA^+) to a negatively charged substrate (SiO_2, indium tin-oxide). The low concentration of

NH_3 prevents bulk precipitation of silica. The oligomers begin collecting around the surfactant at the substrate's surface, particularly favouring the space between two micelles. This encourages the rearrangement of micelles at the substrate interface to organise into vertical rods. Wang *et al* demonstrated the growth of mesoporous silica sandwich structures on graphene oxide.[51] They concluded that strongly attracted, closely packed surfactant micelles on the surface of the support are vital for vertical pore channels.

Electrochemically-assisted self-assembly (EASA) was developed by Walcarius and co-workers.[52] The application of a negative potential to an electrode resulted in the attraction of cationic surfactant to the surface of the electrode. Nitrate ions in solution undergo reduction and generating OH^- at the negatively charged electrode surfaces:

$$NO_3^- + H_2O + 2e^- \rightarrow NO_2^- + 2OH^-$$

Basic conditions are only achieved at the electrode interface due to low pH of the bulk solution, thus restricting the bulk precipitation of silica. The same principle has been widely used in the electrodeposition of solid metal oxide films, such as those of titanium dioxide and zinc oxide.[53] In the EASA process, the result is the formation of hexagonally ordered, perpendicular aligned pore channels within a silica film. Growth of the film is assumed to follow cooperative self-assembly as ionic surfactants are used during the process. Increasing the acidity past pH 3 degrades the resulting structure, possibly due to the protonation of the silica oligomer. This restricts the coordination between the surfactant and the inorganic species.

1.3.4 Templated mesoporous silica rods

The use of AAM as a template material in the fabrication of mesoporous silica rods was established by Yang *et al*.[54] A precursor sol was infiltrated into the channels of the AAM. The confinement of the sol within the channels of the AAM steers the direction of growth along the axis of the pores. This can result in a range of different structure based on parameters, such as the choice of surfactant (ionic/non-ionic), concentrations of structural directing agents (SDA) and the interaction between the sol and the AAM walls. Platschek and co-workers demonstrated a range of pore structure within the AAM using CTAB, Brij56 and Pluronic P123 as SDA.[55] The use of an ionic surfactant (CTAB) led to the formation of hexagonally ordered pores. However, non-ionic surfactants (Brij56/P123) gave both columnar and circular mesophase pore structures. They also investigated the effect of the addition of various inorganic salts and the treatment of the AAM with trimethylchlorosilane (TMCS).[56] They found that increasing the ionic strength of the solutions favoured the formation of a columnar pore structure instead of circular structures. This was related to an increasing interaction between silica oligomers with the alumina channel walls when in the presence of inorganic salts. It was noted that this interaction was key in the formation of mesostructure. Treatment of the AAM walls with TMCS led to organic coated walls, which produced unstructured silica rods.

1.4 Pore size control

1.4.1 Swelling agents

The term swelling agent is attributed to the addition of organic molecule, which is taken into the lipophilic region of the micelle causing it to expand. Consequently, this also enlarges the resulting mesopores. A common group of swelling agents include 1,3,5-trialkylbenzenes for mesoporous silicas, which was demonstrated by Beck and associates in 1992.[37] Fukuoka and co-workers reviewed the effects of 1,3,5-trimethylbenzene (TMB), 1,3,5-triethylbenzene (TEPB) and 1,3,5-triisopropylbenzene (TIPB) on pore expansion.[57] They found

that not only did the swelling agent modify the pore diameter of mesoporous silica powder, but altered the mesophase from hexagonal *P*6*mm* to cubic *Pm*3*n* and *Fm*3*m*. Also it was concluded that based on the alkyl groups present on the aromatic ring, the swelling agents would position itself in different locations within the micelle. Sakai *et al* also demonstrated the effects of other organic swelling agents, which included 1-hexadecanol and decane on mesoporous titania, as well as 1,3,5-trialkylbenzenes molecules.[58] Sayari and colleagues used neutral amine molecules to demonstrate an expansion in the pore diameter of MCM-41 from 3.5 to 7.7 nm.[59]

In recent work by Kao *et al*, organic molecules are used to control the growth of vertically aligned, hexagonally ordered mesochannels with adjustable pore sizes.[60] Without decane, the pores are orientated randomly. When decane is present, the pores expand and orientate perpendicularly to their support and can be replaced by a wide range of other oils.

1.4.2 Functionalisation of Pore Walls

The chemical modification of porous materials has mainly been driven by applications in the targeted uptake of certain hazardous chemicals sensor application[61] or the discrimination of others through size restrictive filtration.[62] This can be achieved through the anchoring of functionalised molecules to hydroxyl groups present on the walls of the support. Beck *et al* demonstrated the grafting of trimethlycholorosilane to surface of the mesoporous silica, which resulted a reduction in the pore diameter.[63] As a result, there has been much work on post-synthesis functionalisation of mesoporous silica. Depending on the size of the grafting agent, the diameter of pore channels can be modified accordingly.[64] Grafting is not just restricted to organosilane molecules. Mokaya and Tompkins demonstrated that the addition of aluminium to the surface of the MCM-41 dramatically improved the hydrothermal stability of the silica.[65] It enabled the mesophase to survive temperatures as high as 900 ˚C in the presence of steam.

Raja et al showed that the grafting of complex organometallic hydrogenation catalyst could be carried out on the pore walls of a support material through multiple step reactions.[66] Initially the external surface of the powder was treated with dichlorodiphenylsilane (Ph_2SiCl_2) to ensure the catalysis only occurred within the internal structure of the support. The walls of the support were then treated with 3-bromopropyltrichlorosilane. 1R,2R-1,2-diphenylethylenediamine was tethered to the functionalised pore walls followed by the addition of $[RhCl(COD)]_2$.

Alternatively *in-situ* synthesis allows for the surface to be functionalised during the fabrication of the support. This method was pioneered by Macquarrie *via* the addition of trimethoxy(3-aminopropyl)silane in the presence of a neutral amine surfactant.[67] The functionalised silane molecules coordinated around the surfactant instead of the inorganic precursor (e.g. TEOS). This leads to the walls on the pores consisting of the functionalised silane molecules. Other examples include vinyl, phenyl and alky silanes.[68,69] Walcarius and co-workers incorporated (3-mercaptopropyl)trimethoxysilane (MPTMS) in the synthesis of mesoporous silica films.[70,71] Using a TEOS:MPTMS ratio of 9:1 they achieved the co-condensation *via* EISA and EASA synthesis methods. Increasing amounts of MPTMS incorporated into the film had a significant impact on the electrochemistry. This resulted in a decrease in the current response due to the restriction caused by the presence of the grafting agents on the analyte.

Chapter 2 - Experimental detail

2.1. X-ray diffraction

X-ray diffraction (XRD) is a well-established method for determining the atomic ordering of a given material based on the elastic scattering of X-ray photons. The sample is exposed to X-rays over a range of angles. The beam is diffracted at particular points based on the lattice planes found in the material's structure. This is because the X-rays scatter off the electrons found within the atoms of the material. Sample with high degree of internal atomic ordering (e.g. crystals) produce large amounts of coherent X-ray scattering at particular angles, which can be used to characterise the material. The higher the degree of ordering, the larger the intensity of the X-ray signal collected by the detector. Figure 4 describes the coherent scattering of X-ray photons from a sample. This is described by Bragg's law where d = distance between planes, 2θ = scattering angle, n = integer, λ = wavelength:

$$n\lambda = 2d\,sin\,\theta$$

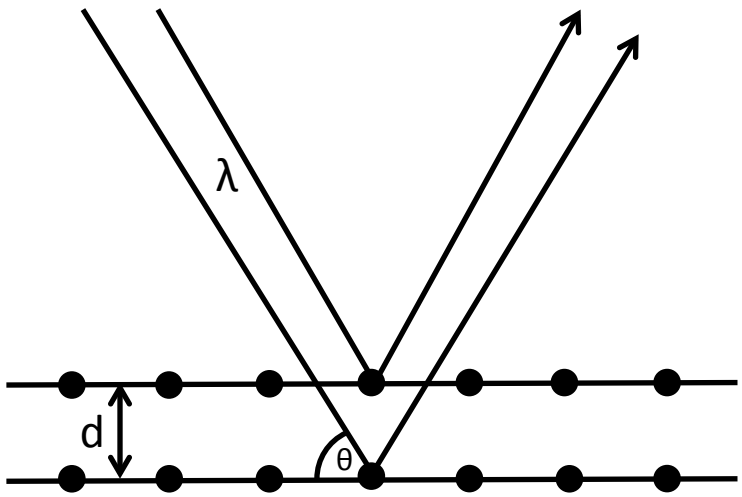

Figure 4 - X-ray scattering off atoms within a lattice plane defined Bragg's law

2.1.1 Small angle X-ray scattering

Small angle X-ray scattering (SAXS) is a low-angle X-ray scattering technique that measures the diffracted beam typically between 0.1 and 10 °. This

technique has been used to characterise the shape and size of macromolecules, such as proteins,[72] nano particles[73] and pores structure within bulk samples.[74] The incident X-rays is passed through the sample using transmission geometry as the detector is scanned directly behind. Samples are commonly mounted in a capillary tube, which are rotated to produces as many reflections as possible (see Fig. 5). This technique has widely been used to measure the pore ordering present mesoporous silica as originally shown by Beck and co-worker.[37]

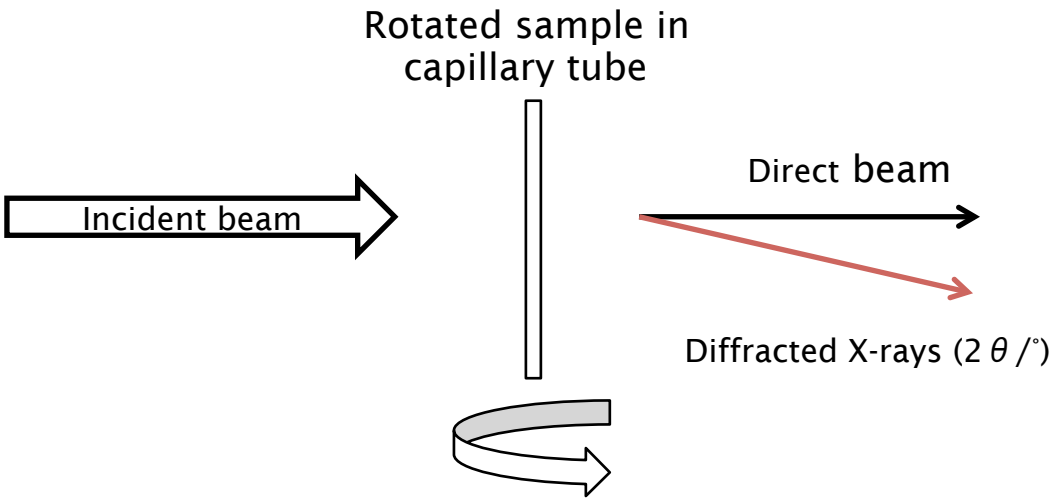

Figure 5 - The schematic of SAXS describing the small degree of x-ray scattering off a sample mounted in a rotating capillary tube.

The ordered pore channels of a mesoporous material can produce coherent X-ray scattering based on the contrast in electron density occurring between pore wall and void. The angle of the reflected beam is small (<10 ˚) and requires collimators increase the resolution of the peaks. The resulting scattering pattern are directly related to the ordering of the pores and can be used to measure changes in the type of mesophase.[57] For example, hexagonal pore arrangement will result in the diffraction peaks relating to the 100, 110 and 200 lattice planes. As a result, the distance between lattice planes can be established from the diffraction patterns. Obtaining the d-spacing can provide information on the interpore distance (a_0). For example, the interpore distance concerning hexagonally arranged pores can be calculated as follows:

$$a_0 = 2d_{100}/\sqrt{3}$$

The distance between pores allows for the determination of the wall thickness, assuming the pore diameter is also known. Expansion and contraction in the d-spacing can also indicate changes in the pore size or wall thickness. In the addition of swelling agents to increase pore diameter, SAXS has been used to follow these changes.[59]

2.1.2 Grazing incidence small angle X-ray scattering

Grazing incidence small angle X-ray scattering (GISAXS) is used to overcome the limitation found when investigating thin films. The incident angle of the X-ray beam is locked in position and the detector scanned across the angle of interest. The grazing incidence geometry uses an angle close to that for total external reflection (the critical angle) in order to maximise the diffraction through the film.[75] This also limits the scattering of X-rays off the support beneath the film.

The geometry in which the X-rays scatter can be used to determine the orientation of pore channels running through a film. Out-of-plane GISAXS can measure the pores channels that run parallel to its substrate. As a result the detector is scanned out-of-plane of the film. This is because the pore ordering occurs perpendicular to the support or out-of-plane. Whereas in-plane GISAXS is capable of determining the pore channels that stand upright on the substrates surface. [76] Therefore the detector is scanned in-plane of the film as that is the direction that the pores are ordered (see Fig. 6). It should be noted that if pore channels were standing perpendicular to its support, out-of-plane GISAXS would not produce any features in the resulting diffraction pattern.[48] Due to the nature of the detector used in this thesis (1D), it can only collect reflections found within the plane it scans. As a result, reflections relating to Miller indices occurring perpendicular to the direction the detector is scanned remain constant. However, this is not a problem for 2D structures, as long as the detector is scanning the appropriate plane.

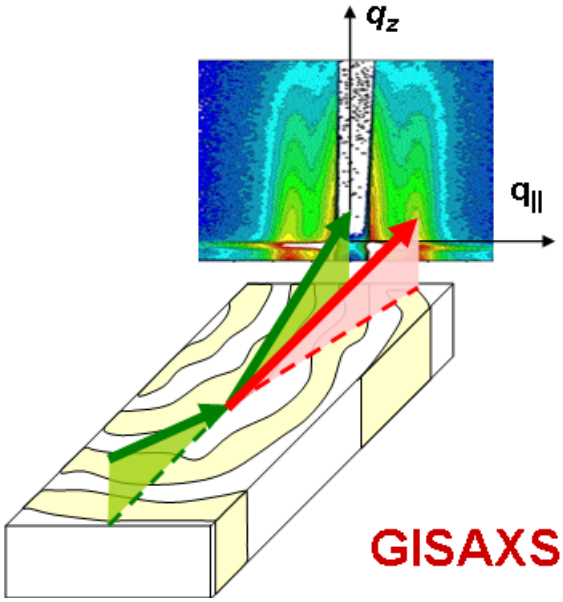

Figure 6 - Image demonstrating the in-plane X-ray scattering while performing a GISAXS experiment[77]

2.2 Electrochemistry

2.2.1 Cyclic voltammetry

Cyclic voltammetry (CV) is a widely used technique that provides an insight into the electrochemical properties and processes of a material within an electrochemical cell. This is achieved sweeping the potential over a range, which gives rise to response in the current based on the redox reactions of a sample or electrolyte probe. The results are generally plotted as current against potential. Other parameter can be controlled, including scan rate speed ($V\ s^{-1}$), which can be used to determine the speed of the redox reactions. Widely used cell configuration is the three-way electrochemical cell. The working electrode performs the desired redox reaction. A counter electrode collects flow of current to complete the circuit. A reference electrode undergoes a reliable, well-known redox reaction to ensure consistent results

and plays no part in the reaction. A simple example of a reversible redox reaction performed may proceed as follows:

$$O + ne^- \rightleftharpoons R$$

Multiple sweeps may be performed as the initial scan might differ due to changes in the behaviour or state of a material. Various parameters can be investigated using CV these include mass transport, diffusion and redox reactions present at or near the surface of the working electrode. In turn this information can be used to probe the structures of materials on an electrode based shape and chemical properties.

Walcarius and co-workers used cyclic voltammetry to characterise EASA silica films. Diffusion studies were used to investigations variations in the synthesis of the film based on the flux of analyte through the channels of the film to the electrode beneath.[78] This was achieved by recording changes in the effective rate coefficient (k_{eff}). Where I_{lim} (limiting current) n (number of electrons), F (Faraday's constant, C mol^{-1}), A (area of electrode, cm^2), C (concentration of redox probe, mol cm^{-3}), P (partition coefficient), D_f (diffusion coefficient, $cm^2\ s^{-1}$) and d (film thickness, cm).

$$k_{eff} = \frac{I_{lim}}{nFAC} = PD_f/d$$

Walcarius *et al* noted as the size of the surfactant decreased, the peak current was found to diminish. This was attributed to the reduction in the size of the pores, which restricted the mass transport of redox probe through the film. Hence the peak current was used to measure the permeability of the films.[78] This was reversed with the addition of a swelling agent (1,3,5-trimethyl benzene) lead to an increase peak current, resulting from larger pore channels.

As a result, more analyte could diffuse through film to give a larger current response.[79]

2.2.2 Electrochemical impedance spectrometry

Electrochemical impedance spectrometry is a technique that measures the electrical impedance within a system over a given frequency range. It is a common method for studying corrosion[80] and batteries.[81,82] This differs from resistance, as it is not limited by the simplified properties of Ohm's law and becomes useful with complex electrical systems. Impedance is defined as (where applied potential, E and current response, I):

$$Z = \frac{E}{I}$$

EIS involves applying an alternating current (AC) potential to an electrochemical cell, then measuring the response of the resulting current. This is achieved by applying a sinusoidal potential, which results in a similar response from the current but phase is shifted. The shift is explained by electrode reactions behaving in the same manner to the electrical circuit, which contains capacitances and resistances. The applied potential (E), (where f = frequency, ϕ = phase angle):

$$E = \Delta E \sin 2\pi f t$$

$$I = \Delta I \sin(2\pi f t + \phi)$$

It is challenging to display the data obtained from AC impedance in a simple and meaningful manner. The Nyquist plot compares the real impedance (Z_{im}) against imaginary impedance as of frequency. The in-phase component (sin $2\pi ft$) consists of the real component and the imaginary is the shifted phase (sin $2\pi ft + \pi/2$). Figure 7 describes the Randles cell circuit schematic based on the corrosion model was used in this thesis, which accounts for double layer

capacitance (C_{dl}) and charge transfer resistance (R_{ct}) in parallel, the uncompensated solution resistance (R_u) is positioned in series. Plotting the data results in the formation of a semi circle, which is the result of the parallel combination of the dielectric capacitance and the film's resistance. The diameter of the semi circle denotes charge transfer resistance (R_{ct}) (see Fig. 8).

$$Z_{im} = \frac{1}{2\pi f C_{dl}}$$

$$f = \frac{1}{2\pi R_{ct} C_{dl}}$$

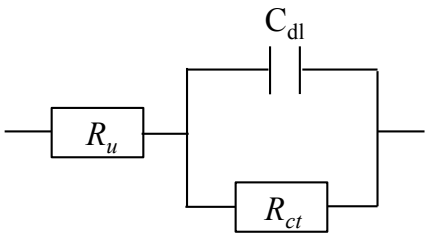

Figure 7 – Randles cell equivalent circuit schematic

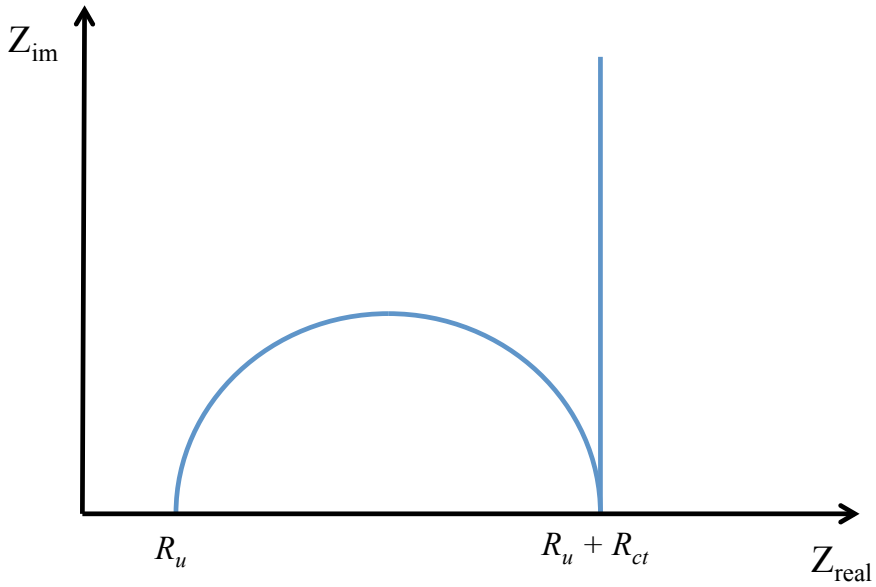

Figure 8 - Typical Nyquist plot with labelled parameters

2.3 Microscopy

2.3.1 Scanning electron microscopy

Scanning electron microscopy (SEM) is a powerful imaging technique capable of achieving a resolution below 1 nm. This involves accelerating a focused beam of electrons onto a sample contained within a vacuum. As the electron beam scans over the sample, secondary electrons are generated at the surface of the material and collected by a positively charged detector. The focus can be altered by a series of magnetic fields that concentrate the electron beam. In order to ensure high-resolution images electrically conductive samples are preferred, as the beam can displace electrons off atoms present at the samples surface. In nonconductive samples this results in the build up of charge at the sample surface, decreasing the resolution of the image. Covering the sample in a thin layer of conductive material (carbon or gold) is commonly used to overcome this problem. However, this can obstruct and blanket fine detail present on the surface of the sample. Another method for suppressing charging is to lower the accelerating voltage, which also improves topographic resolution.[83] However, care must be taken to ensure that the minimum amount of electrons is collected in order to form the image. Alternatively, environmental SEM introduces a gas to the vacuum (commonly water vapour).[84] As negative charge builds on the surface of the sample, water molecules that have been ionised by the electron beam are attracted and cancel this build up.

2.3.2 Transmission electron microscopy

Transmission electron microscopy (TEM) is an extremely effective imaging technique capable of achieving resolutions that can distinguish carbon atoms present within graphene.[85] This is achieved by passing an electron beam through a thin sample. As the electrons travel through the sample, they scatter off of the electrons of atoms within the material. The difference between areas of higher and lower electron density provide the contrast in resolution within an image. Samples must be prepared with a sufficient depth to allow the

electron beam to pass through it. This can be achieved in a number of different ways. The simplest method of preparing a film or powder sample is to scrape/wash material to be imaged onto TEM grid. The grid can be made of a copper mesh or lacey carbon. Manual grinding is another simple way of reducing sample thickness. This is achieved by exposing the surface of the sample to an abrasive surface, which grinds material down to a desired thickness. However, care must be taken to ensure the process does not destroy the underlying structure of the sample. Ion beam milling involves the bombarding the sample with ions, which breaks down the surface of the material. When paired with a SEM, focused ion beam (FIB) instruments are capable of etching samples with astonishing accuracy. A sample can effectively be prepared with a uniform thickness in nanometres.[86]

2.3.3 Energy-dispersive X-ray spectroscopy

A consequence of bombarding a sample with electrons is the production of X-rays, which can be used to characterise the composition of a material. This technique is known as energy-dispersive X-ray spectroscopy (EDX). The incident beam displaces inner shell electrons from atoms in the samples. Electrons from higher energy orbitals fill the empty orbital, which release the excess energy as X-ray photons. As the photon has a specific energy, it can be used to characterise the elements present within the sample. It should be noted that it is harder to accurately determine lighter elements as the X-rays photons produced are low in energy and can readily be reabsorbed. Also certain orbitals overlap in terms of energy bands, which can complicate resolving the element composition of a sample.

2.3.4 Helium-ion microscopy

Helium-ion microscopy (HIM) works in principle like an electron microscopy. Ionised helium ions are fired from tip of a tungsten needle sharpened down to a point consisting of three atoms. The ions are fired and scattered off the sample, generating secondary electrons (SE), back scattered helium (BSHe) and photons.[87] Helium ion have a small de Broglie wavelength and high source

brightness that allows it to achieve images with higher resolution than SEM.[88] It also provides better imaging of samples consisting of lighter elements, such as carbon.[87] The technique is capable of achieving extraordinarily high images of insulating materials. As such they are capable of achieving images with surface resolutions of below 0.35 nm.[89]

2.4. Sorption techniques

2.4.1 Nitrogen sorption

Nitrogen sorption is a method for determining the porosity of a material by modelling the behaviour of the gas within the confined space. This allows for the determination of pore size distribution (PSD), pore volume and surface area. Nitrogen is the most commonly used gas as it is both inert, user-friendly and widely available. Adsorption modelling is primarily based on work by Langmuir. He established the Langmuir model (ideal localised monolayer adsorption), which describes the behaviour of molecules forming a monolayer on planar surfaces.[90] Brunauer–Emmett–Teller (BET) theory expands this work in order to determine the surface area of a material using multilayer adsorption. In 1951, Barrett, Joyner and Halenda (BJH) published the most commonly used model for determining the PSD, which is still used widely even today.[91]

The Kelvin equation is used to model the filling of pores based on the capillary condensation of liquid nitrogen within cylindrical channels. This is applicable to mesopores ($2 < x < 50$ nm). (Where γ is surface tension, V_m, molar volume, r_K, radius of droplet, p, actual pressure, p_0, saturate vapour pressure)

$$r_K = \frac{2\gamma V_m}{RT}\, In(\frac{p_0}{p})$$

The condensation of gas within pores of the material can be used to determine the PSD. This uses on the principle that the smallest pores are filled first, followed by large ones as the pressure of the system is increased incrementally. This occurs until the point saturation of the gas, providing the adsorption isotherm. This is followed by reducing the pressure to establish the desorption isotherm, which results in the liquid evaporating from the pore channels. The isotherm can be separated into six different types, which relate to the different sizes and shapes of the pore channels within a sample (see Fig. 9). Type I isotherms are observed for samples consisting solely of micropores. This noted by the large change in volume of gas absorbed at low pressure, denoting the formation of a large number of micropores. Type II consists of non-porous powders, which form small voids between each of the particles. Type III isotherms are due to samples with little porosity. Type IV/V are samples with mesopores, which undergo slower desorption as it is harder for the gas to evaporate from the pores resulting in a hysteresis loop between the adsorption and desorption curve. However, type IV consists of materials, which bind the gas more strongly to the samples surface, such as silica/alumina, whereas type V materials bind the gas more weakly and mainly consists of materials like activated carbon. Type VI indicates the presence of a multiple layer sample such as graphite.

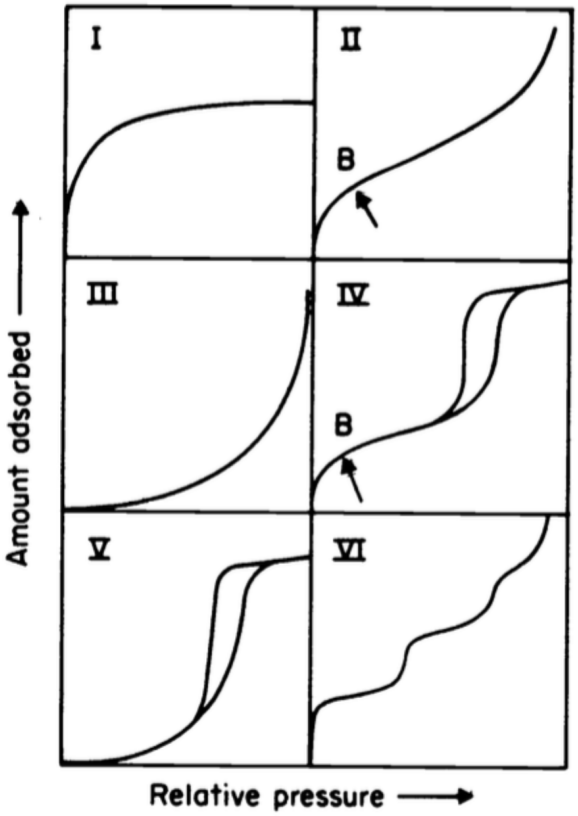

Figure 9 – Sorption isotherms resulting from the different types of porous materials. Taken from ref 92 with copyright permission (1985) IUPAC.[92]

2.4.2 Ellipsometric porosimetry

Measuring the porosity of films has only recently been established using ellipsometric porosimetry (EP). It utilises the technique of ellipsometry and applies it to porosimetry. Previously, in order to determine parameters such as surface area and pore size distribution for a film, sufficient amounts of sample had to be made so that nitrogen sorption could be used. Ultimately this would evolve scraping the film from the surface of its substrate, destroying the sample in the process. For thin/ultra thin films this requires a very large amount of sample, which may not be neither practical nor cost-effective. Therefore, an alternate method was devised based around the same modelling principle used for gas sorption.

Ellipsometry is a technique used for measuring the thickness of thin films. It involves reflecting a laser off the surface of the film. A detector collects the reflected beam and measures its change in phase. By modelling the behaviour of the light, changes in film density can also obtained based on alternation in the refractive index of the sample. For example, Baklanov and co-workers have used ellipsometric porosimetry (EP) to measure the pore diameter of porous xerogel films utilising changes in the sample's density by varying the partial pressure of solvent within a vacuum.[93] When the atmosphere of the chamber is removed, the film is in its least dense state. As the humidity is increased, the solvent undergoes capillary condensation within the pore channels of the films. This results in a change in the refractive index of the film, which can be translated into an adsorption/desorption isotherm. The Kelvin equation, as a well-established equation is an example of an equation used to determine the pore size distribution for EP.[93]

2.5 Nuclear magnetic resonance spectroscopy

Nuclear magnetic resonance (NMR) spectroscopy is a widely used technique for determining the structural composition of a compound by examining the chemical environments found within it. This is achieved by exploiting the magnetic properties of the nuclei present in the sample. Placing the NMR active nuclei into a magnetic field results in the absorption of electromagnetic radiation. The radiation is re-emitted as the nuclei relax from their excited state. This observable NMR signal is known as the free induction decay. When in the presence of an external magnetic field, there will be spin states that align and oppose its direction. This result in a difference in energy between the two states and is proportional to the strength of the field applied and the magnetic moment of the nuclei. Importantly, even if the protons have the same magnetic moment, they may not produce resonant signals at the same frequency values. This is related to differences in the individual electronic environment of each atomic nucleus (i.e. chemical bonds). Local magnetic fields are generated can be "shielded" from external magnetic field that is applied. Therefore stronger fields are required in order to obtain a response

and are measured in parts per millions (ppm). NMR active nuclei are defined as having a spin of 1/2 and are magnetically active. This occurs in abundance naturally in most elements, but for carbon (^{12}C) and oxygen (^{16}O) it does not. For example, ^{13}C natural abundance is only 1.1 %, whereas ^{1}H is over 99 %.

Magic angle spinning (MAS) NMR enables the analysis of solids, which is not possible with conventional NMR. This is due to the limited movement of molecules within solids, where leads to anisotropic dominated responses. In liquids, this can be averaged out due to Brownian motion. MAS allows for a solid to mimic the conditions that molecules suspended in a liquid are exposed too. Samples are spun at an angle (θ_m = 54.74 $^{\circ}$) relative to the direction of the magnetic field, known as the magic angle. This is because at this angle the signal response becomes narrower and other interactions can be averaged out. This has been used analyse mesoporous silica in a number of different ways. Simonutti *et al* used ^{13}C and ^{29}Si MAS NMR to study the interaction of CTAB with the silica walls.[94] Comparing the powders before and after calcination, the team determine the changes in surface chemistry of the silica on removal of surfactant from the sample. Zhao and Lu used ^{29}Si MAS NMR to investigate the silylation of MCM 41 with trimethylchlorosilane.[95] They observed a new silicon environment (-$OSiR_3$) and a reduction in the intensity of the hydroxyl groups at the surface of the powder (-SiOH).

Chapter 3 – Stöber-derived mesoporous silica films

3.1 Introduction

The primary aim of the project was to fabricate aligned nanoporous template materials on top of electrodes. We need a template that can produce well-ordered channels that run perpendicular to the electrode interface. This is needed to ensure the bottom-upward growth of the nanowires during deposition process.

Ordered mesoporous silicas have shown large advancement since their discovery in 1992 by Mobil researchers.[37] However, it is only relatively recently that control over the orientation the pore channels of mesoporous silica films have been achieved. Teng *et al* have developed a hydrothermal method of growing vertically aligned pore channels on indium-tin oxide (ITO) substrate based on a Stöber-derived method.[49] The film forms due to the cooperative self-assembly of a cationic surfactant at an anionic surface. In solution the surfactant forms micelles on the substrate surface. Silica oligomers then collect around the micelle to neutralise the charge on the surfactants. As a result, the repulsion between the polar heads of the surfactant is reduced and the micelle may begin to open and grow upwards through cooperative self-assembly with silica oligomers in solution. Using this method, Teng and co-worker have managed to produce perpendicularly aligned pore channels on both silica and ITO with pore diameter of 2.3 nm and a film thickness of between 34 to 110 nm.

Consequently, the Stöber-based method of producing vertically aligned mesoporous silica films is of particular interest to the SCFED project. Utilising this fabrication method in order to grow nanoporous templates directly onto electrodes limits the need for post processing of the films. This prevents damaging or deforming the film before deposition occurs and makes them easer to handle.

3.2 Experimental Detail

3.2.1 Synthesis of Stöber-derived mesoporous silica film

This method was taken from Teng *et al.*[49] Deionized water (35 mL) and ethanol (15 mL) mixed with ammonia solution (35 wt%, 3.5 μL). Tetraethyl orthosilicate (TEOS) (40 μL) was added and the mixture was stirred for 2 mins. This was followed by hexadecyltrimethylammonium bromide (CTAB) (0.08 g). The solution was stirred for a further 5 mins to ensure the CTAB was properly dissolved. The substrate (25 × 75 mm) was submerged in the solution, sealed in a Parr autoclave (125 mL) and heated at 60 °C for 3 days. The resulting film was washed with deionized water and dried at 130 °C overnight.

3.2.2 Soxhlet extraction of surfactant from pores of mesoporous silica film

The surfactant was removed using Soxhlet extraction. The films were placed so that any drips fell on the back of substrates so that solvent did not erode the surface of the film during Soxhlet extractor and washed in a solution of 0.1 M $HCl_{(aq)}$ in ethanol at 110 °C for 6 hrs. The films were heated at 350 °C at 0.5 °C min^{-1}.

3.3 Characterisation of Stöber-derived mesoporous silica films

3.3.1 Grazing incidence small angle X-ray scattering

Grazing incidence small angle X-ray scattering (GISAXS) experiments were performed using a Rigaku Smartlab thin film diffractometer with a 9 kW Cu-Kα source, with parallel line beam optics, in-plane arm and a DTex250 1D detector. The incident beam was a 0.1 *x* 5 mm line fixed at 0.251 incidence angle, and data was collected between 1–10 ° 2θ using in-plane and out-of-plane modes. For in-plane scans 0.5 ° Soller slits were used on the incident side and a 0.228 ° in-plane analyser on the detector side.

3.3.2 Transmission electron microscopy

Transmission electron microscopy (TEM) was conducted in a JEOL JEM2100 LaB_6 instrument operating at 200 kV and an aberration corrected JEOL ARM200F operating at 200 kV. For cross-sectional imaging, samples were prepared by conventional mechanical polishing followed by ion beam milling, or lamellar sections were prepared in a Jeol 4500 FIB/ SEM instrument. Plan view samples were prepared by scraping the mesoporous films directly onto lacey carbon grids.

Samples were prepared and imaged by both Dr Richard Beanland and Dr Reza Kashtiban.

3.3.3 Helium-ion microscopy

Sample imaging was performed by Dr Stuart Boden. Helium-ion microscopy used an Orion Plust scanning helium ion microscope (Carl Zeiss), with an accelerating voltage of 32.2 kV, a beam current of 0.3 pA, a working distance of 8.6 mm, zero degrees tilt and a beam limiting aperture of 10 mm. The sample was cleaned for 8 minutes using an Evactron remote plasma cleaner

(XEI Scientific, Inc) in the load lock of the microscope to reduce hydrocarbon contamination on the sample surface for high resolution imaging. 35 Secondary electron images were collected using an Everhart–Thornley in-chamber secondary electron detector with a grid bias of 500 V.

3.3.4 Cyclic voltammetry (CV)

CV was performed using a solution of decamethylferrocene (2 mM) in acetonitrile (50 mL) with 0.1 M tetrabutylammonium tetrafluoroborate (TBATFB, Aldrich, 99 %) using the custom cell described in section 4.3.1. An Ag rod pseudo reference electrode was used with a stainless steel cone counter recorded using a scan rate of 100 mV s^{-1}.

3.3.5 AC impedance

Electrochemical impedance spectra were collected in 2-electrode cells *vs.* Pt gauze counter electrode with a Biologic SP150 potentiostat. 10 mV AC amplitude centered on 0 V was scanned over a frequency range 1 MHz–1 Hz. The electrolyte was 20 cm^3 of a 0.05 mol dm^3 solution of $^nBu_4NBF_4$ (99%, Sigma Aldrich) in acetonitrile.

3.4 Results and discussion

3.4.1 Stöber-derived mesoporous silica film using ammonia solution

The fabrication of vertically-aligned mesoporous silica on both indium-tin oxide (ITO) and glass was originally developed by Teng and co-workers.[49] This work is particularly attractive as it allows for the growth of nanoporous template materials directly on to the surface of a conductive electrode. However, the surface needs to be negatively charged in order to grow perpendicular channels. The main disadvantage of ITO is that its potential window is narrow (i.e. it is not stable) at potentials required to deposit electropositive elements, such as germanium and silicon.

In this chapter we investigate the Stöber-derived growth of mesoporous silica films onto titanium nitride (TiN). TiN has a large electrochemical window and has been extensively used as a diffusion barrier in many electronic devices. The formation of an oxide monolayer was expected to allow for good adhesion between substrate and silica film even at high temperatures and pressures.

The films produced on both glass and ITO were tinted coloured films, generally appearing green, blue or purple, whereas films on sputtered TiN-coated silicon emerged dark bronze in colour. The incident beam was set to 0.25 ° ($2\theta = \omega$), above the critical angle of silica and below that of TiN and the in-plane X-ray scattering ($2\theta_x$) was collected (generally between 1-8 °). The incident angle was chosen to maximise the X-ray beam passage through the silica film and not into the substrate. The in-plane GISAXS pattern produced a single diffraction peak on all substrates (see Fig. 10), which was attributed to the (10) lattice plane of a hexagonal pore lattice. Generally, films on TiN produced the most intense peaks at 1.92 °, followed by 2.00 ° (ITO), then 2.04 ° (silica). The noise of the peaks was reduced on TiN, which can be related to an improved reflectioned of X-rays off of the substrate based on a contrast in electron density between film and substrate. A broad feature at ~ 4 ° was witnessed and was related to a combination of both the 11 and 20 peaks. The ordering of the

pores remains very similar, only a slight shift of a few angstroms was witnessed in the interpore distance (see Table 1)

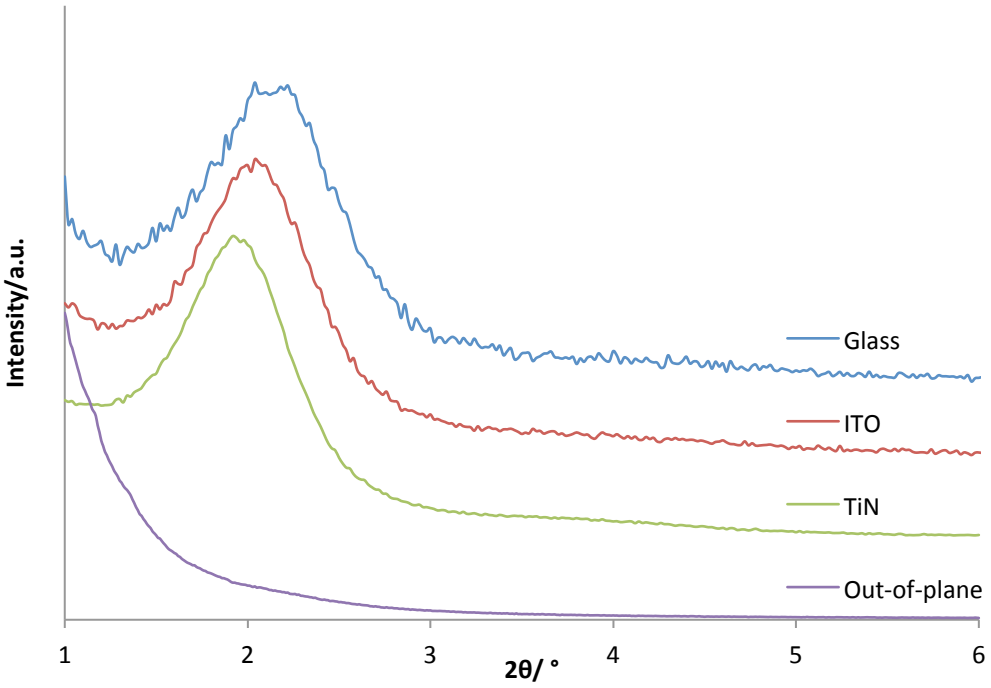

Figure 10 – In-plane GISAXS pattern of Stöber films on various substrates, which include glass, ITO and TiN. Out-of-plane diffraction included demonstrating that no features were witnessed on TiN. Reproduced from Ref. 97 with permission from the PCCP Owner Societies (http://dx.doi.org/10.1039/C4CP05730A).

Table 1 - Summary of peak position and lattice spacing of Stöber-derived mesoporous silica films on Silica, ITO and TiN.

Substrate	Peak posn. (2θ/˚)	d_{10} (nm)	a_o (nm)
Glass	2.08	4.24	4.90
ITO	2.00	4.41	5.09
TiN	1.92	4.60	5.31

The pore diameter of the films was measured at ~2.6 nm using TEM imaging (see Fig. 11 left). Scraping sections of Stöber film on TiN into a lacey carbon grid shows the presence of pore running throughout the whole of the flake. No discrete ordering of the pores is observed, which correlates with the data obtained from the GISAXS patterns (see Fig. 9). Cross-sectional TEM imaging of

the film shows the presence of pores running through the whole of the film, allowing access to the conductive substrate beneath (see Fig. 11 right). During the calcination of the film to remove the surfactant from the pore channels (450 ˚C, 0.5 ˚C min^{-1}, 5 hrs) an oxide layer formed at the film/substrate interface. This was attributed to oxygen diffusing down the pores and oxidising the TiN to TiO_2 at the film/substrate interface:[96]

$$2TiN + 2O_2 \rightarrow 2TiO_2 + N_2$$

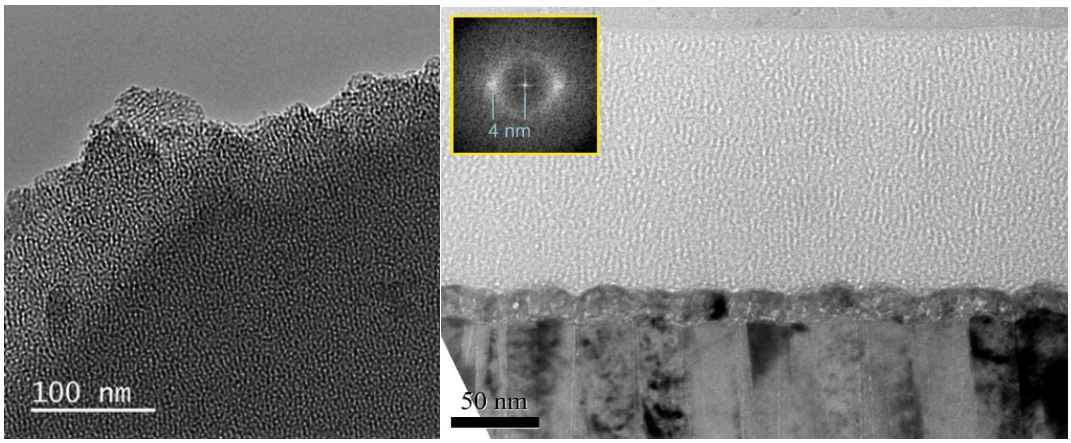

Figure 11 - (Left) Top down TEM image of the Stöber-derived mesoporous silica film grown on TiN scraped into a lacey carbon grid. (Right) Cross sectional image of calcined film on TiN, where an oxide has formed at the film/electrode interface (inset) fast fourier transform showing splitting on the electron beam due to the alignment of the vertical pores. Reproduced from Ref. 97 with permission from the PCCP Owner Societies (http://dx.doi.org/10.1039/C4CP05730A).[97]

In order to determine the effects that oxidation at the film/substrate might have on the electrode, small TiN sections were calcined at various temperatures (ranging between 350 to 450 ˚C). A visible change in the colour of the TiN was witnessed when exposed to temperature above 350 ˚C (0.5 ˚C min^{-1}, 5 hrs). When subjected to 375 ˚C, the bronze of the TiN began to turn red/purple and by 400 ˚C it had become blue. Yellow regions could be seen when exposed to 425 ˚C, which eventually covered the sample by 450 ˚C (see

Fig. 12). The resistivity of the calcined TiN section was measured using AC impedance. The impedance spectra calcined TiN films using AC impedance can be seen in Figure 13 using the conditions described in section 3.3.4. As the temperature that the sample was exposed to increased, the charge transfer resistance of the films grew. This is particularly evident at 450 ˚C, where the charge transfer resistance reached 550 kΩ.

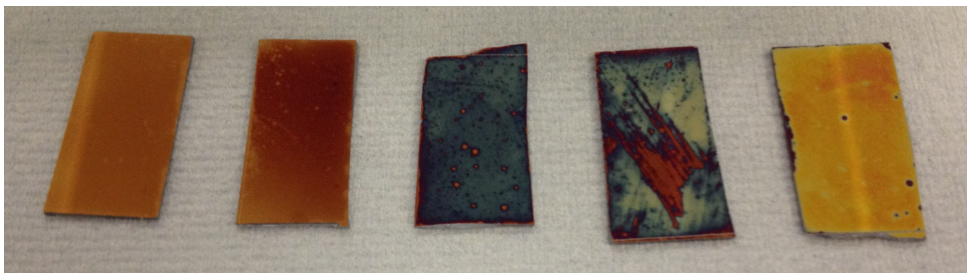

Figure 12 – Photo of TiN-coated silicon films calcined at 350, 375, 400, 425 and 450 ˚C

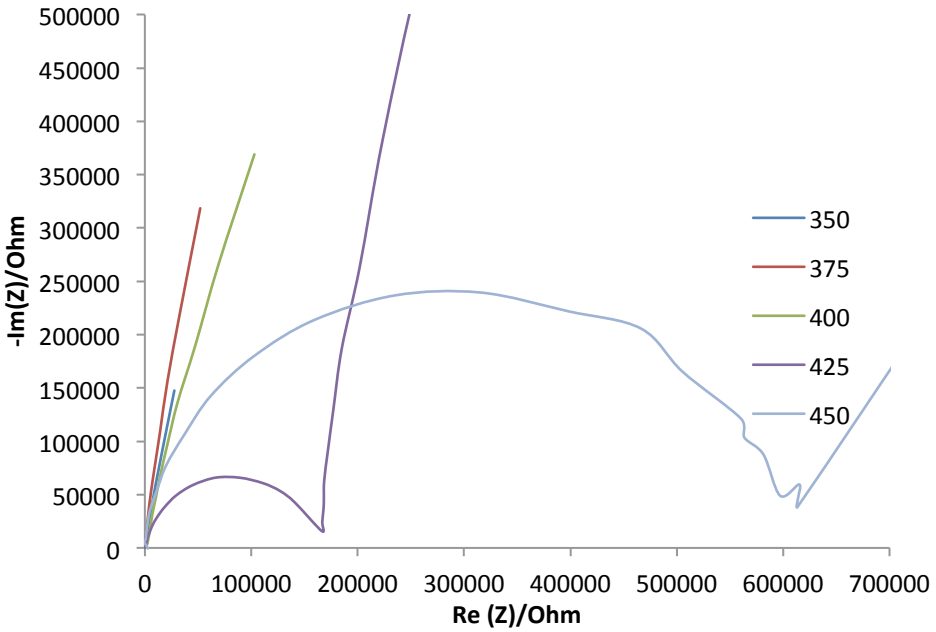

Figure 13 - AC Impedance of TiN-coated silicon films calcined at 350, 375, 400 and 450 ˚C performed using $^{n}Bu_4NBF_4$ (0.05 mol dm^3) in acetonitrile

A low temperature method of removing the surfactant from the pore channels was required in order to avoid passivating the TiN beneath the porous film. Soxhlet washing the films in acidified organic solvent to displace CTAB from

the pores was developed to achieve this (see section 3.2.2). After washing, the films were dried and calcined at 350 ˚C (0.5 ˚C min^{-1}). EDX analysis compared amounts of carbon in untreated, calcined and washed films in order to gauge the displacement of surfactant. This showed that Soxhlet washing resulted in a smaller presence of carbon within the film than calcined samples. Cross-sectional TEM images, also confirmed that there was no indication of an oxide layer at the film/electrode interface (see Fig. 14 left).

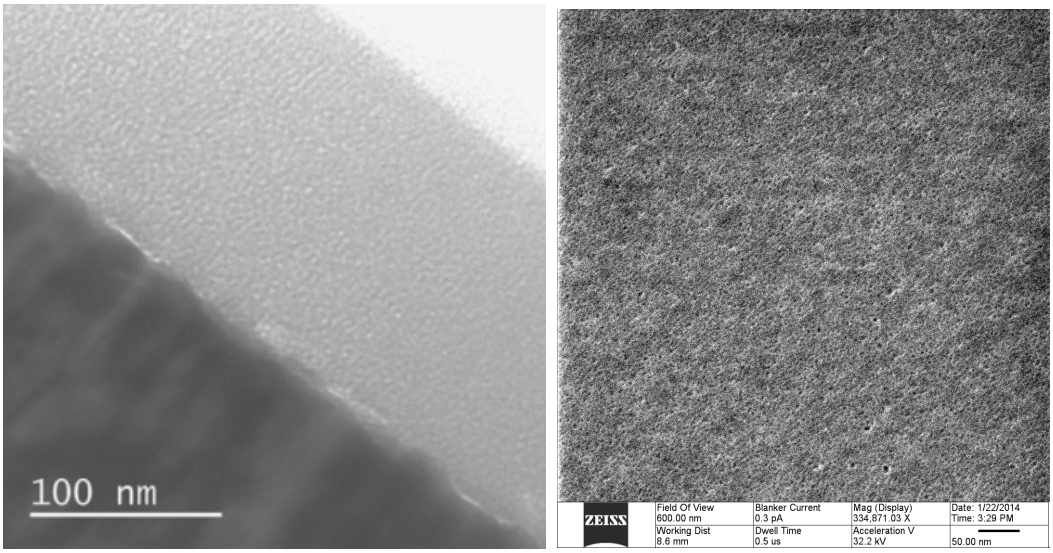

Figure 14 – (Left) Cross-sectional image of Stöber-derived mesoporous silica film that has been soxhlet washed in Ethanol with 0.1 M HCl then calcined at 350 ˚C at 0.5 ˚C min^{-1}. (Right) He-ion Microscope image of surface of Stöber-derived mesoporous silica film. Reproduced from Ref. 97 with permission from the PCCP Owner Societies (http://dx.doi.org/10.1039/C4CP05730A).

In order to ensure that the pores were open, helium-ion microscope (HIM) was used to image the surface of the Stöber-derived silica film. It produces images of the surface of samples with higher resolution than SEM. Helium ions are less susceptible to diffraction effects, which electrons are due to their wave like properties.[98] Images of the film show that open pores cover the surface of the sample with no discrete ordering (see Fig. 14 right). No scratches or cracks were observed showing the method produces films that are both robust and uniform. Very few silica aggregates were spotted on the surface of the film, unlike other methods of producing mesoporous silica films, vindicating the perpendicular orientation during deposition.[78]

Cyclic voltammetry (CV) was used to probe diffusion of redox probe through the film to the conductive electrode beneath. Only films with pore channels aligned perpendicular would allow the probe to access the electrode surface. This method has been used previously by Walcarius *et al* and has shown to measure differences in pore diameter of films.[78] The CV traces allow comparison between the different results obtained from plain TiN-coated silicon, a film with the surfactant with in the pores and without (see Fig. 15). On the plain TiN electrode a standard redox couple is observed using decamethylferrocene as the analyte in acetonitrile. The presence of an empty Stöber film (surfactant removed) on top of the electrode results in a drop in current from the redox peaks. A further reduction in the current was observed with the surfactant remaining in the pores, due it restricting the flux of analyte through the pore channels. It should be noted that decamethylferracene has been shown to travel through the micelle structure of films produced by a different method and produce redox peaks.[99] This is seen in the weak current peaks visible in the voltagramm with the surfactant remaining in the pores.

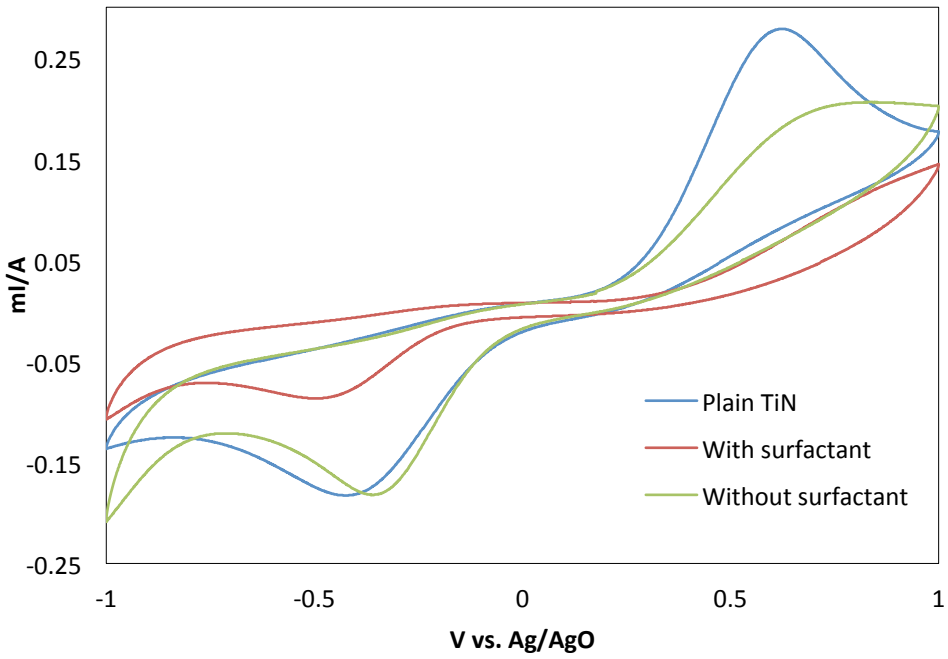

Figure 15 - Cyclic voltammetry performed using Pt gauze of plain TiN-coated silicon, Stöber film with surfactant and without surfactant on TiN-coated silicon using decamethylferracene

Using the data we have obtained sufficient evidence demonstrating that the pore structure of the Stöber-derived silica film produces channels perpendicular on a range of supports, which include TiN, ITO and silica. Transferring the films onto TiN proved highly successful indicated by in-plane GISAXS, TEM imaging and CV diffusion studies. This opens up the range of materials capable of being electrodeposited into the templates.

3.4.2 Effect of reaction time on thickness of Stöber-derived mesoporous films

Control of the film thickness of the Stöber derived mesoporous silica films can be achieved by altering length of heating, whilst the substrate is submerged in solution. At room temperature no film growth is witnessed on the support. A typical three-day reaction at 60 °C produced a film thickness of 148 nm, as noted in the TEM cross-sectional images (see Fig. 16). The elevated temperature of solution encourages the formation of silica oligomers in solution away from the surface of the support. As the temperature of the solutions was increased to 100 °C, this also resulted in the oxidation of TiN with no film growth observed. The reaction time was investigated by measuring the thickness of the Stöber films on TiN-coated silicon through cross-sectional images by FEGSEM. The film thickness of a sample exposed for one-day was measured at 100 nm (see Fig. 16 left). Whereas, increasing the reaction time to two-days (see Fig. 16 right), the film thickness increases to ~150 nm. Charging of the surface of the film made it harder to determine the exact thickness of each of the samples. From this it can be concluded that two-thirds of film growth occurs within the first day, with any remaining film growth finishing by the second. The film growth appears to be self-limiting, as no increases in film thickness are observed after a third day of heating.

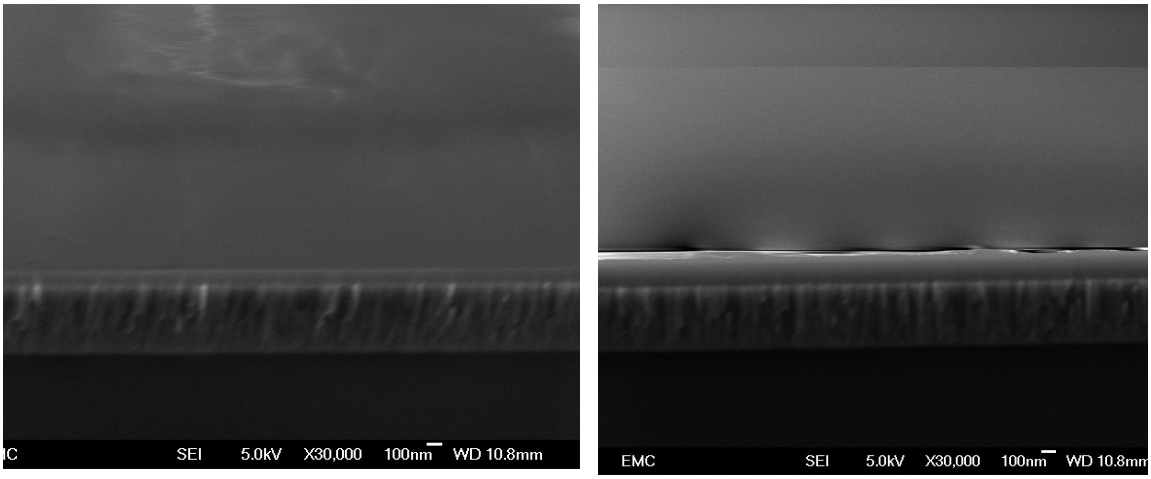

Figure 16 - Thickness of Stöber-derived mesoporous silica films exposed to growth conditions for one day (left) or two days (right) using FEGSEM

It was suggested by Teng *et al* that ammonia plays important role in inducing hydrogen bonding between surfactant and silica oligomer in order to reduce the curvature energy of micelle which would lead to the formation of mesochannels. However, this is counter-intuitive, as hydrogen bonding due to the presence of water in solution would also reduce the repulsion between the polar head of the surfactant reducing curvature energy of the micelle. Silica is widely understood to form negatively charged species in basic and neutral solutions. Therefore this would be electrostatically attracted to the positively charged exterior of the micelle, again reducing the curvature energy. Consequently it is more likely that the silica forms a double layer around the micelles positioned on the surface of the support. This would encourage the reorganisation of the CTAB to maximise its interaction with the silica oligomers. Hence the presence of ammonia simply acts as a base, deprotonating the silanol within the oligomer chains to induce nucleophilic attack between the molecules ($Si\text{-}O^{-}$ + Si-OH → Si-O-Si). However, this does not explain the self-limiting nature of the film growth. Therefore, a concentration gradient must develop close to the surface of the substrate, resulting from the consumption of inorganic precursor during film growth. This limits further growth of the film either as the reagents collecting in solution to form silica aggregates.

It has been concluded that the Stöber-derived method for the fabrication of vertical aligned pore channels is limited by the reaction time and exhaustion of the reagents. Without modifying the reaction conditions established by Teng et al, film growth is limited around 150 nm. It was found that the majority of the film growth occurred within the first day of the reaction.

3.4.3 Effect of different concentrations of ammonia solution (35 wt %) on Stöber-derived mesoporous silica film

The presence of ammonia in solution acts as a catalyst in order to deprotonate the silanol groups and encourages nucleophilic attack between silica oligomers. As was previously stated, Teng et al proposed that ammonia assists hydrogen bonding between surfactant and the silica oligomers to favour the formation of mesochannels.[49] This was investigated by varying the concentration of ammonia within solution. These films were produced on glass slides due to their availability.

As shown in the in-plane GISAXS patterns, there is little to no difference in pore ordering of the films apart from a slight shift in the pore spacing (see Fig. 17). The introduction of larger concentrations of ammonia to solution led to the precipitation of silica aggregates away from the surface of the substrate. This precipitation is commonly used to fabricate mesoporous powders, where the concentration of the base can be used to control the particle size.[100] As expected, increasing the amounts of the ammonia in solution led to the pore structure of the film breaking down. As shown with the addition of 28 μL of ammonia (35 wt%), which shows a reduction in the intensity of the 10 peak when compared against samples with lower concentrations of base. This increase in pH would lead precipitation of TEOS in solution and away from the film growth. A trend in the peak position was also observed, which shows that with more base in solution, a reduction in lattice spacing was observed. This can be ascribed to a reduction in the repulsion between the polar heads of the surfactant as the ammonia molecules could coordinate around the micelle. Therefore the micelles are capable of organising a lot closer together.

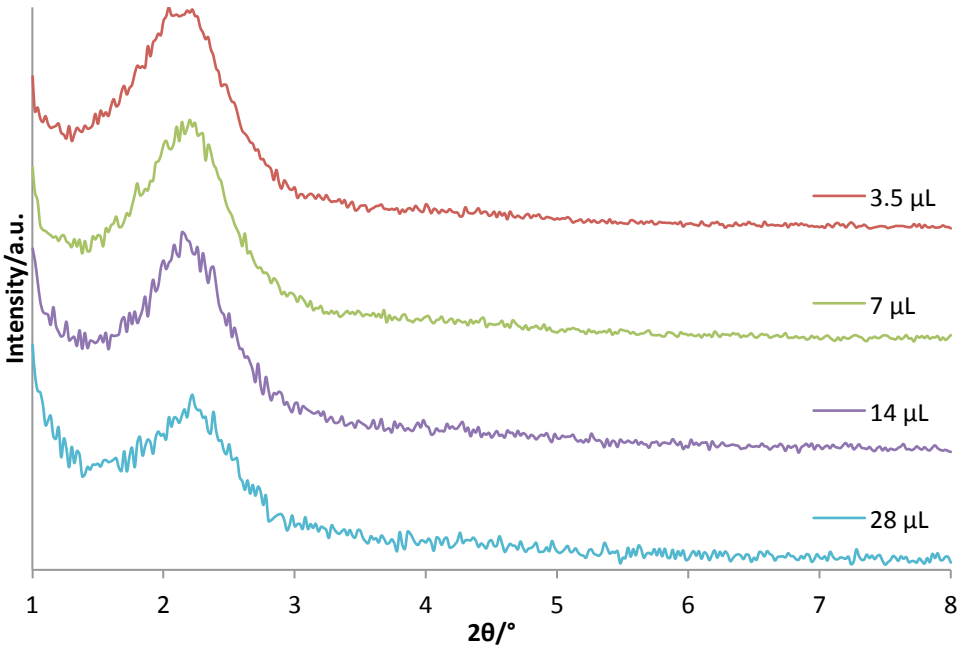

Figure 17 – In-plane GISAXS pattern of Stöber-derived mesoporous silica film with various concentration of ammonia solution on silica

Table 2 - Summary of the peak positions of Stöber-derived mesoporous silica film with varying concentration of ammonia

NH_3 (µL)	Peak posn. (2θ/˚)	d_{10} (nm)	a_0 (nm)
3.5	2.08	4.24	4.90
7	2.14	4.13	4.77
14	2.16	4.09	4.72
28	2.24	3.94	4.55

3.4.4 Effect of CTAB concentration on Stöber-derived mesoporous silica film

An important parameter that determines the ordering of the pores is the concentration of surfactant within solution. It has been shown that varying the amount of surfactant in solution, the structure of the film can be modified.[101] This has been used to fabricate a range of different pore structures within both

mesoporous silica films and powders. These include hexagonal, cubic and lamellar structure formations. The concentration of CTAB in solution was investigated to determine its effect on the structure of the Stöber-derived mesoporous silica films, which were produced on glass-slides.

Though no significant changes to the in-plane GISAXS pattern was witnessed, a small scatter in peak position was observed with no indication of a trend (see Fig. 18). It should be noted these films were synthesized in different batches of surfactant. Though the same supplier and grade of CTAB was used, samples 0.06g to 0.12 g were from an older supply, whereas 0.15 g to 0.30 g was from a new stock (both Sigma Aldrich, Bioextra, >99 %). The presence of more surfactant at the surface may lead to greater repulsion between the micelle, increasing the interpore distance. For each batch of films, the peak position remains fairly constant, with films between 0.06g to 0.12 g maintaining a peak position of ~1.85 °. Other samples between 0.15 g to 0.30 g produced a feature in the XRD pattern around 1.72 °. Nonetheless, no significant changes denoting the formation of new pore structures were witnessed with a 8-fold increase in the concentration of CTAB in solution.

Table 3 - Summary of the lattice parameter obtained from the in-plane GISAXS patterns of Stöber-derived mesoporous silica film with varying concentration of CTAB

CTAB (g)	Peak posn. ($2\theta/^{\circ}$)	d_{10} (nm)	a_0 (nm)
0.06	1.86	4.75	5.48
0.08	1.92	4.60	5.31
0.10	1.88	4.70	5.43
0.12	1.84	4.80	5.54
0.15	1.74	5.07	5.85
0.20	1.70	5.19	5.99
0.25	1.70	5.19	5.99
0.30	1.76	5.02	5.80

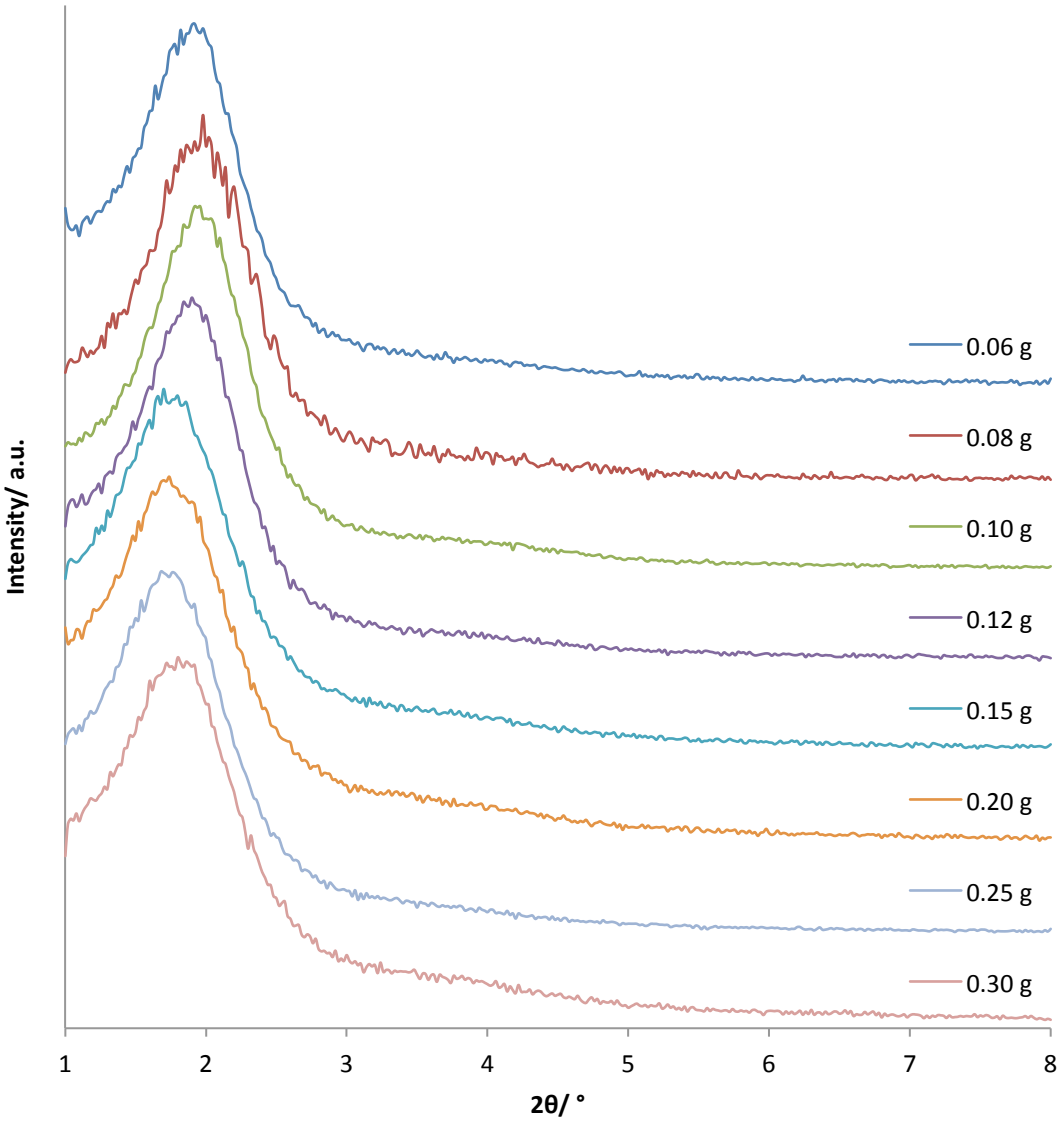

Figure 18 - GISAXS pattern of Stöber-derived film synthesied using different amounts of CTAB which varied from 0.06 g to 0.30 g

Consequently, in order to ensure more consistent results, samples were made in batches so that slight alteration in their fabrication would be constant across the samples. These include cooling times (which can be affected by the temperature within the labs). Others results based on variations of the surfactant concentration with similar tail lengths showed no significant deviations their GISAXS patterns (see sections 3.9.1 and 3.9.4).

3.5 Effect of different concentrations of sodium salts on Stöber-derived mesoporous silica film

In a review by Leontidis, he summarise the effect of cationic and non-ionic surfactant self-assembly based on the Hofmeister anions series.[102] Typically for cationic surfactants, most anions fall within the Class I, which do not bind to the polar head. Instead, they behave like counter-ions. There is a sub-group within Class I ions, which are more hydrophilic and can interact with water through acid-base equilibria. These ions include OH^-, CH_3COO^-, $HCOO^-$. Class II anions are more polarizable, usually larger complexes and include I^-, SCN^- and ClO^-. Class III consists of transition metals that covalently bond with amine headgroups. Finally, Class IV ions are hydrophobic and promote the formation of wormlike micelles in cationic surfactants.

The effect of various sodium salts on the structure of Stöber-derived films was examined by varying their concentrations within solution. Salt additions have been shown to increase the hydrothermal stability of MCM-41 and result in pore expansion. [103,104] For example the addition of fluoride ions in solution has shown to favour the formation of hexagonal phase in mesoporous silica.[105] It is believed that the counter ions compete with the silicate ions coordinating with the polar heads of the surfactant in solution. As a result, they can influence the rate at which the mesophases are formed.

3.5.1 Sodium nitrate

Echchahed et al showed the effect of various mineral acids HX (X^- = Cl^-, NO_3^-, SO_4^{2-}) and cations on micelle templated silicas structure.[106] In particular, the addition of certain ratios of $NaNO_3$ could influence the mesophase based on the NO_3^-/Si. This was seen in the SAXS pattern based on ratios of NO_3^-/Si from 0.15 (lamellar) to 0.4 (hexagonal).

The concentration of sodium nitrate in solution was varied between 0.013 to 0.1 M. The in-plane GISAXS pattern of the films shows a shift in the 10 peak to a larger lattice parameter as the concentration of $NaNO_3$ increased. An

expansion of 0.4 nm was seen with the addition of 0.1 M $NaNO_3$ (see Table 4). This can be attributed to the NO_3^- ion collecting around the cationic surfactant heads. The charge on the anion would be neutralised by the ammonium groups and not restrict the silica oligomers from coordinating around the micelle (assuming all the sites are not occupied). Consequently this led to the increase in interpore distance as witnessed in the GISAXS pattern because of the added steric bulk of NO_3^- ions (see Table 4). However no changes in the pore structure were discerned (see Fig. 19).

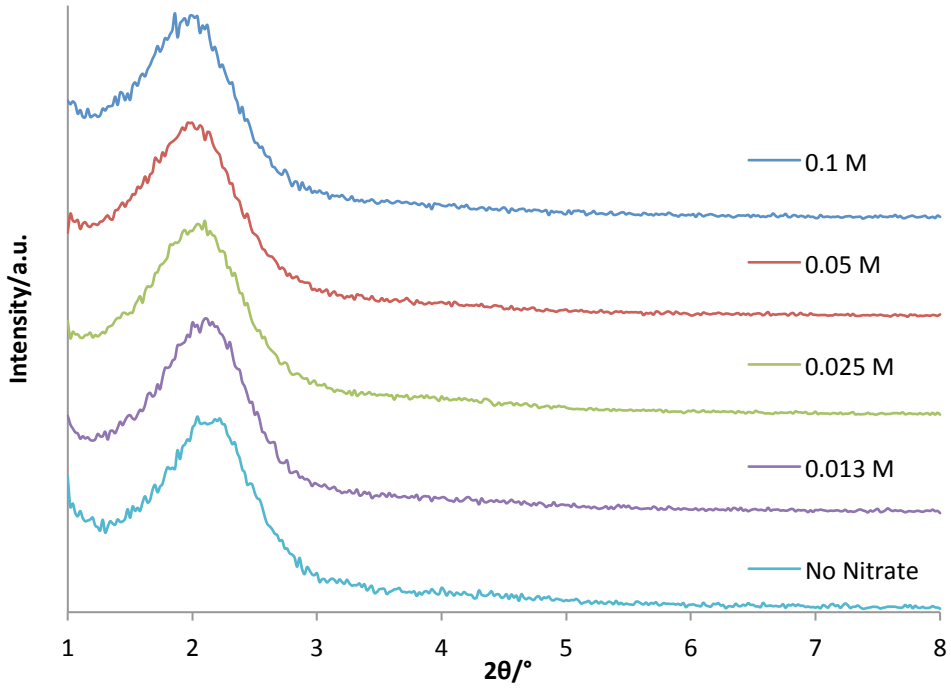

Figure 19 - GISAXS patterns of Stöber-derived mesoporous silica film with various concentration of $NaNO_3$

Table 4 - Summary of the lattice parameters obtained from the GISAXS pattern to due to the addition of $NaNO_3$

NO_3^- conc. (M)	Peak posn. (2θ/°)	d_{10} (nm)	a_o (nm)
0.1 M	1.90	4.65	5.37
0.05 M	1.94	4.55	5.25
0.025 M	1.98	4.46	5.15
0.013 M	2.04	4.33	5.00
None	2.08	4.24	4.90

3.5.2 Sodium bicarbonate

The dissolution of sodium bicarbonate in aqueous solution leads to the release of hydroxyl ions as the anion reacts with water:

$$HCO_3^- + H_2O \rightarrow H_2CO_3 + OH^-$$

It is therefore used to gently increase the pH of solutions and neutralise acids. Initially this was investigated on glass slides, using the same concentrations as used for $NaNO_3$. An additional feature was observed at ~ 4.1 ° in the in-plane GISAXS pattern for all films containing $NaCHO_3$ (see Fig. 20). This becomes clear when the feature is compared the feature with a plain Stöber film without $NaCHO_3$ in solution. The extra peak could be related to enhancement in the amount coherent X-ray scattered off pores, which have become more regularly ordered or an increase the thickness of the films. Otherwise the peaks remain consistent with that of Stöber films, where the 10 peak is positioned close to 2°.

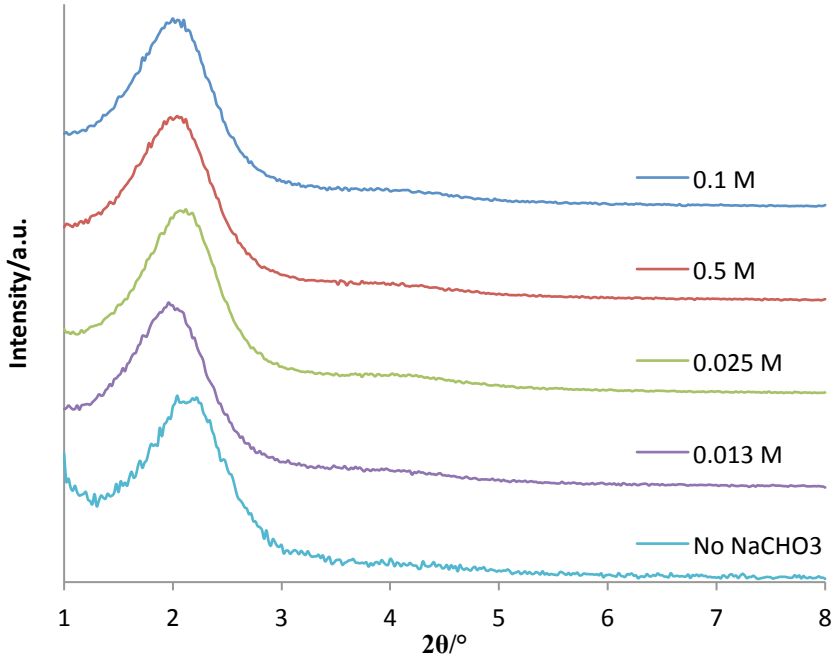

Figure 20 - GISAXS pattern of Stöber-derived mesoporous silica film with various concentration of $NaCHO_3$ on silica

Table 5 - Summary of the in-plane GISAXS pattern of Stöber films with the addition of various concentrations (0.1 to 0.013 M) of $NaCHO_3$

$NaHCO_3$ conc.	Peak posn. (2θ/˚)		d_{10}	a_0
(M)	(10)	(20)	(nm)	(nm)
0.1 M	2.00	3.94	4.50	5.20
0.05 M	1.98	3.92	4.50	5.20
0.025 M	2.02	4.04	4.37	5.05
0.013 M	1.92	3.90	4.60	5.31
None	2.08	/	4.24	4.90

This work was transferred onto sputtered TiN-coated silicon in order to increase the contrast between substrate and film. The film changed colour based on the scattering of light. A further improvement in the in-plane GISAXS pattern is observed with the 10 peak becoming more defined and the additional feature more pronounced at 2 ˚ and 4 ˚, respectively (see Fig. 21). Using FEGSEM, a cross-sectional image shows a significant increase in the thickness of the films from ~140 nm to around 400 nm (see Fig. 22 Right). This is an expansion in thickness of 300 % over the conventional Stöber method. TEM imaging of a scraped film sample shows that addition of $NaHCO_3$ has made no major improvements in the ordering, though pockets of hexagonal arranged pores were witnessed (see Fig 22 left).

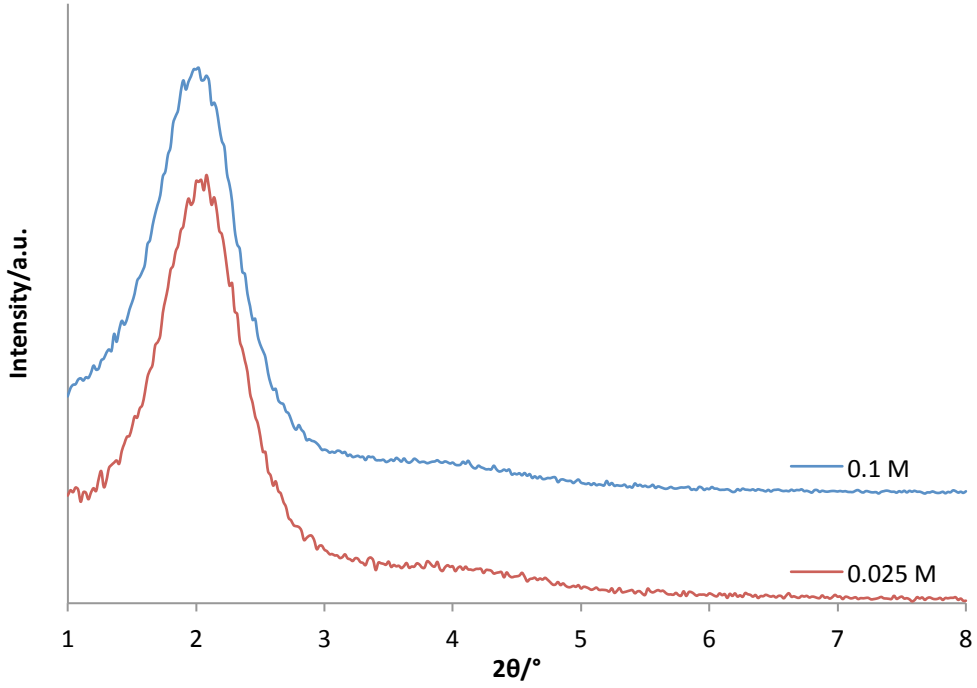

Figure 21 - GISAXS pattern of Stober-derived mesoporous silica film with various concentration of $NaHCO_3$ on TiN coated silicon

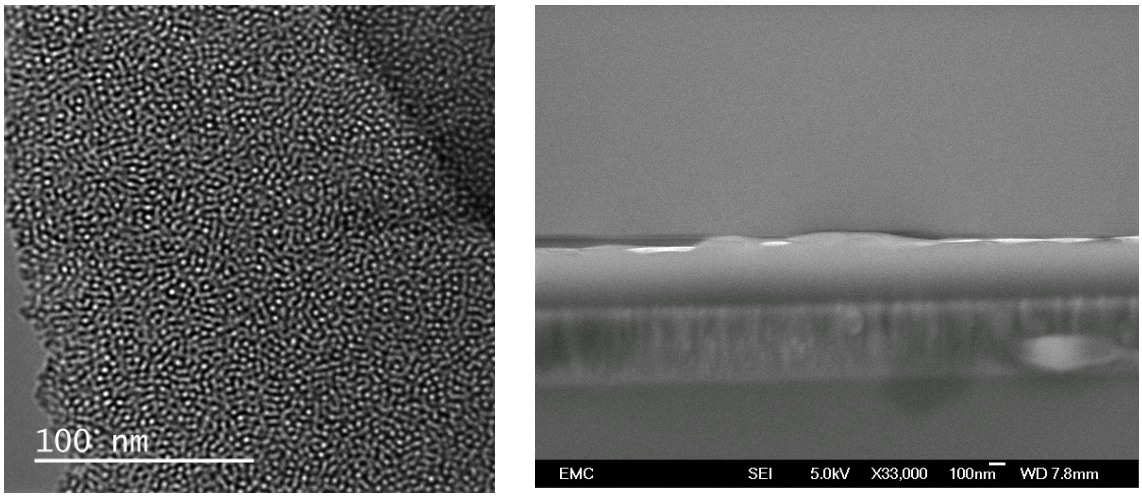

Figure 22 - (Left) TEM image of scrapped Stöber-derived mesoporous silica film with the addition of $NaCHO_3$ (0.025 M). (Right) Cross-sectional FEGSEM image of Stöber-derived film on TiN-coated silicon synthesised with addition of $NaCHO_3$ (0.1 M)

Table 6 - Summary of the in-plane GISAXS pattern of Stöber films on TiN with the addition of 0.1 and 0.025 M of $NaHCO_3$

$NaHCO_3$ conc.	Peak posn. ($2\theta/^{\circ}$)		d_{10}	a_0
(M)	10	20	(nm)	(nm)
0.1	1.98	4.02	4.46	5.15
0.025	2.00	4.10	4.41	5.09

The addition of sodium bicarbonate has led to an increase in the thickness of the Stöber-derived mesoporous silica films. It was understood that due to the increased concentration of hydroxyl ion in solution, a larger amount of silicate ions could hydrolyse without precipitating into solution.

3.5.3 Sodium carbonate

The higher charge density of sodium carbonate was investigated in order to measure its effects of the pore ordering of Stöber-derived mesoporous silica films. In aqueous solutions, sodium carbonate releases twice the amount of hydroxyl ions compared to sodium bicarbonate, which was shown to increase film thickness of samples in the previous section:

$$CO_3^{2-} + H_2O \rightarrow HCO_3^{-} + OH^{-}$$

$$HCO_3^{-} + H_2O \rightarrow H_2CO_3 + OH^{-}$$

Using the same concentrations of sodium carbonate, as used the previous sodium salts would lead to larger increase in the pH. Glass-slides were used as the substrates for growing the Stöber films in the presence of Na_2CO_3. In-plane GISAXS patterns indicate a collapse in the pore ordering of the films when compared against other Stöber films. The lowest concentrations of sodium carbonate (0.013 to 0.05 M) retained a feature at around 2.2 ° in the scattering patterns. However, the peaks broadened indicating a clear reduction in pore ordering (see Fig. 23). No visible features were witnessed when the highest

concentration of sodium carbonate (0.1 M) was used, signifying no ordered pores present within the film.

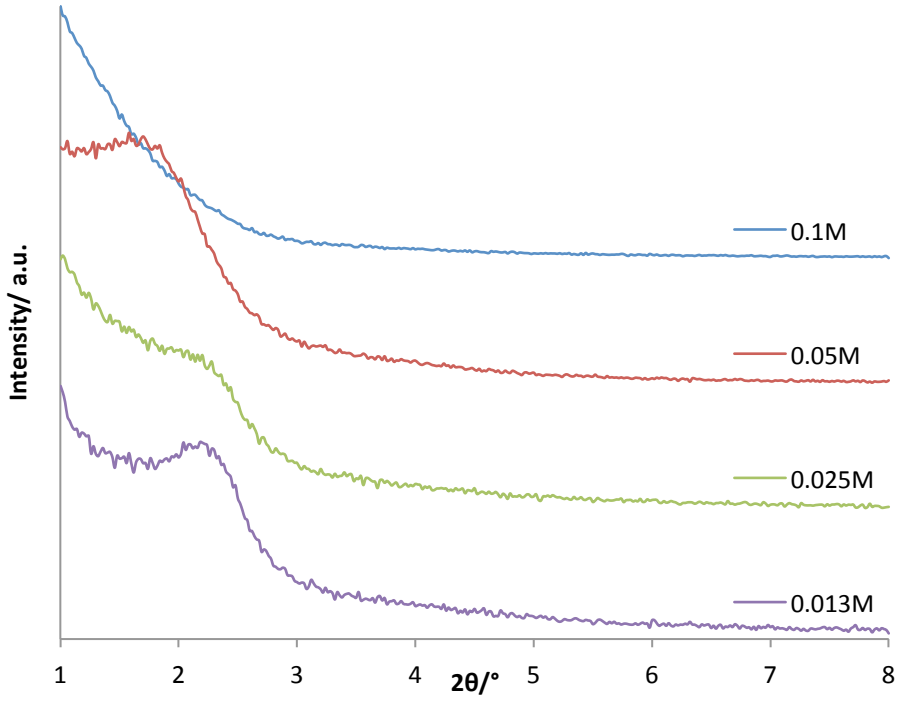

Figure 23 - GISAXS pattern of Stöber-derived mesoporous silica film with various concentration of Na_2CO_3 to a Stöber sol.

The larger amounts of hydroxyl ions in solution have clearly disrupted film growth, possibly due to the precipitation of silica away from the substrate surface. Also due to the higher charge density on the carbonate anion (-2) compared with the nitrate and bicarbonate (-1) could result in them collecting around the cationic micelle. This would prevent cooperative self-assembly by forming a double layer around the exterior of the micelle repelling silicate oligomers from the polar head of the surfactant. This has previously been used to prevent repulsion in order to encourage self-assembly of surfactants and titania with matching charges.[107] However, here this has led to an unfavourable result.

Table 7 - Summary of the GISAXS data obtained from the addition of various concentrations of Na_2CO_3 to Stöber sol.

Na_2CO_3 conc. (M)	Peak posn. (2θ/°)	d_{10} (nm)	a_0 (nm)
0.1M	/	/	/
0.05M	1.64	5.38	6.21
0.025M	2.16	4.09	4.72
0.013M	2.18	4.05	4.68
None	2.08	4.24	4.90

3.5.4 Sodium sulphate

The addition of sodium sulphate to solution was investigated on the synthesis of Stöber-derived mesoporous silica films. However, this had a negative effect on the pore ordering when analysed using in-plane GISAXS pattern. No features were observed in the scattering pattern with the addition of sodium sulphate (between 0.1 and 0.013 M) into deposition onto glass slides. No changes in the pH could be accredited to the addition of sodium sulphate; therefore coordinating around the positively charged micelle would be the main effect. It led to the negatively charged silica oligomers being repelled by the charge on the anion. This has been observed in the synthesis of mesoporous titania powders made with CTAB from titanium ethoxide ($TiOEt_4$).[107] Instead of disrupting the attraction of titania to CTA^+, the sulphate attracted in order neutralise the repulsion between surfactant and metal. As a result, it forms a double layer around the micelle repelling the negatively charged silica oligomers needed to solidify the pore structure.

3.5.5 Summary

The effect of various sodium salts has been shown have various to effects on the resulting structure of the Stöber films depending on the properties of the anion. The largest effect came from the addition of $NaCHO_3$, which led to a significant increase in the thickness of the film of almost 300 %. This increase resulted in an increase in coherent X-ray scattering, resulting an enhancement

witnessed in the XRD pattern. Adding anions with higher charge density, such as CO_3^{2-} and SO_3^{2-} disrupted the formation of the mesophase. No features were observed in the GISAXS pattern with the addition of SO_3^{2-} and increasing the concentrations of the CO_3^{2-} resulted in a collapse in the pore structure. $NaNO_3$ had little effect apart from reducing the noise of the scattering pattern. The addition of NaCl and KBr resulted in increasing the interpore distance.

3.6 Addition of swelling agents on Stöber-derived silica films

Controlling the pore size was an important aim of the project. This would enable the diameter of the resulting nanowires to be altered based on the inverse void left by the pores of the template. The addition of organic groups during the synthesis of mesoporous silica powder has been shown to increase the size of the resulting pores, based on their uptake in the surfactant micelle. On entering the hydrophobic region of the micelle, the organic molecules cause it to swell and hence increase the size of the pore channels.

Fukuoka et al reviewed the effect of various 1,3,5-trialkylbenzene molecules on the pore expansion of mesoporous silica powders.[57] They determined that based on the size and shape of the molecule, they sit within different regions of the micelle. For example, smaller trialkybenzene molecules, such as 1,3,5-trimethylbenzene (TMB) sit close to the polar heads of the surfactants. Whereas larger, more sterically bulkier molecules, like 1,3,5-triisopropylbenzene (TIPB) were posited closer to the centre of the micelle. They found that a larger concentration of TIPB relative to TMB could be added to solution before a collapse in the pore structure of the powder recorded.

Another noted swelling agent is 1-hexadecanol ($C_{16}OH$), of which Sakai and co-workers investigated the effect on mesoporous titania powder.[58] This study included other organic groups, such as decane and TMB. Again, depending on the properties of the swelling agents, they posited themselves in different regions of the micelle. Sakia *et al* used changes XRD patterns to measure the expansion of the pores caused by the swelling agents.

3.6.1 - 1,3,5-trimethylbenzene (TMB)

Various molar equivalent amounts of TMB were added to the Stöber solution relative to CTAB (0.1, 0.5 and 1 molar eq.) once the surfactant had dissolved in solution. This was to ensure the uptake of the swelling agent before formation of any pores. Shifts in the d-spacing of the resulting peaks were used to measure changes in the pore size due to the addition of the organic groups. This was based on the principle that as the pore size increased; the interpore distance would also increase relative to the pore expansion. Figure 24 demonstrates the effect of the addition of TMB on the XRD pattern when compared against a standard Stöber film, a noticeable shift in peak position is observed. Utilising d-spacing of the peak shows an increase in the interpore distance when compared against a Stöber film without the swelling agent. Therefore this increase in the lattice parameter can be attributed to an increase in the size of the pore based on the addition swelling agent. The addition of 0.1 (3.1 μL) and 0.5 (16 μL) molar equivalents of TMB to solution resulted in a shift in peak position from 2.08 ° to 1.81 °. Whereas adding 1 molar equivalent TMB (31 μL) led to further movement of the peak position to 1.60 °. Based on the calculated interpore distance, this was an increase of ~1.3 nm. A scraped sample of the one molar equivalents of TMB film was imaged using TEM, which showed the surface to have no irregularities when compared against the standard films (see Fig. 25). The pore diameter was measured at ~2.9 nm, demonstrating an expansion of around 10 % with the addition of TMB.

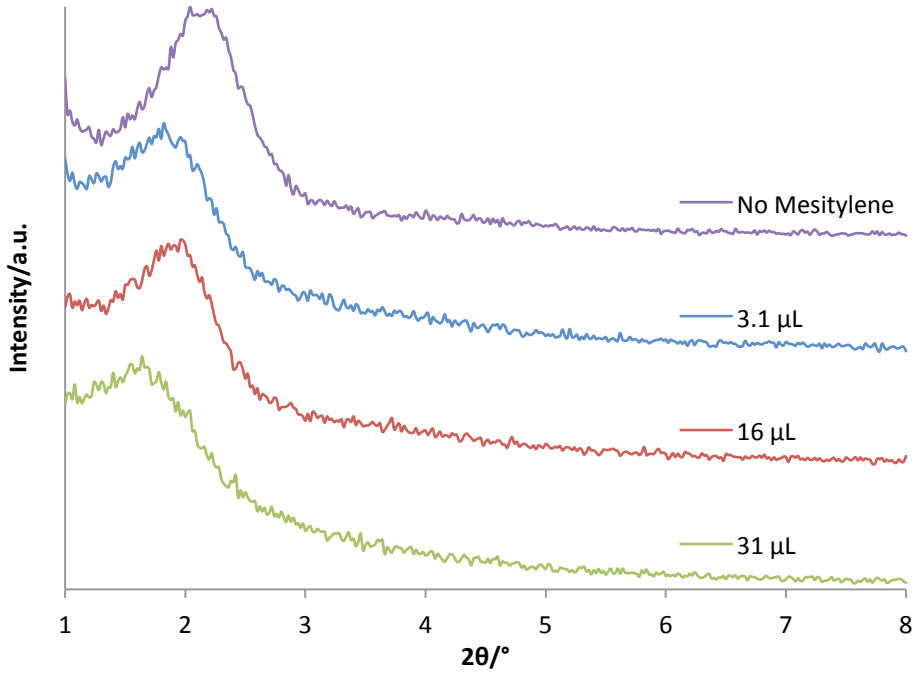

Figure 24 - GISAXS pattern Stöber-derived mesoporous silica films with the addition of mesitylene in order to expand the pores. Reproduced from Ref. 97 with permission from the PCCP Owner Societies (http://dx.doi.org/10.1039/C4CP05730A).

Table 8 – Summary of the d-spacing of Stöber-derived film with the addition of increasing concentrations of TMB based on the molar ratio (0.1, 0.5, 1) with surfactant (TMB/CTAB)

Molar eq (TMB/CTAB)	Volume of TMB (µL)	Peak posn. (2θ/˚)	d_{10} (nm)	a_0 (nm)
0.1	3.1	1.82	4.85	5.60
0.5	16	1.80	4.90	5.66
1	31	1.64	5.38	6.21
No TMB	0	2.00	4.41	5.09

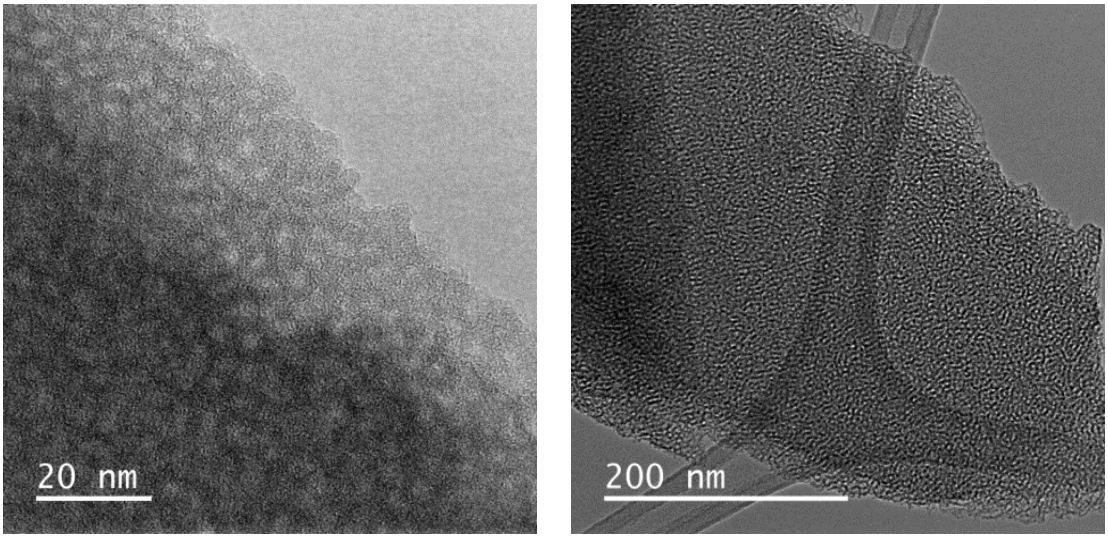

Figure 25 - TEM images of Stöber films with the addition of TMB (31 μL) show a 10 % increase in the pore diameter when compared against films without the swelling agent. Reproduced from Ref. 97 with permission from the PCCP Owner Societies (http://dx.doi.org/10.1039/C4CP05730A).

3.6.2 - 1,3,5-triisopropylbenzene (TIPB)

1,3,5-triisopropylbenzene (TIPB) was investigated as a swelling agent, in order to increase the pore size of the Stöber films and determine the effects of a larger organic molecule on pore expansion. It has been suggested by Fukuoka that TIPB molecule positioned itself within the centre of the micelle as it is taken up in solution.[57] This was found to be the most stable position, enabling larger concentrations of TIPB to be used before resulting in the collapse of the mesopores, which increase the pore diameter of the powder by as much as 1.6 nm. As the concentration of TIPB increased, the mesostructure altered from hexagonal (*P*6*mm*) to cubic (*Fm*3*m*) at 0.22 molar eq. (TIPB/CTAB).

TIPB was added based on various molar equivalent levels against CTAB and grown on glass-slides. Compared against a standard Stöber film, the increasing amounts of TIPB in solution resulted in shift in in plane GISAXS peak position from 2.08 ° to 1.94 ° (5.3 μL), 1.88 ° (27 μL) and 1.82 ° (105 μL) (see Fig. 26). The peaks become increasingly noisy with the presence of TIPB. Compared with a standard Stöber film, the d-spacing increased from 4.24 nm to a maximum of 4.90 nm. Unexpectedly this was a smaller change in peak position than observed when TMB was added. Expansion in the d-spacing

resulted in the interpore distance swelling to maximum distance of 5.66 nm or an increase of around 0.8 nm.

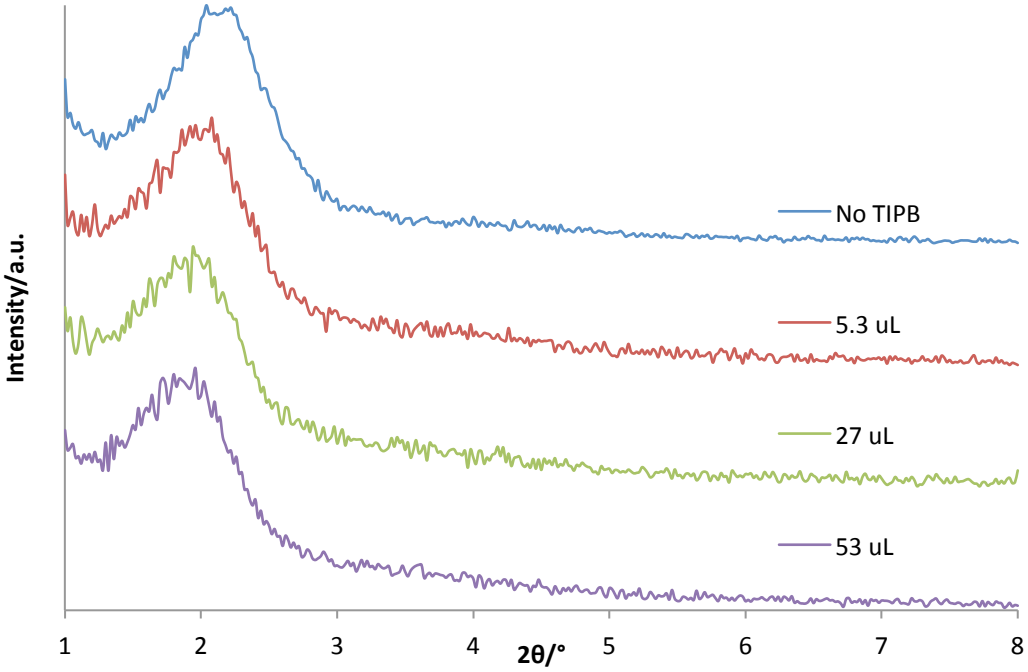

Figure 26 - GISAXS pattern of Stöber-derived mesoporous silica (NH_3 cat.) with the addition of increasing concentrations of TIPB

Table 9 - Summary of the in-plane GISAXS pattern data obtained from Stöber films with the molar eq. (0.1, 0.5, 1) of TIPB against CTAB

Molar eq. (TIPB/CTAB)	Volume of TIPB (µL)	Peak posn. (2θ/˚)	d_{10} (nm)	a_0 (nm)
0.1	5.3	1.94	4.55	5.30
0.5	27	1.88	4.70	5.43
1	53	1.80	4.90	5.66
No TIPB	0	2.00	4.41	5.09

SEM images of the surface of films show the development of cracks across the surface of the film (see Fig. 27). This is not witnessed in other Stöber films, which generally have smooth, defect-free surfaces. Fukuoka et al showed that the addition of particle morphology of the mesoporous silica powder became

more rough with the increasing amount of TIPB, which they related to the change in phase of the pores.[57] The pores of the powder maintained stable through the change in mesophase, whereas Stöber films that have been exposed to 1 molar equivalent begin to split. TEM images of film scrapings show the presence of pores. Unlike powders, which are free to undergo more dramatic changes in volume whilst suspended in solution, the films are directly bonded to their support. During its contraction as the film dries, more stress is applied to the walls of the pore leading to possible splintering. As the swelling agent offers no additional support for the pore structure, this leads to a weakening of the pore walls.

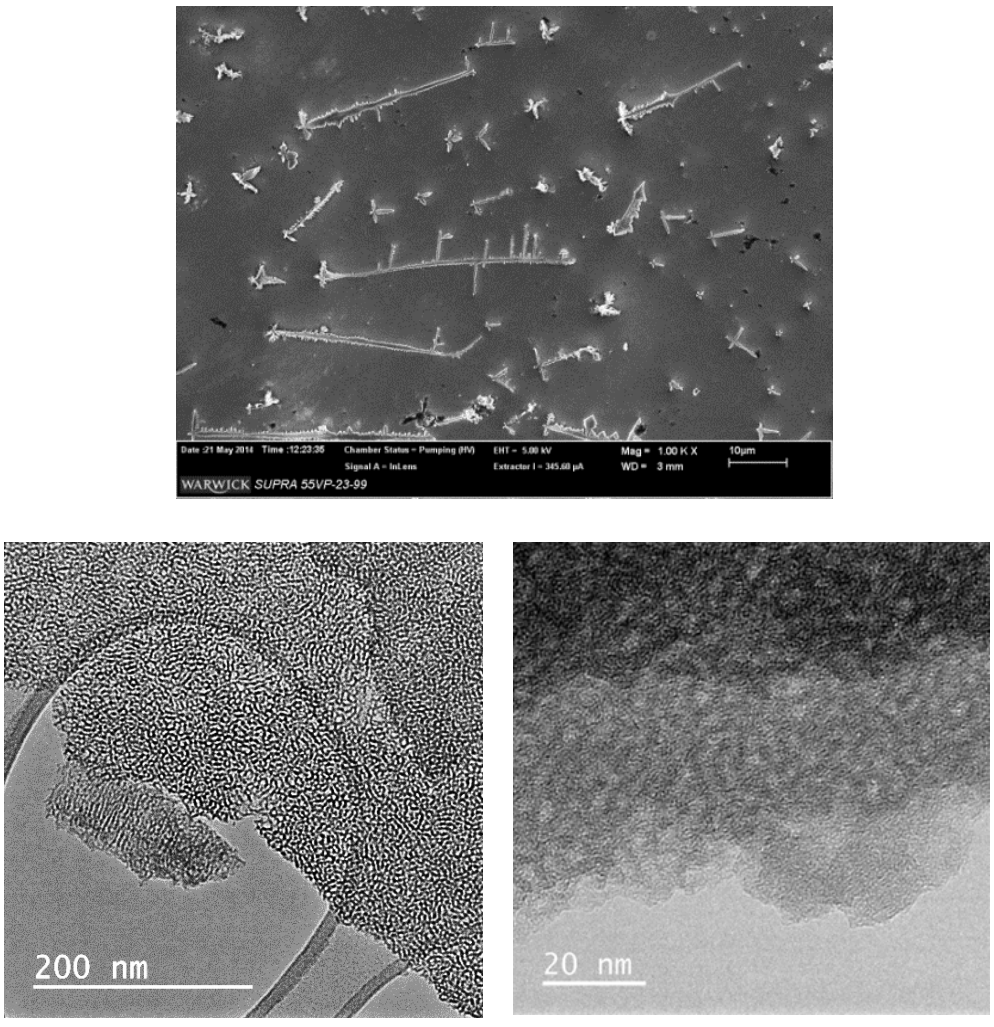

Figure 27 – (Top) SEM of the surface of Stöber-derived film with TIPB (105 µL), which exhibits cracks across its surface. (Bottom Right) TEM image of the surface of the same film presenting the formation of pores. (Bottom Left) TEM image of same sample at higher magnification.

3.6.3 - 1-Hexadecanol ($C_{16}OH$)

The various amounts of $C_{16}OH$ was added to solution in order to replace CTAB (0.1, 0.2, 0.3 and 0.5 molar eq.). This was investigated using on the in-plane GISAXS pattern of films, which were grown on glass-slides, are shown in Fig. 28). The presence of $C_{16}OH$ in solution clearly disrupts the ordering of the mesostructure. It proved hard to dissolve the swelling agent into solution due to its waxy nature. However, there is a significant shift in the peak position when compared against the standard Stöber film. This has led to a movement in peak position from 2.08 ° to around 1.40 ° (see Fig. 28). The disruption in the mesostructure structure could possibly be attributed to the positioning of the alcohol in between the CTAB molecules. Therefore reducing the attraction to the micelle with the surface of the substrate.

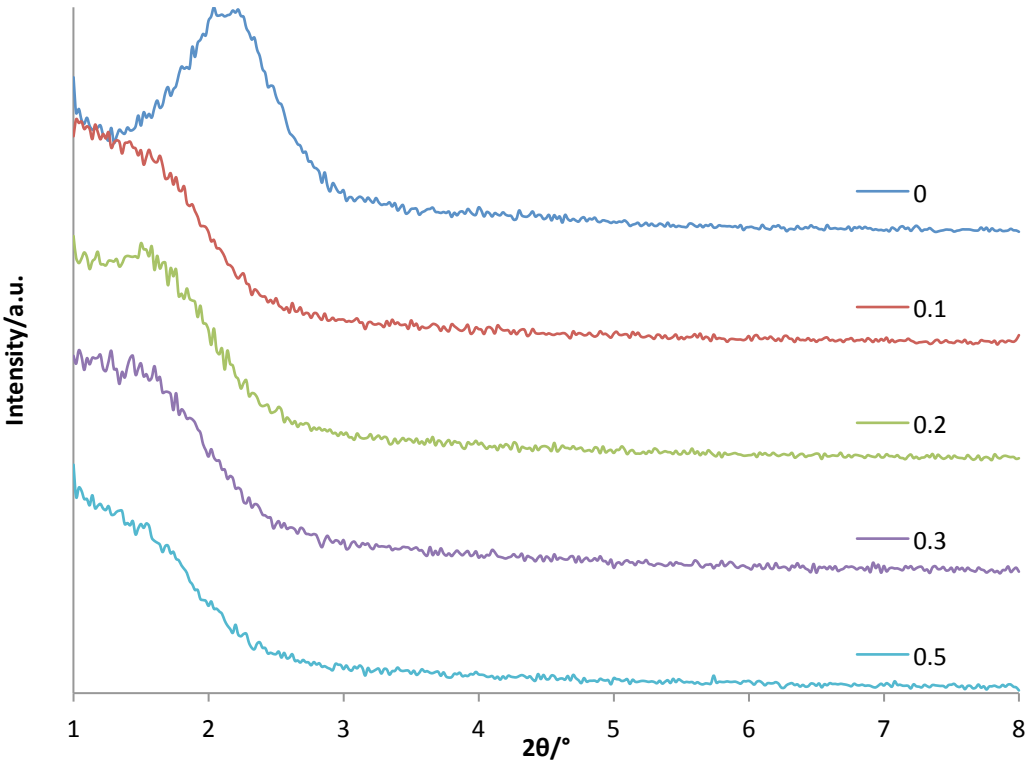

Figure 28 - GISAXS pattern of Stöber-derived mesoporous silica film replacing CTAB with molar equivalents of $C_{16}OH$ (0.1, 0.2, 0.3 and 0.5)

Table 10 - Summary of the in-plane GISAXS pattern data obtained from Stöber films with the addition of $C_{16}OH$

Mass of $C_{16}OH$ (mg)	Molar eq.	Peak posn. ($2\theta/^{\circ}$)	d_{10} (nm)	a_0 (nm)
5.3	0.1	1.42	6.22	7.18
11	0.2	1.48	5.96	6.88
16	0.3	1.38	6.40	7.39
27	0.5	/	/	/
0	0	2.00	4.41	5.09

3.6.4 Summary

The addition of organic swelling agents during the synthesis of the Stöber-derived films has affected the pore structure of the resulting samples. This was clearly picked up on in the XRD patterns of the samples, which all displayed shifts in their peak positions. A trend has developed showing that the larger the organic group added to solution, the less stable to the resulting sample is (i.e. TMB > TIPB > $C_{16}OH$). The addition of TMB produced the largest increase in pore expansion by 10 %, whilst visibly retaining its pore structure. TIPB caused a smaller expansion in the pore size with the film developing cracks across its surface. $C_{16}OH$ showed the largest shift in the peak position of its XRD pattern. However the peaks appear less resolved, denoting a lack of ordered pores.

3.7 Stöber-derived mesoporous silica film using triethylamine catalyst on silica

The effect of the catalyst on the growth of the Stöber-derived silica films was investigated by replacing ammonia with triethylamine (Et_3N). It is a stronger base than NH_3 (pKa_{Et3N} 10.78 and kPa_{NH3} 9.25 respectively) because of the three ethyl groups surrounding the nitrogen atom, which provide electron density.

These terminal groups also make the base far more organic solvent soluble. In the case of the organic swelling agent this may allow them to more readily diffuse through the exterior of the micelle. Teng *et al* suggested that the ammonia catalyst facilitates hydrogen bonding between the CTA^+ micelle and silica oligomers. Replacing the ammonia may confirm this, as Et_3N should not act as the proton source for hydrogen bonds but able to accept them.

3.7.1 Effect of different concentrations of triethylamine on Stöber-derived silica film

The effect of Et_3N on the formation of Stöber-derived silica films was explored by varying the amount added to solution, which were grown on glass. In-plane GISAXS patterns of the films were very similar to those obtained using ammonia solution (see Fig. 29). When 1 μL is added to solution, the peak position is roughly 1.80 °. As this is increased to 20 μL, the peak position has shifted by 0.34 ° to 2.14 °. No features in the scattering pattern were observed with the addition of 100 μL of Et_3N. A relationship between peak position and Et_3N concentration indicates that as the amount of base increases, the interpore distance reduces (see Table 11). This was also seen when varying the concentration of ammonia in solution (see section 3.4.1). The micelles contraction may be due to a reduction in repulsion between the polar heads of the CTA^+ groups as the Et_3N molecules coordinate around them. Therefore, with higher concentrations of Et_3N in solution, more base can organise about the micelle and reduce repulsion further. This agrees with the result obtained by Sayari and Yang who were investigating pore expansion of mesoporous MCM-41 silicas following the addition of amines.[59] They found that the addition of smaller amine molecules (i.e. triethylamine and trimethylamine) resulted in a contraction in the pore size and d-spacing when compared against samples without either.

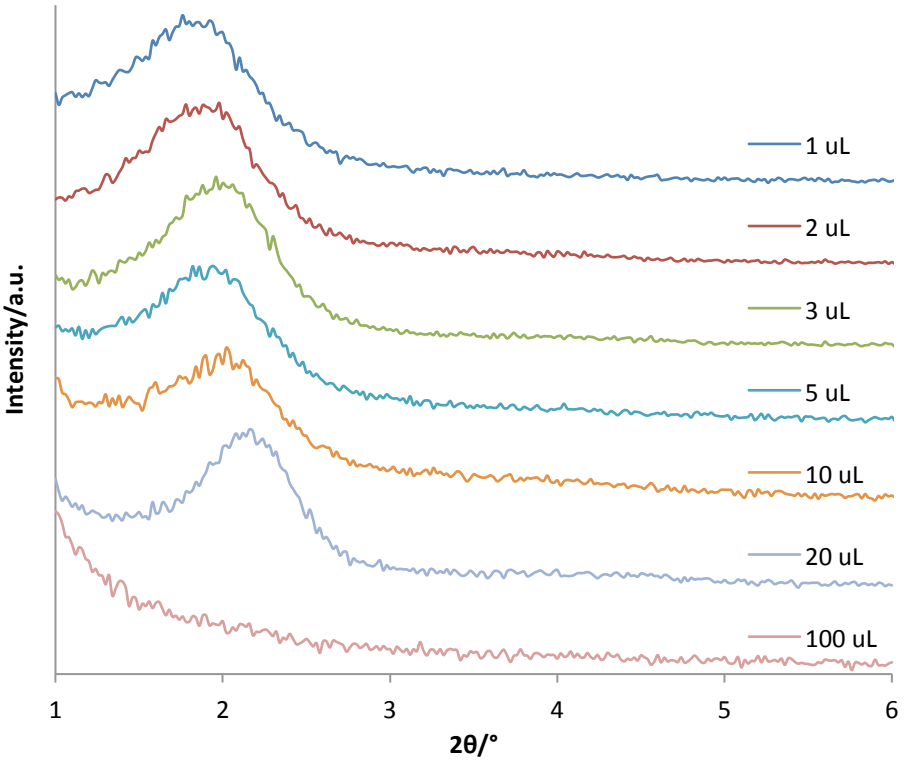

Figure 29 - Varying the concentration of Et_3N used in the growth of Stöber-derived mesoporous silica films

Table 11 - Summary of the in-plane GISAXS pattern obtained from varying the concentration of Et_3N present when fabricating Stöber films

Et_3N (µL)	Peak posn. (2θ/°)	d_{10} (nm)	a_o (nm)
1	1.84	4.80	5.54
2	1.88	4.70	5.43
3	1.94	4.55	5.25
5	1.92	4.60	5.31
10	2.00	4.41	5.09
20	2.14	4.13	4.77
100	/	/	/

3.7.2 The effect of 1,3,5-trimethylbenzene (TMB) to Stöber-derived mesoporous silica films with triethylamine catalyst

The effect of a more organically soluble catalyst was investigated with the addition of TMB as a swelling agent in the growth of Stöber-derived mesoporous silica films. As previously demonstrated of the ammonia Stöber films, an increase in the interpore distance was witnessed. The effect of a more organically soluble catalyst may result in the large uptake of organic swelling agent, due to a lower charge density surrounding the exterior of the micelle. Therefore act as less of a barrier for the uptake the TMB molecules.

Each solution contained 3.5 μL of Et_3N during the fabrication Stöber-derived, which were grown on glass-slides. TMB was added based on molar mixing ratios of 0.1, 0.5 and 1 (TMB/CTAB). Based on the in-plane GISAXS patterns obtained, the films made with Et_3N appear much more stable, producing peaks with less noise with the addition of TMB (see Fig. 30). A film with no TMB contained a feature at 2.04 ˚. The presence of 3.1 μL molar equivalence of TMB resulted in a shift in peak position to 1.94 ˚. This increased to ~1.82 ˚ for both 16 μL and 31 μL of TMB. This was a change in interpore distance of over half nanometre. However, overall this is a smaller change in lattice spacing then the ammonia Stöber films.

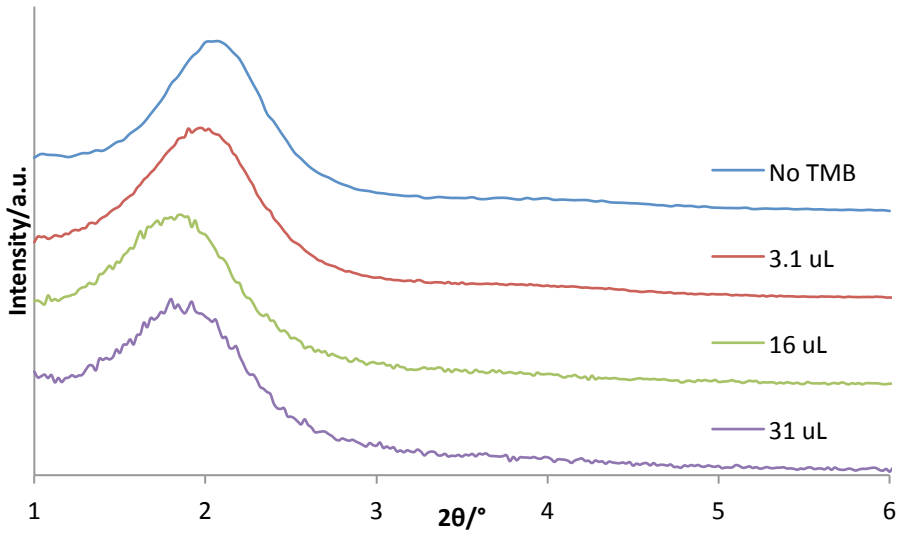

Figure 30 - GISAXS pattern Stöber-derived mesoporous silica films (Et_3N) with the addition of swelling agent TMB

Table 12 - Summary of the in-plane GISAXS patterns of Stöber film with the addition of TMB in the presence of Et_3N

Molar eq. (TMB/CTAB)	TMB (µL)	Peak posn. (°)	d_{100}, (nm)	a_0 (nm)
0.1	3.1	1.94	4.55	5.25
0.5	16	1.80	4.90	5.66
1	31	1.82	4.85	5.60
No TMB	0	2.04	4.33	5.00

Therefore it can be concluded that adding TMB to the Stöber solution has produced more stable mesopores. However, when compared against the ammonia Stöber films, a larger change in the interpore distance is witnessed. As the catalyst is the only parameter changed, this must regulate the diffusion of TMB through the micelle. The organic properties of Et_3N could disrupt the positioning of TMB within the micelle. As previously described, the base would position itself close to the polar head of CTAB. Due to its increased organic solubility (when compared with NH_3) Et_3N could position itself within the micelle, thus superseding TMB. Therefore producing lower amounts suitable sites within the micelle for the TMB, reducing its uptake and preventing the expected expansion in pore diameter. The higher charge density on Et_3N would be more favourable than TMB, which has been shown to reduce the repulsion between the ammonium groups present on CTAB (see section 3.7.2).

3.7.3 The effect of 1,3,5-triisopropylbenzene (TIPB) on Stöber-derived mesoporous silica films with triethylamine catalyst

The effect of TIPB was also investigated using Et_3N catalysed Stöber films. Like TMB, the effect of Et_3N of the uptake of TIPB was investigated to determine the effect of the more organically soluble base. As previously mentioned, TIPB has sterically bulky organic terminal groups, which result in the molecules positioning itself within the centre of micelle when it is absorbed.[57] Here the

Et_3N presence in the synthesis of Stöber film with the addition of TIPB has been investigated. As previously shown, ammonia-catalysed films showed an increase in the interpore distance in the XRD pattern with increasing concentrations of TIPB. However, images of the surface showed large amounts of cracking across the surface of the films (see section 3.6.2).

In-plane GISAXS patterns when various mixing ratios of TIPB (0.1, 0.5 and 1 molar eq.) were added to CTAB/TIPB show an expansion in the d-spacing with increasing concentration of the swelling agent (see Fig 31). Unlike when TMB was added, TIPB in the presence of Et_3N does not appear to reach a limit with the amount of swelling agent absorbed into the micelle at 1 molar equivalent (5.3 µL). When compared against a film with no TIPB, a steady reduction in peak position is witnessed, denoting an expansion in the pore volume. The addition of 0.1 molar equivalence resulted in a peak shift from 2.04 ˚ to 1.92 ˚. This was decreased further with larger concentrations of TIPB to 1.80 ˚ (0.5 molar eq.) and 1.60 ˚ (1 molar eq.). This resulted in a change in the interpore distance close to 1.4 nm.

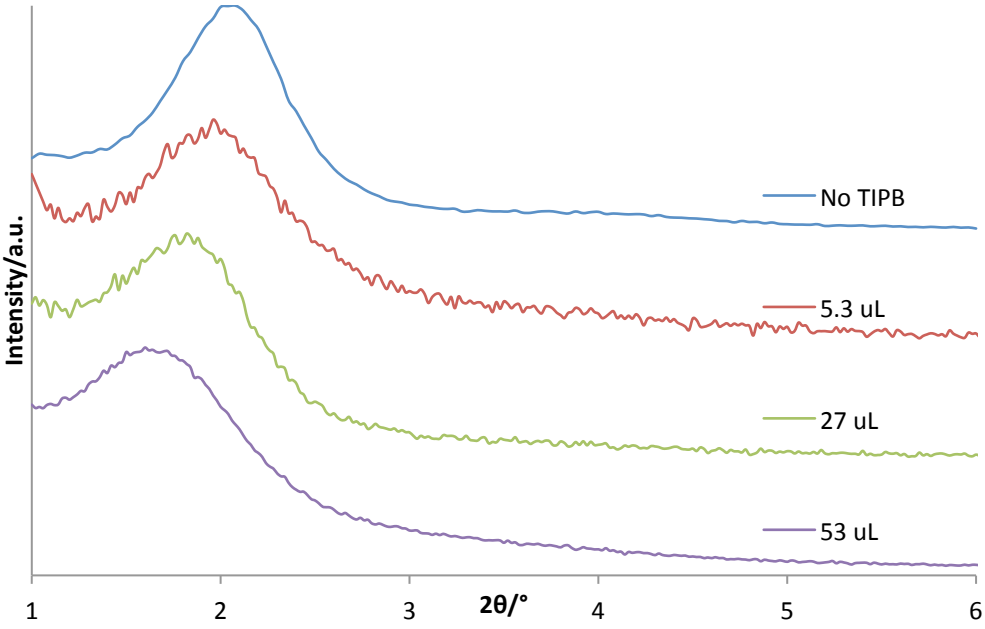

Figure 31 – GISAXS pattern of Stöber-derived mesoporous silica (Et_3N cat.) with the addition of increasing concentrations of TIPB

Table 13 - Summary of data obtained from XRD pattern of Stöber films with the addition of TIPB

Molar eq. (TIPB/CTAB)	TIPB (µL)	Peak posn. (2θ/°)	d_{10} (nm)	a_o (nm)
0.1	5.3	1.92	4.60	5.31
0.5	27	1.80	4.90	5.66
1	53	1.60	5.52	6.37
No TIPB	0	2.04	4.33	5.00

Increasing amounts of TIPB in solution shows a gradual increase in the interpore distances in the presence of Et_3N. Its behaviour mimics that of the addition of TMB to the ammonia Stöber films instead of TIPB, with a larger amount of swelling agent having been absorbed. This could again be related to the position of the swelling agent within the micelle. As discussed with TMB in the presence of Et_3N, with the base displacing the swelling agent. With TIPB being positioned within the centre of the micelle, it may be unaffected by the Et_3N allowing more absorption.

3.7.4 Summary

The effect of replacing NH_3 with Et_3N has shown to reverse the stabilities of the two swelling agents. TMB was shown to have a smaller effect of the peak positions, whereas TIPB had a much larger one. This was related to the increase in organic solubility of Et_3N and the positioning of the swelling agent within the micelle. As a result the base was capable of displacing TMB, but not TIPB.

3.8 Stöber-derived silica film using urea catalyst on silica

The thermal decomposition of urea has been used to gradually alter the pH of a given solution by slowly releasing ammonia as it breaks down. This property has been used to homogenously precipitate a range of materials, such as metal oxides in solution to synthesis nanoparticle with uniform sizes and shapes.[108] The mechanism for the thermal decomposition of urea proceeds as stated:[109]

$$(NH_2)_2CO + 3H_2O \rightarrow CO_2 + 2NH_4^+ + 2OH^-$$

The controlled release of base into solution is attractive in the synthesis of thin films as the reaction temperature could be used to control the growth. It has been widely used in the formation of mesopores within alumina[110,111] and titania.[112]

Concentrations of between 0.1 and 0.013 M of urea were added to the water used in the synthesis of the Stöber-derived mesoporous silica films without NH_3. The solution was heated to 60, 80, 100 and 120 ˚C to induce the thermal decomposition of urea in order to release ammonia. The film growth was performed on glass-slides. No features were observed in the in-plane GISAXS pattern of Stöber-derived film generated at 60 ˚C, though this was partly expected as the thermal decomposition of urea occurs above 80 ˚C.[110] On increasing the reaction temperature to 80 ˚C the scattering pattern shows weak feature denoting the beginnings of the formation of the 10 peak (see Fig. 32). However, no changes in scattering patterns were observed based on the concentration of urea in solution due to the broad nature of the features.

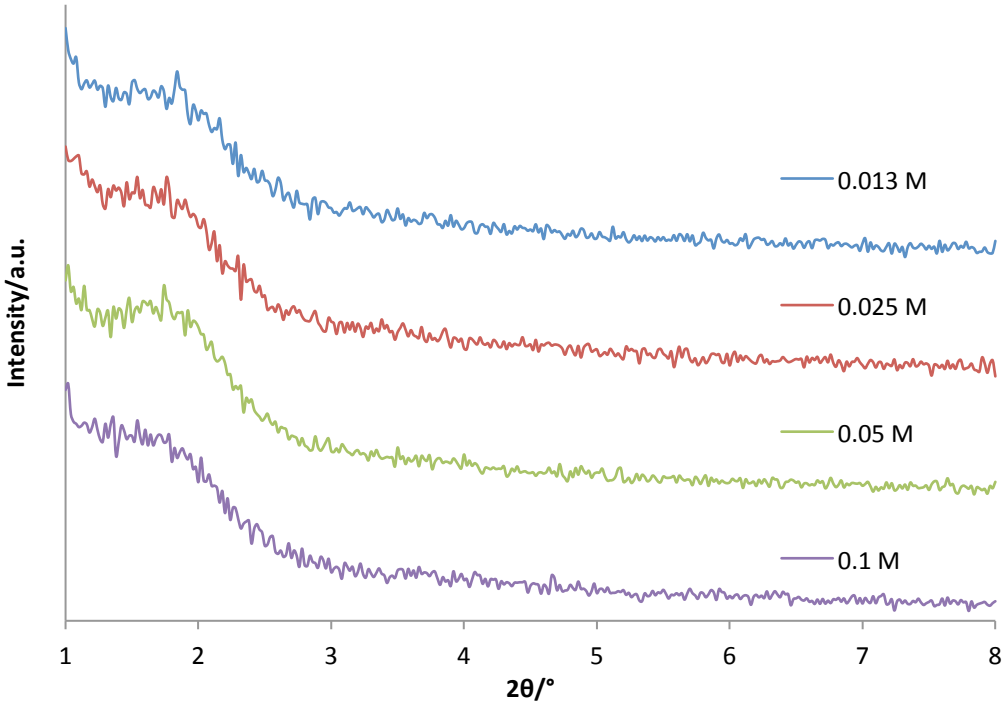

Figure 32 - Stöber-derived mesoporous silica film with concentrations of urea at 80 ˚C

Table 14 - Summary of data obtained from the in-plane GISAXS patterns of the Stöber-derived silica film generated using urea at 80 ˚C

Urea conc. (M)	Peak posn. (2θ/˚)	d_{10} (nm)	a_0 (nm)
0.1	~1.67	5.29	6.11
0.05	1.72	5.13	5.92
0.025	1.70	5.20	6.00
0.013	1.82	4.85	5.60

As the temperature was increased to 100 ˚C, the feature witnessed in the 80 ˚C synthesis scattering pattern become far more pronounced. Again at all concentrations we see the formation of a peak at 1.94 ˚ in the in-plane GISAXS patterns, (see Fig. 33). This can be related to a larger amount of NH_3 released by urea thermally decomposing. As a result, thicker films would be produced, which would increase the intensity of X-ray scattered by the pores. Unfortunately, if this work were to be carried out on TiN substrate instead of

the glass slides, it would likely lead to the oxidation of its surface. As seen in the section 3.3.4, this would be unfavourable for SCFED due to the increased resistivity of the electrodes surface.

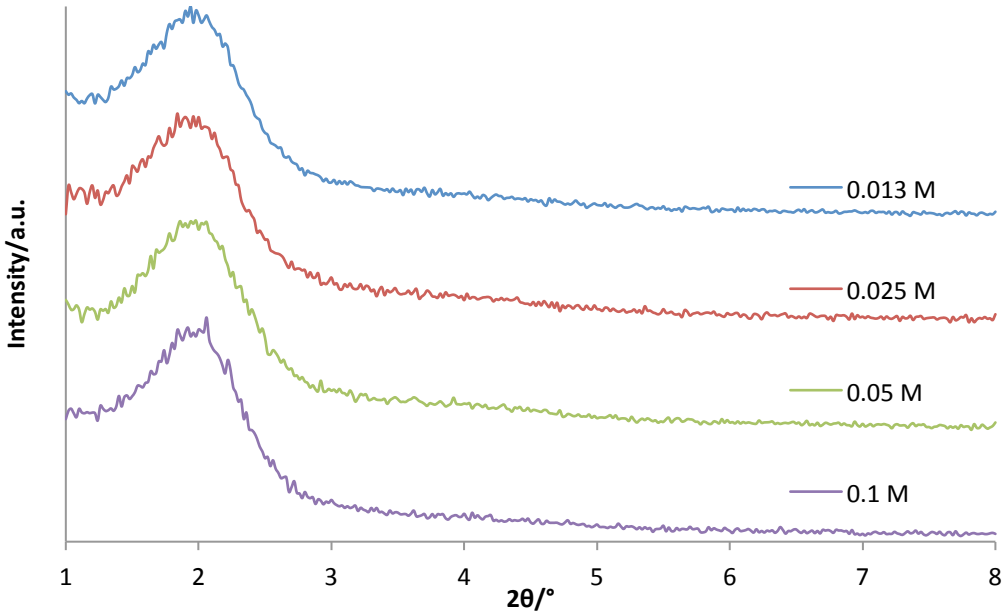

Figure 33 - Stöber-derived mesoporous silica film with concentrations of urea at 100 ˚C

Table 15 - Summary of data obtained from the in-plane GISAXS patterns of the Stöber-derived silica film generated using urea at 100 ˚C

Urea conc. (M)	Peak posn. (2θ/˚)	d_{10} (nm)	a_o (nm)
0.1	1.94	4.55	5.25
0.05	1.94	4.55	5.25
0.025	1.94	4.55	5.25
0.013	1.94	4.55	5.25

Increasing the reaction temperature further to 120 ˚C, achieved very similar results to films grown at 100 ˚C. Again, a single peak at 1.94 ˚ was witnessed in the in-plane scattering patterns for each film regardless of the concentration of urea (see Fig. 34). This clarifies that the controlled release of ammonia into

solution proceeded to produce highly uniform films with little shift in the peak position.

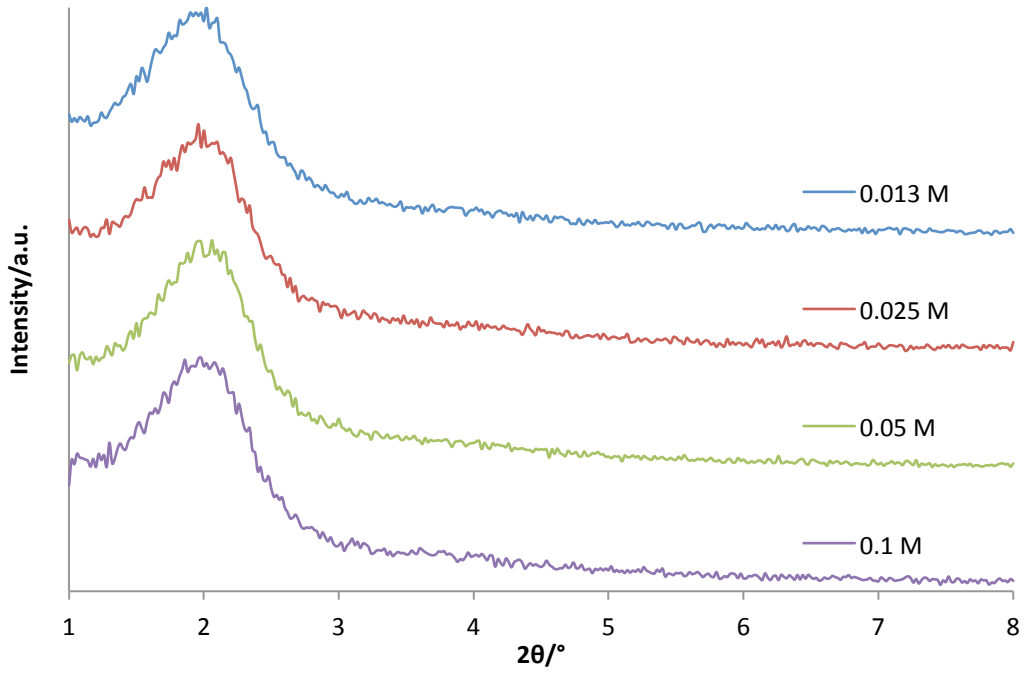

Figure 34 - Stöber-derived mesoporous silica film with concentrations of urea at 120 ˚C

Table 16 - Summary of data obtained from the in-plane GISAXS patterns of the Stober-derived silica film generated using urea at 120 ˚C

Urea conc. (M)	Peak posn. (2θ/˚)	d_{10} (nm)	a_o (nm)
0.1	1.94	4.55	5.25
0.05	1.94	4.55	5.25
0.025	1.94	4.55	5.25
0.013	1.92	4.60	5.31

As determined by the in-plane GISAXS pattern, the formation of a peak at 1.94˚ was witnessed in both the films synthesized at 100 ˚C and 120 ˚C regardless of the concentration of urea. This shows a high degree of reproducibility when using urea not seen with other catalysts. Only films synthesized at 80 ˚C

exhibited any difference, which can be explained by the lack of ammonia released due to the lower temperature. However, the higher temperatures (> 80 ˚C) required fabricating the films to make the process unfavourable for growing on TiN, leading to the electrically passivating of its surface.

3.9 Stöber-derived mesoporous silica films with varying alkyltrimethylammonium bromide carbon chain lengths

Control over pore size is a key parameter under investigation in order to regulate the diameter of nanowires grown within the templates. The addition of a swelling agent has led to the production of larger pores, based on the uptake of organic molecules by the surfactant. In this section, the aim is to decrease the size of the pores by reducing the tail length of the alkytrimethylammonium surfactant. With shorter alkyl tails on the surfactant, the hydrophobic region of the surfactant would decrease in diameter and hence reduce the size of the pores within the film. An advantage of this process is that the pore size can be controlled based simply on the number of carbon atoms within the surfactant tail, thus providing a high degree of control of the pore size.

3.9.1 Tetradecyltrimethylammonium bromide (MyTAB)

When myristyltrimethylammonium bromide (or tetradecyltrimethylammonium bromide or MyTAB) was used instead of CTAB, a peak was found using the same molar amount of surfactant (0.074 g, 0.22 mmol) in the GISAXS pattern of the films at around 2.12 ˚ (see Fig. 35). The concentration of MyTAB was increased two (0.15 g), three (0.22 g) and four-fold (0.30 g) in relation to CTAB, in order to determine the optimum conditions required to fabricate the films. All samples stay within ± 0.04 ˚ of each other. Comparing the interpore distance of MyTAB films with CTAB films reveals a reduction of around 0.5 nm, indicating a reduction in pore diameter and/or wall thickness. TEM imaging of a sample (0.074 g) shows no visible changes in pore structure, which had no discrete arrangement. These results indicate that MyTAB behaviours in a

similar manner CTAB Stöber films (see section 3.4.1). Therefore, based on the average peak position gathered from the various amounts of MyTAB used, a decrease in the interpore distance is established, which is smaller then any seen in the scattering patterns of films synthesised using CTAB.

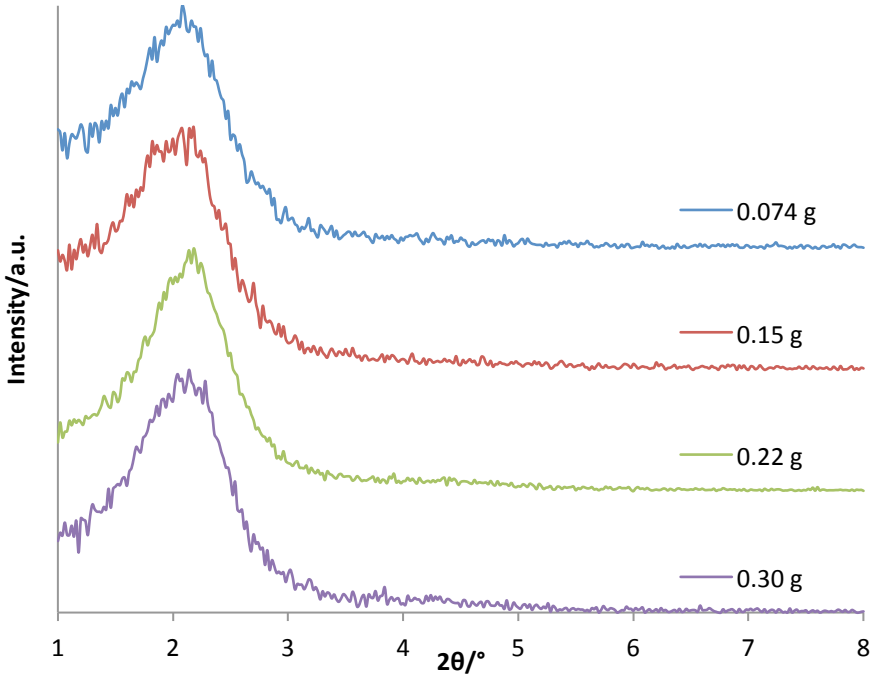

Figure 35 - In-plane GISAXS of Stöber-derived mesoporous silica film using MyTAB

Table 17 - Summary of the in-plane GISAXS pattern data obtain from the synthesis of Stöber films using different amounts of MyTAB surfactant

MyTAB (g)	Peak posn. (2θ/˚)	d_{10} (nm)	a_o (nm)
0.074	2.12	4.16	4.80
0.15	2.10	4.20	4.85
0.22	2.14	4.13	4.77
0.30	2.12	4.16	4.80

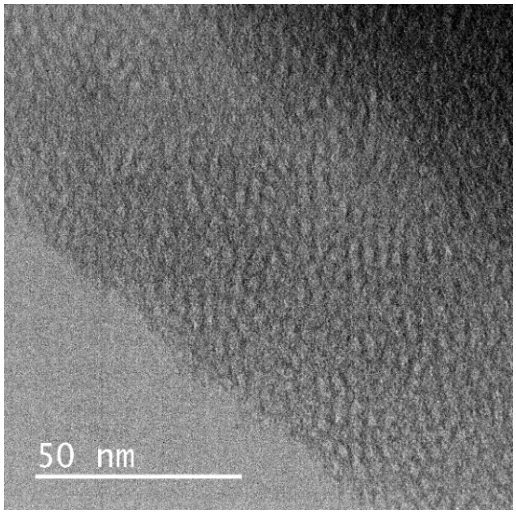

Figure 36 - TEM image of the surface of MyTAB Stöber-derived film. Reproduced from Ref. 97 with permission from the PCCP Owner Societies (http://dx.doi.org/10.1039/C4CP05730A).

3.9.2 Dodecyltrimethylammonium Bromide (DoTAB)

Dodecyltrimethylammonium bromide (DoTAB) was used in the synthesis of Stöber-derived mesoporous silica to reduce the pore size further then MyTAB. It contains a tail consisting of twelve carbon atoms in length. The amount of DoTAB was varied in order to find the ideal conditions required to fabricate the films and was grown on glass slides. A feature in the in-plane GISAXS pattern was observed at ~1.94 ° when the same molar equivalents of DoTAB were used to replace CTAB. Subsequently, increasing the concentration of DoTAB by three to four-fold produced a more prominent reflection at around 2.20 ° (see Fig. 37). Comparing the interpore distance with CTAB reveals a further reduction of 0.8 nm. TEM imaging of a DoTAB film (0.28 g) showed the formation of pores across the surface of the sample, indicating vertical orientation structure, which correlates with the diffraction data (see Fig. 38). Walcarius *et al* also observed this behaviour during electrochemical diffusion studies on similar mesoporous silica films fabricated using DoTAB.[78] He noted an improvement in the current response during cyclic voltammetry when higher concentrations of DoTAB were used in the synthesis of the mesoporous silica films. Therefore, an enhancement in the formation of the channels was concluded, allowing the analyte better access to the electrode surface under the film.

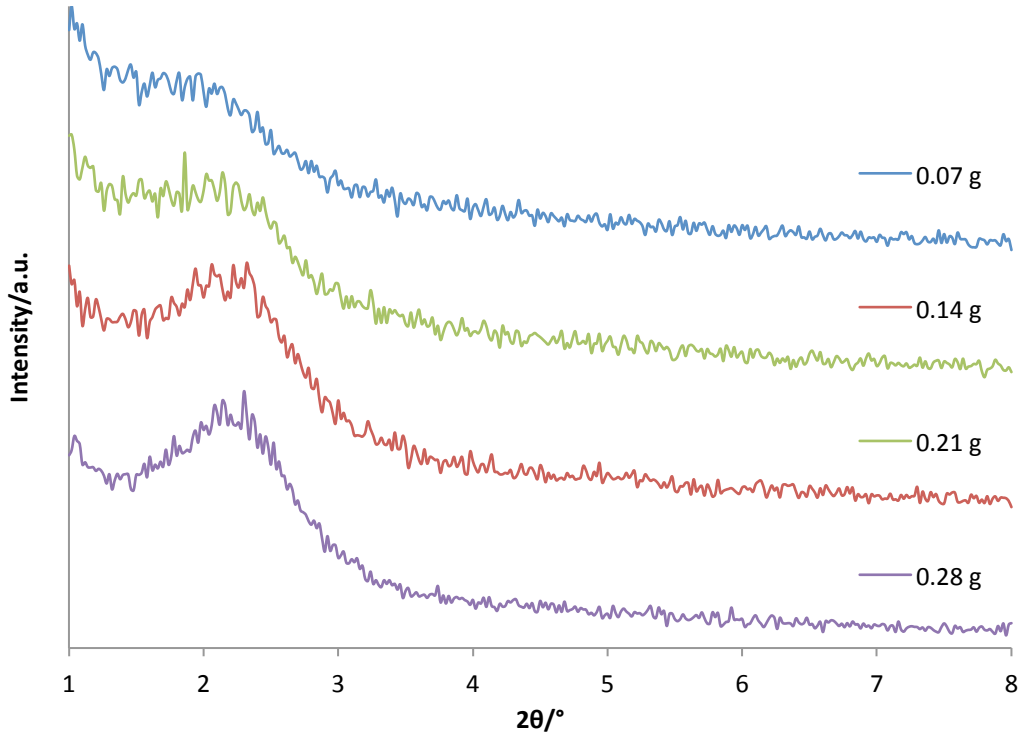

Figure 37 - In-plane GIASXS pattern of Stöber-derived mesoporous silica film using various amount of DoTAB

Table 18 - Summary of the data obtained from the in-plane GISAXS pattern of Stöber synthesized with different amount of DoTAB

DoTAB (g)	Peak posn. (2θ/˚)	d_{10} (nm)	a_o (nm)
0.07	1.94	4.55	5.25
0.14	2.18	4.05	4.68
0.21	2.24	3.94	4.55
0.28	2.25	3.92	4.53

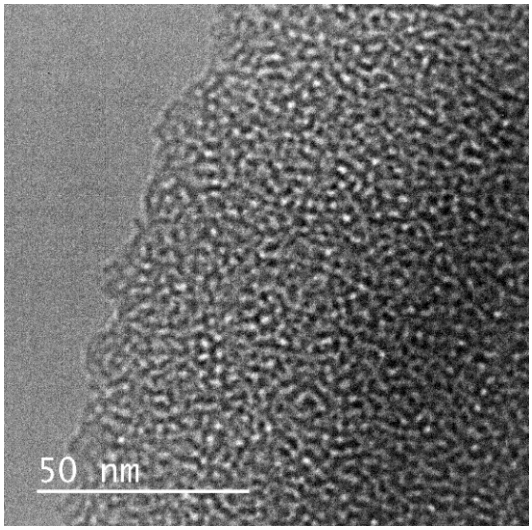

Figure 38 - TEM images of both in focus (left) and under focus (right) DoTAB templated films demonstrating difference in resolution. Reproduced from Ref. 97 with permission from the PCCP Owner Societies (http://dx.doi.org/10.1039/C4CP05730A).

3.9.3 Decyltrimethylammonium Bromide (DeTAB)

Decyltrimethylammonium bromide (DeTAB) was the shortest surfactant investigated to determine the effect of reducing the tail length of the surfactant on Stöber-derived silica films. No peaks appeared in the in-plane GISAXS patterns until a three-fold (0.18 g) increase in the molar equivalence (compared with CTAB) was used (see Fig. 39), which produced a broad feature at roughly 2.34 °. The strongest peak was observed at 2.40 °, when using a four-fold increase in the amount of DeTAB (0.24 g). This is reminiscent of using DoTAB, which required higher concentrations of surfactant to generate features in the XRD pattern. The d-spacing is the shortest so far and decreased the interpore distance in relation CTAB by 1 nm. This agrees with the trend seen in TEM image of the film (0.24 g) and indicates the formation of smaller channels within the film. It should be noted it is hard to determine the exact difference based on pore diameter (see Fig. 40).

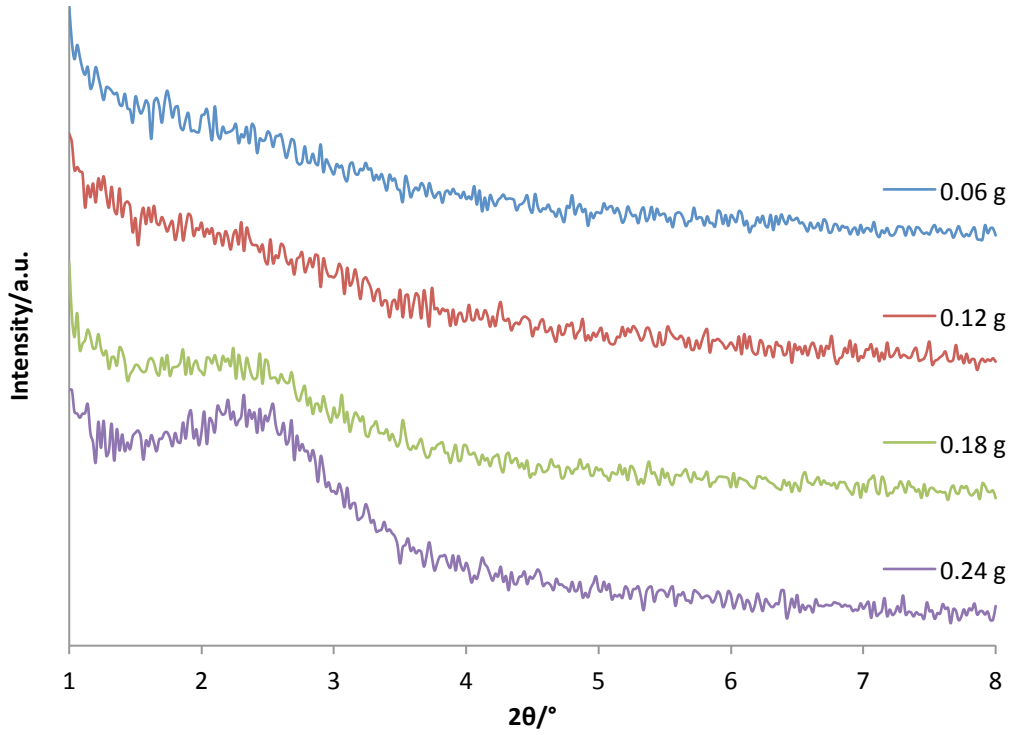

Figure 39 - In-plane GISAXS pattern of Stöber-derived mesoporous silica film using various amount of DeTAB

Table 19 - Summary of the data obtained from the in-plane GISAXS pattern of Stöber synthesized with different amount of DeTAB

DeTAB (g)	Peak posn. (2θ/˚)	d_{10} (nm)	a_o (nm)
0.06	/	/	/
0.12	/	/	/
0.18	2.34	3.77	4.35
0.24	2.38	3.71	4.28

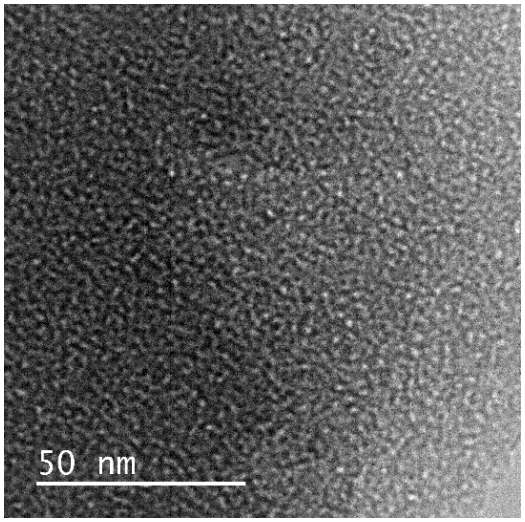

Figure 40 - In-focus image of DeTAB Stöber-derived film scraped into lacey carbon grid. Reproduced from Ref. 97 with permission from the PCCP Owner Societies (http://dx.doi.org/10.1039/C4CP05730A).

3.9.4 Cetylpyridinium bromide (CPyB)

The effect of a different class of cationic surfactant was investigated on the synthesis of Stöber-derived silica films by replacing the trimethylammonium head of CTAB with cetylpyridinium bromide (CPyB). Both ammonia and Et_3N were used as catalysts in order to investigate any difference in the resulting pore structure of the films.

3.9.4.1 Ammonia

Using the same conditions as those used in previous synthesis route (see section 3.2.1), CTAB was replaced by varying concentrations of CPyB using ammonia as the catalyst (3.5 μL, 35 wt%), with the films grown on glass slides. Initially, using the same molar equivalents as CTAB, CPyB (0.09 g, 0.22 mmol) show analogous results in terms of pore structure, based on its in-plane GISAXS pattern (see Fig. 41). A shift in peak position is witnessed when the same molar eq. of CTAB and CPyB are used, moving from 1.92 ° to 1.82 ° respectively. This implies that the decrease in steric bulk of the polar head on CPyB has lead to an increase in the interpore distance, possibly through more tightly packed surfactant. As a result, this reduces the curvature of the micelle and increasing its diameter. No meaningful change in the scattering was

observed with increasing amounts of CPyB double in solution. TEM imaging of a CPyB film (0.09 g) reveals a pore structure akin to that seen in the CTAB samples, showing the formation of pores across the surface of the film (see Fig. 42).

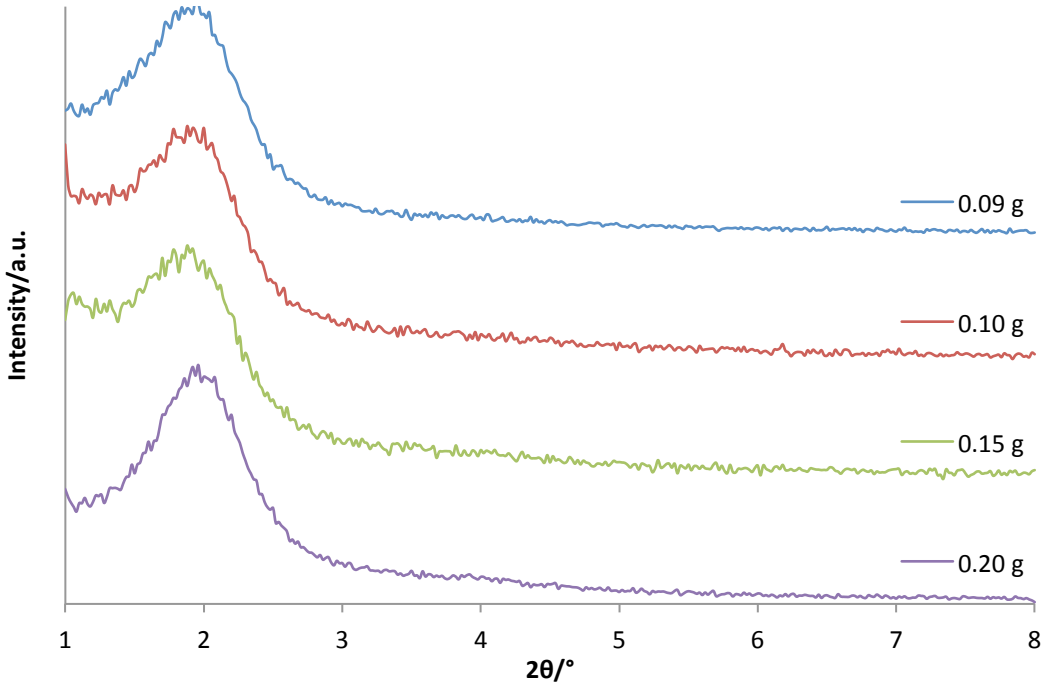

Figure 41 - GISAXS pattern of Stöber-derived mesoporous silica film with various amounts of CPyB using ammonia solution catalyst

Table 20 - Summary of the data obtained from the in-plane GISAXS patterns from CPyB Stöber films

CPyB (g)	Peak posn. (2θ/˚)	d_{10} (nm)	a_o (nm)
0.09	1.82	4.80	5.54
0.10	1.86	4.75	5.48
0.15	1.84	4.80	5.54
0.20	1.86	4.75	5.48

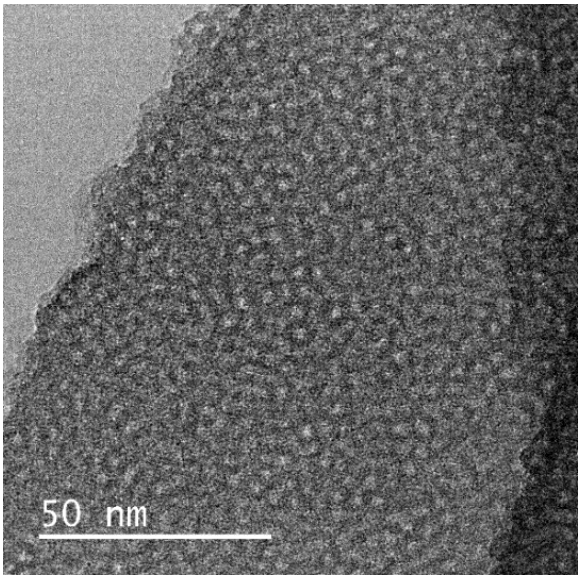

Figure 42 – Under-focus TEM image of Stöber film fabricated with CPyB surfactant. Reproduced from Ref. 97 with permission from the PCCP Owner Societies (http://dx.doi.org/10.1039/C4CP05730A).

TMB was added to investigate its effect on the pyridinium of CPyB. Using 0.09 g of surfactant in the synthesis of the Stöber films, molar eq. of TMB was also added (using same molar eq. as seen in section 3.6.1). The addition of 3.1 μL of TMB to solution produced a feature in the in-plane GISAXS pattern at 1.84 ˚ (see Fig. 43). When compared a film without TMB, a small shift in peak position of less than 0.02 ˚ to 1.82 ˚. Further amounts of TMB produce a larger degree of movement in the peak position to around 1.73 ˚ for the addition of both 15.5 μL and 31 μL with decreasing intensity as with CTAB.

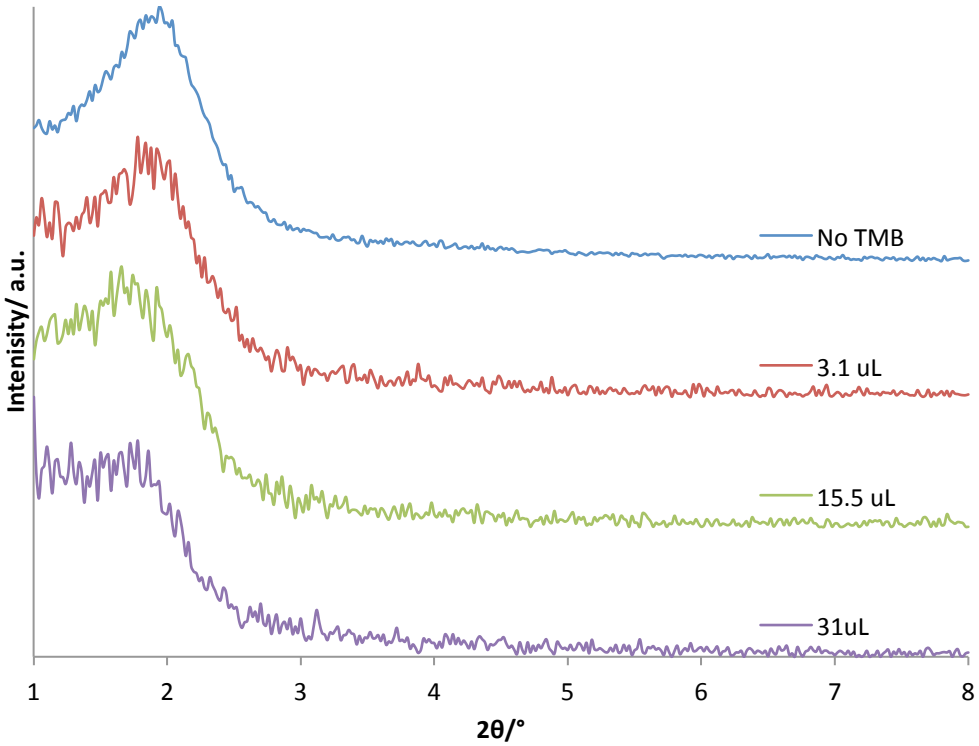

Figure 43 - In-plane GISAXS pattern of Stöber-derived silica film with the addition of various concentrations of TMB added to solution (NH_3).

Table 21 - Summary of the data obtained from the in-plane GISAXS pattern resulting from the addition of TMB to NH_3 Stöber films using CPyB surfactant

TMB (µL)	Peak posn. (2θ°)	d_{100} (nm)	a_o (nm)
3.1	1.82	4.85	5.60
15.5	1.74	5.07	5.85
31	1.72	5.13	5.92
No TMB	1.84	4.80	5.54

Replacing CTAB with CPyB in the presence of NH_3 has successfully produced pore structures based on the evidence in both the in-plane GISAXS pattern and the TEM images. The decrease in steric bulk of the surfactant's ionic head produced a shift in the lattice spacing, indicating an increase in the interpore distance due to an expansion in the pores. The addition of TMB required larger amounts (0.5 molar eq.) of the swelling agent in order enlarge the pores

significantly. This may be the result of the steric bulk of the pyridinium group providing voids, which TMB could fit in. Therefore higher concentrations of swelling agent were needed inflate micelles, but at the cost of pore ordering.

3.9.4.2 Triethylamine

Ammonia was replaced with Et_3N (3.5 μL) and the films were produced on glass-slides. The data obtained from in-plane GISAXS patterns of the resulting films were again analogous to the results obtained from both the CTAB and CPyB with NH_3 films (see Fig. 44). A feature in the in-plane scattering pattern was witnessed at 2.04 °, which was higher than those obtained using with the NH_3 solution. As the concentration of CPyB increased in solution, this result a shift in peak position, from 2.04 ° (0.09 g) to 1.94 ° (0.10 g) and 1.92° (0.15, 0.20 g). Higher concentrations of surfactant in solution have led to a small increase in the interpore distance, which stabilises at 0.15 g.

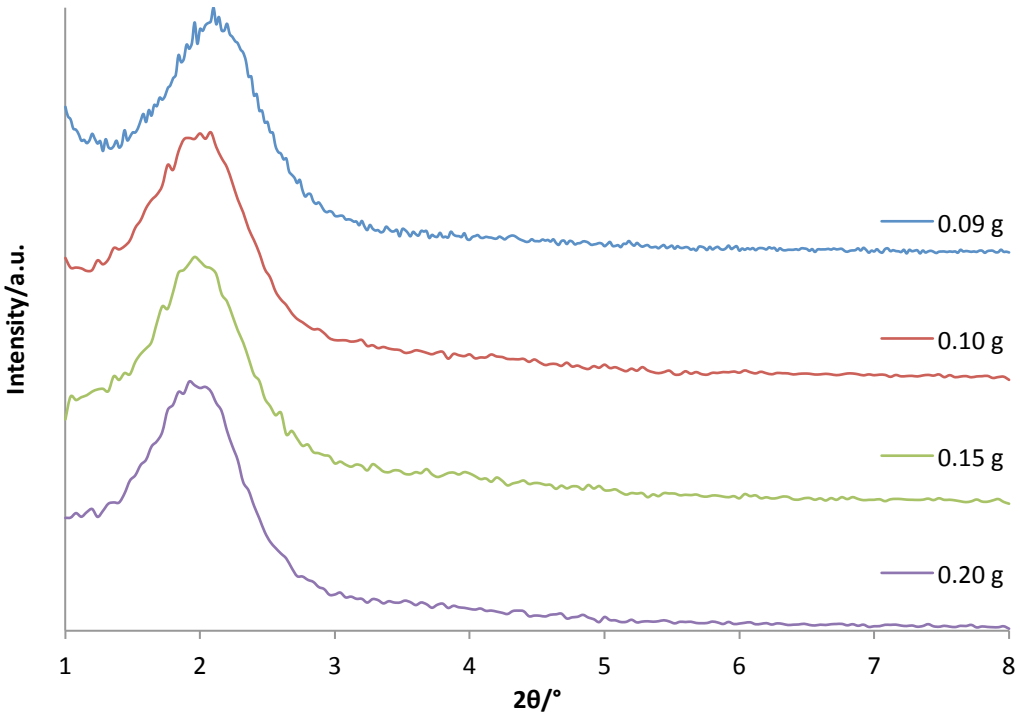

Figure 44 - GISAXS pattern of Stöber-derived mesoporous silica film with various amounts of CPyB using Et_3N catalyst

Table 22 - Summary of the in-plane GISAXS data obtained from CPyB Stöber films made using Et_3N

CPyB (g)	Peak posn. (2θ/°)	d_{10} (nm)	a_0 (nm)
0.09	2.04	4.33	5.00
0.10	1.94	4.55	5.25
0.15	1.92	4.60	5.31
0.20	1.92	4.60	5.31

3.9.4.3 Summary

Based on the data obtained from the CPyB Stöber films made using NH_3 and Et_3N, the in-plane GISAXS patterns indicate the formation of vertically aligned worm-like pore structure present. When compared against films made using CTAB, a shift in the peak position signifying an increase in the interpore distance could be related to an expansion in the pores. This was due to the increased steric bulk of the pyridinium groups, which is larger than the trimethylammonium had on CTAB. TEM images of the surface of the film confirm this behaviour, though it hard to confirm the exact expansion of the pores due to the pyridinium groups on the CPyB. Addition of TMB to the film grown in the presence of NH_3 showed a further expansion in the interpore distance, but only with larger amounts of swelling agent in solutions. Et_3N showed no indication of varying from results obtained when using NH_3.

3.9.5 Comparison of the surfactants used in the synthesis of Stöber-derived silica films

The direct comparison of the best in-plane GISAXS patterns from each of the surfactant films was compiled in Figure 45. A clear trend is visible based on the reduction in length of the surfactants (i.e. CTAB > MyTAB > DoTAB > DeTAB), which leads to a reduction in the d-spacing detected in the diffraction patterns (see Table 23). This clarifies that decreasing the tail length of the surfactant, results in a reduction in the interpore distance within Stöber films due to the formation of smaller pores. As well as varying the tail length,

increasing the steric bulk of the cationic heads of the surfactant, which suggested an enlargement of the resulting pores.

Other trends present are the broadening of the XRD peaks as the surfactant tail length decreases. Also larger concentrations of shorter surfactant in solution were required in order to produce a feature in the XRD pattern. A possible explanation for this effect is that the smaller the diameter of the micelle, the higher the concentration of surfactant needed in order to cover the same surface of the substrate to form pore structures. Both DoTAB and DeTAB, required larger amounts of surfactant in solution to observed peaks. The longer tails provide a higher contrast between the hydrophilic and hydrophobic domains, which is seen to improve the formation of pores as shown with the longer surfactant (CTAB, CPyB and MyTAB).

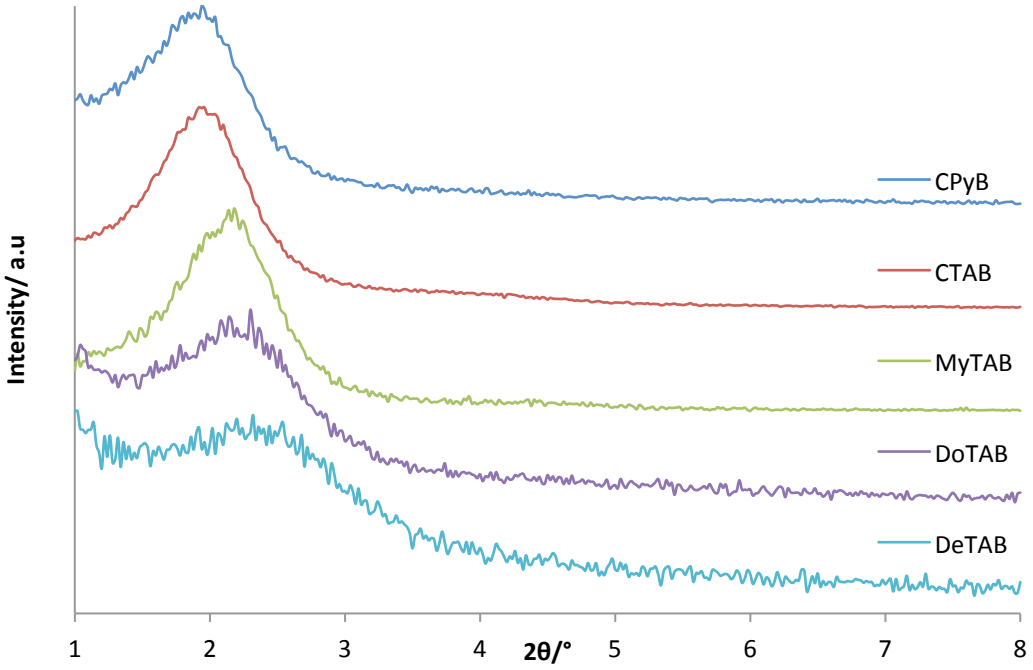

Figure 45 - Comparison detailing the change in peak position resulting from variations both the tail lengths alkyltrimethylammonium and an increase in steric bulk by cetylpyridinium bromide. Reproduced from Ref. 97 with permission from the PCCP Owner Societies (http://dx.doi.org/10.1039/C4CP05730A).

Table 23 - Summary of the peak positions, d spacing and interpore distance from Stöber-derived films fabricated with a range of different surfactant

Surfactant	Peak posn. ($2\theta/^{\circ}$)	d_{10} (nm)	a_0 (nm)
CPyB	1.82	4.85	5.60
CTAB	1.92	4.60	5.31
MyTAB	2.12	4.16	4.80
DoTAB	2.24	3.94	4.55
DeTAB	2.38	3.71	4.28

3.10 Summary

Through the application of Stöber-derived method of fabrication, the production of mesoporous silica films with pore channels running perpendicular to its support has been demonstrated. Additionally, the diffusion of decamethylferrocene through the resulting films has indicated access to the electrode beneath it. Current response was very limited with the surfactant remaining in the pore of the film, but dramatically increased once cleared. HIM imaging shows the presence of pore opening at the surface of the films.

Stöber-derived films have been successfully deposited onto TiN. This now increases the available potential window for the electrodeposition of more electropositive elements, such as germanium and silicon. Limitations were discovered when fabricating films on TiN, which were revealed when exposed to high temperatures (> 375 ˚C) resulting the surface of the material beginning to oxidise. As a result, a resistive layer develops at the film/support interface, which is unfavourable for electrodeposition. This was further investigated using AC impedance, where plain pieces of TiN were calcined between 350 ˚C to 450 ˚C. Soxhlet washing the each film in acidic ethanol removed the surfactant from the pores and prevent the formation of an oxide layer.

Sodium salts were added to investigate the effects on the growth and pore ordering of the Stöber-derived films. The addition of sodium bicarbonate had the largest effect, resulting in the growth of films that were almost x3 the thickness of conventional films. Under standard reagents and conditions the films were ~140 nm thickness. Whereas, the addition sodium bicarbonate the films grew to have a thickness of 400 nm. Other salts, such as sodium carbonate and sodium sulphate resulted in a large reduction in the pore ordering, due to the disruption of the cooperation self-assembly between surfactant and silica oligomers.

The pore sizes of the films were increased with the addition of swelling agents functionalised benzene molecules with different alky terminal groups. Both swelling agents TMB and TIPB have a direct effect on increasing the lattice spacing of the films. However, as higher concentrations were used, it led to the reduction in the pore ordering of the films. With TIPB, cracking also occurred across the film. Yet replacing NH_3 with Et_3N reversed the stability of the TMB and TIPB.

Choice of surfactant was also investigated, in order to reduce the size of the pores of films. Features in the in-plane GISAXS patterns indicate a clear reduction in d-spacing based on the tail length of the surfactant. This related to a contraction of the interpore distance as the diameter of the micelle collecting at the substrates contracted. TEM imaging of scraped samples confirmed this trend, as visible pores are comparatively smaller though its hard to clarify by how much. Also, as the tail length was reduced, the concentration of surfactant required to form pores increased. This was noticeable in the in-plane GISAXS patterns of DoTAB and DeTAB, which needed a three/four fold increase relative to CTAB and MyTAB. A different polar head, pyridinium, was explored in the form of CPyB. This bulkier group increased the pore size of the resulting films. This was both seen in TEM imaging of the films and in-plane GISAXS patterns.

Chapter 4 – Electrochemically-assisted self-assembly (EASA)

4.1 Introduction

Electrochemically-assisted self-assembled (EASA) mesoporous silica films have been shown to contain highly ordered pores, which are orientated perpendicular to their support. The technique was devised by Walcarius and co-workers and involves electrodepositing a porous silica film directly on a conductive substrate.[52] The orientation of the pores is a result of the attraction between positively charged surfactants (CTAB) and induced negative charge of the electrode, which causes the surfactant to organise on the surface of the support. The current also results in the electrodecomposition of nitrate ions in solution causing the release of hydroxide ions in solution. Consequently, a TEOS-derived sol condenses due to the increase in pH at the electrode interface. This is kept in check, as the solution is made acidic to prevent the precipitation of silica.

These films are of particular interest as nanoporous templates for the SCFED project as they produce highly ordered pores with a convenient orientation. As the films can be grown directly onto the electrodes, minimal post processing would be needed to then deposit into the pores. Previously, the technique had been shown to work best on negatively charged conductive surfaces, such as ITO. Positively charged conductive surfaces, (e.g. gold) result in poor adhesion between film and support. This is particularly unfavourable for SCFED, as the films must remain well adhered to the electrode's surface if they are to survive the harsh condition of a supercritical solvent.

In the previous chapter the preparation of Stöber-derived films has been transferred from ITO to TiN. This provides the films with a conductive substrate that is far more stable at lower potentials than ITO. As a result, during SCFED, lower potentials can be reached which are required to deposit more electrically positive elements, such as germanium and silicon. This chapter examines EASA growth of porous silica films on TiN, which was shown to be an effective substrate of the Stöber films.

4.2 Experimental Detail

4.2.1 Synthesis of electrochemically-assisted mesoporous silica films

Taken from Goux and co-workers.[78] Aqueous sodium nitrate (0.1 M, 20 mL) and ethanol (20 mL, Fisher) made to pH 3 using aq HCl solution (0.2 M). TEOS (905 μL, Sigma Aldrich, 98 %) was added and the solution allowed to stir at room temperature for 90 mins. CTAB (0.47 g, 1.29 x 10^{-3} mol, Sigma Aldrich, >99 % bioextra) was added to solution and left to stir for a further 30 mins.

Deposition of the film was carried out based on a custom-built PTFE cell, which used a silver rod pseudo reference electrode and stainless steel counter electrode. Electrochemical experiments were controlled using a Biologic SP150 potentiostat. The working electrode consisted of either titanium nitride coated silicon wafer (200 nm TiN deposited onto resistive Si wafers by medium frequency plasma-assisted magnetron sputtering (Leybold Optics HELIOS Pro XL) at room temperature) or indium-tin oxide (ITO, Sigma Aldrich, surface resistivity 8–12 Ω/sq) coated glass. A potential of -2.0 V for 5 s was applied to the TiN electrode and -1.3 V for 20 s for the ITO. The resulting films were washed with deionized water immediately after deposition and dried at 130 ˚C overnight.

4.2.2 Grazing incidence small angle X-ray scattering

Grazing incidence small angle X-ray scattering (GISAXS) experiments were performed using a Rigaku Smartlab thin film diffractometer with a 9 kW Cu-Kα source, with parallel line beam optics, in-plane arm and a DTex250 1D detector. The incident beam was a 0.1 *x* 5 mm line fixed at 0.251 incidence angle, and data was collected between 1–10 ˚ 2θ using in-plane and out-of-plane modes. For in-plane scans 0.5 ˚ Soller slits were used on the incident side and a 0.228 ˚ in-plane analyser on the detector side.

4.2.3 Supercritical fluid electrodeposition of Sn in EASA films on TiN

Supercritical fluid electrochemical studies was performed by Dr Peter Richardson in a stainless steel high-pressure cell, the details of which have been described in previous publications.[11,14] The dry powdered reagents and electrolyte complexes, $[N^nBu_4][SnCl_3]$ and $[N^nBu_4]Cl$, were transferred into the cell inside a nitrogen-purged glove box (Belle Technology). All electrolytes were prepared with 2×10^{-3} mol dm^{-3} of the $[N^nBu_4]_x[MCl_y]$ as the redox species and 50×10^{-3} mol dm^{-3} of the $[N^nBu_4]Cl$ as the supporting electrolyte. Once sealed, the cell was removed from the glove box, connected to a high-pressure rig and heated to the desired temperature using a band heater under PID (proportional-integral-derivative) control. The sc-CH_2F_2 was then introduced using a specialized carbon dioxide pump (PU-1580-CO_2, JASCO) until the desired pressure was achieved. To ensure that the solution was homogeneous, the system was stirred during pumping using a magnetic stirrer. Stirring was stopped at least 5 minutes prior to electrochemical measurements in order to allow any insoluble components in the solution to settle. All experiments were carried out at 17.2 MPa and 358 K. The electrochemical experiments were performed using a three-electrode system. A platinum mesh was used as the counter electrode, and a 0.5 mm diameter platinum disk was used as a pseudo-reference electrode. After cleaning with acidified methanol, the mesoporous silica electrodes were dried overnight at 100 ˚C under vacuum. Cyclic voltammetry measurements were recorded at potential sweep rates of 50 mV s^{-1}. Electrodeposition experiments were performed potentiostatically by holding the electrode at a potential where no reaction occurred for 2 s and then switching to a constant deposition potential. After depressurisation, the electrode samples were cleaned in dichloromethane.

4.2.4 Effect of moderator addition on an EASA silica sol

Acetyl acetone (Acac, Sigma Aldrich, 99 %) or diethylamine (DEA, Sigma Aldrich, 98%) was added to a standard EASA silica sol in 1:1 molar ratio against TEOS. Aqueous $NaNO_3$ (0.1 M, 20 mL) and EtOH (20 mL) was acidified to pH 3 using HCl_{aq} (0.2 M). TEOS (905 μL, 98%, Sigma Aldrich)) was added after the moderator (Acac or DEA, 4.66 mmol) and the solution was stirred for 90 min at

room temperature, resulting in a green solution. CTAB (0.47 g, >99 % Bioextra, Sigma Aldrich) was added and the solution was left to stir for 30 mins. Deposition occurred on TiN with potential of -2.0 V for 5 s using a Biologic SP150 potentiostat with a pseudo Ag rod reference electrode and stainless steel cone counter electrode. The films were then dried in an oven overnight at 130 ˚C. The samples were then washed in acidified EtOH (0.1 M) for 5 minutes before being returned to the oven to dry overnight.

4.2.5 Varying the ratio of Ti:Si present in EASA sol

Aqueous $NaNO_3$ (0.1 M, 20 mL) was added drop-wise to a solution EtOH (20 mL), Acac (415 μL) and $Ti(O^iPr)_4$ (95 %, Sigma Aldrich). The solution was adjusted to pH 3 using HCl_{aq} (0.2 M). Various ratios of TEOS were added to make the total amount of inorganic precursor to 4.66 mmol, followed by stirring for 90 minutes at room temperature. CTAB (0.47 g) was added and the solution was stirred for a further 30 minutes. Si:Ti ratios used were; 0.8:0.2, 0.5:0.5, 0.2:0.8 and 0:1. Electrodeposition was performed using a Biologic SP150 potentiostat with a pseudo Ag rod reference electrode and stainless steel cone counter electrode. Resulting films were washed with water and dried in oven at 130 ˚C overnight.

4.3 Results and Discussion

4.3.1 Electrochemically-assisted self-assembled (EASA) mesoporous silica films on ITO

Initial attempts at reproducing Walcarius' work were performed on ITO. This involved fabricating a custom cell design based on Walcarius and coworkers, in which a cone shape was cut out of a Teflon cylinder (see Fig. 46). This left an 8 mm diameter hole at the bottom, where the working electrode would sit. A rubber o-ring was placed between top of the substrate, which was connected to the potentiostat by a copper wire (0.125 mm diameter). The precursor solution would be placed in the Teflon cell; with its weight on the o-ring ensuring no solution leaked. A cone of stainless steel was used as a counter electrode and a silver rod as a pseudo reference.

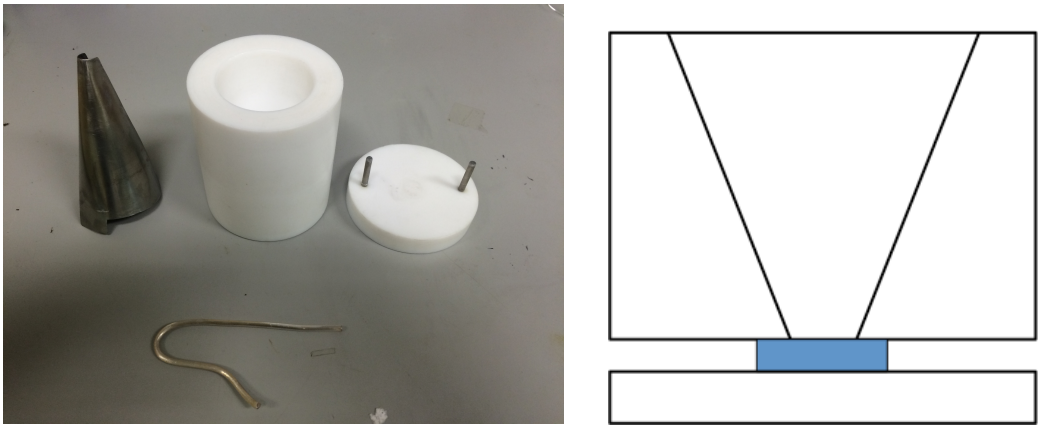

Figure 46 – (Left) Image of the custom cell used in the fabrication of EASA mesoporous silica films. (Right) Schematic showing a cross-section of cell showing a film (highlighted in blue) positioned ready for deposition.

The films deposition was altered slightly from Walcarius' technique by simply suspending the working electrode from a crocodile clip into solution. The films could be swapped more easily, therefore minimising the loss of solution. The films were then washed in distilled water immediately on removal from solution to ensure no remaining reagents were left on the surface and placed in an oven at 130 ˚C to age. The films produced on ITO appeared transparent in nature with a green/blue tint when performed on ITO-coated glass. The

geometry of the substrate during deposition produced loosely attached silica aggregates on the films surface, which could be brushed off leaving a smooth film beneath. This did make comparing differences in current harder as the exposed area of the electrode in solution varied between each sample. However, the formation of fewer surface aggregates was advantageous and using the potential to control film growth meant variations in the area of the electrode would have less of an effect between samples.

The optimum conditions were determined for the electrochemically-assisted self-assembled (EASA) mesoporous silica films by varying the potential applied to the ITO. The pore structure and ordering were determined using in-plane GISAXS pattern. Figure 47 shows the GISAXS pattern of films generated a potential of -1.2 V and -1.3 V for 20 s against a silver rod pseudo reference and a stainless steel cone as a counter electrode. The diffraction patterns show the presence of vertically aligned pores ordered hexagonally (*P*6*mm*). This was in line with results obtained by Walcarius and co-workers.[78] In order to achieve the most intense scattering of the X-rays, the incidence angle of the beam (omega) was positioned at 0.25 ˚. This was found to produce the most intense peak in the scattering patterns. Any variation away from this angle led to a reduction in the intensity of the peaks. This was particularly important in order to maximise the intensity of the second (11) and third (20) degree ordered peaks, positioned at 4.02 ˚ and 4.68 ˚ respectively. Films deposited below -1.3 V, resulted in a significant darkening in the colour of the ITO denoting its electrochemical reduction due to the applied current. Out-of-plane GISAXS resulted in no features in the diffraction pattern confirming the orientation of the pores.

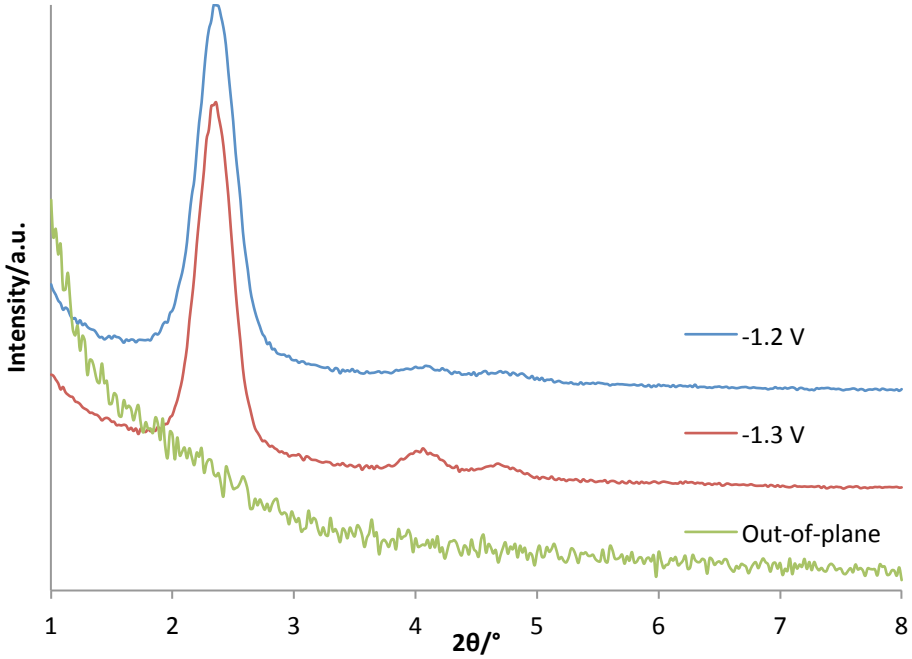

Figure 47 - GISAXS pattern of EASA mesoporous silica film generated at -1.2 V or -1.3. V for 20 s. When potentials below -1.3 V were applied to the ITO, the surface of the electrode turn brown/black due to reduction. No features witnessed in the out-of-plane diffraction pattern.

Table 24 - Summary of the data obtained from in-plane GISAXS pattern of EASA films fabricated on ITO-coated glass grown using different applied potentials

Applied potential (V)	Peak Position (°)			d_{100} (nm)	a_o (nm)
	10	11	20		
-1.2	2.34	4.02	4.68	3.77	4.36
-1.3	2.34	4.02	4.68	3.77	4.36

4.3.2 Electrochemically-assisted self-assembly mesoporous silica films on Au

Electrodes are commonly made of gold due to their high conductivity, low resistance and chemical stability. As a result the potential window of gold is far superior to that of ITO and an ideal replacement. Reagent concentrations were

carried over from those used in the fabrication of EASA films on both ITO (see section 4.2.1). The films were fabricated on a 200 nm layer of gold vacuum deposited onto glass slides. The films generated at different potentials and deposition times with the Au-coated glass suspended vertically in the sol. The application of -2.0 V led to a significant decline in the pore ordering when applied to gold based on in-plane GISAXS patterns (see Fig. 48). This was not observed with ITO, as it was not stable at such low potentials (<1.3 V). Deposition at -1.6 V (10 s) produced an improvement, where the features previously seen in other EASA films denoting hexagonal ordering became far more pronounced at 2.18 ˚, 3.92 ˚ and 4.61 ˚. The conditions that produced the best in-plane scattering patterns were the same as those which were used to produce films on ITO (-1.3, 20 s). The features were both clear and well resolved, and were positioned at 2.33 ˚, 4.05 ˚, 4.65 ˚ and 6.20 ˚. These were related to the hexagonal lattice planes, 10, 11, 20 and 21 respectively.

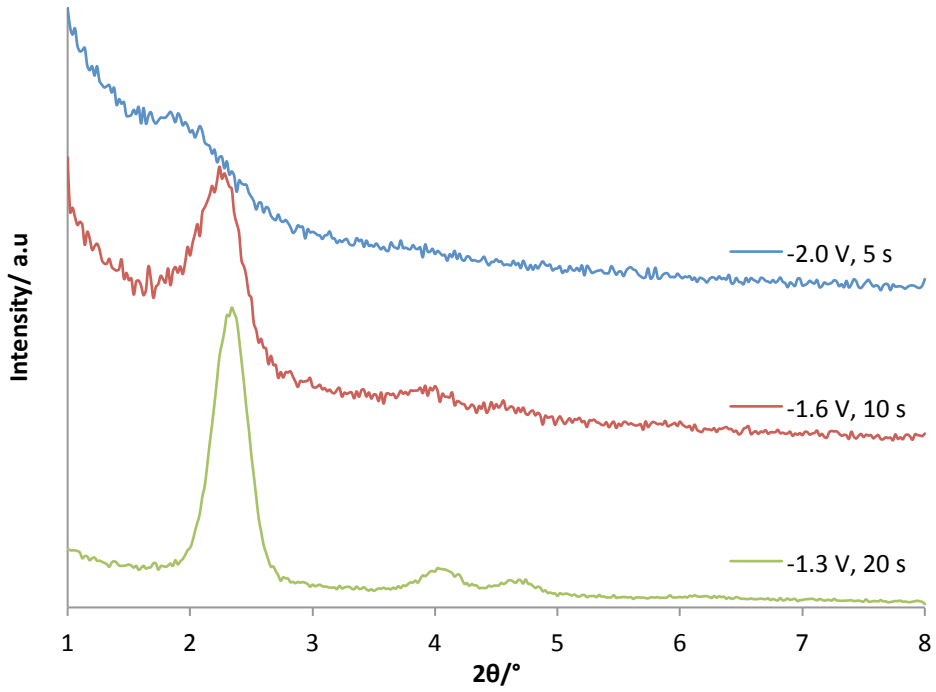

Figure 48 - In-plane GISAXS pattern of EASA films grown on Au using various potentials.

Table 25 - Summary of the data obtained from the in-plane GISAXS pattern of EASA grown on gold-coated glass slides grown using different applied potentials

Applied potential (V)	Peak posn. (2θ/°)				d_{10} (nm)	a_o (nm)
	10	11	20	21		
-2.0	~1.86	/	/	/	4.75	5.48
-1.6	2.18	3.92	4.61	/	4.05	4.68
-1.3	2.33	4.05	4.65	6.20	3.78	4.36

Images of the surface of the -1.3 V film were taken using a FEGSEM in order to gauge surface coverage and uniformity. The films appeared to be patchy and poorly adhered to the electrodes surface (see Fig. 49 left), despite the strong GISAXS pattern. Cross-sectional images of the film show the thickness to be uniform with a depth around 120 nm. Flakes and particle matter can be seen in the background of Figure 49 (right).

The reasoning behind this poor adhesion can be based on the lack of bonding occurring between the gold and silica film. This can be associated with gold's high resilience to chemical attack, which ironically makes it such a good electrode. The silica film bonds with the metal/ oxygen framework at the surface ITO electrode. Application of the negative potential allows Au to influence both the attraction and arrangement of the micelle, followed by the release of the hydroxyl ions. The subsequent drying of the film and its shrinkage led to cracks developing as it is loosely held on the electrode's surface. Though the films produce excellent in-plane GISAXS features, showing perpendicularly aligned hexagonal pore structure; the FEGSEM images show poor adhesion between film and support. As a result, the survival of the film within a supercritical solvent is highly unlikely, consequently unsuitable for SCFED.

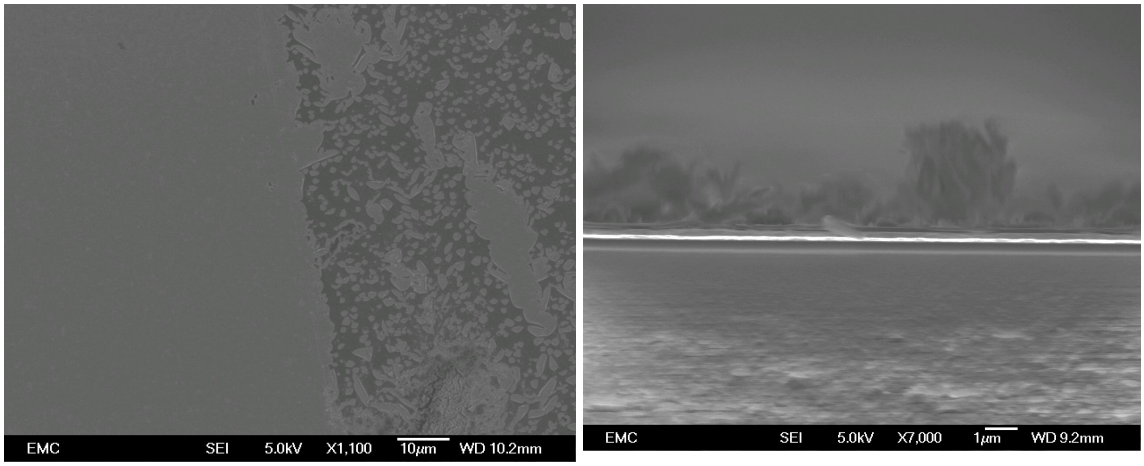

Figure 49 - FEGSEM image of the surface of EASA mesoporous silica film on gold-coated glass. Right image shows the film to be patchy and poorly adhered to the gold surface. Left image is of the film's cross-section showing the build up of aggregates on surface.

4.3.3 Electrochemically-assisted self-assembly mesoporous silica films on TiN

The advantage of TiN is that it has a thin negatively charged oxide surface layer, which can provide strong adhesion between the silica film and substrate. This would allow films grown on TiN to survive the harsh conditions of a supercritical solvent as shown with the Stöber film in Chapter 3. The potentials between -2.4 V to -1.4 V were applied to TiN-coated (approximately 10 *x* 10 mm) silicon for a period of 5 s by submerging them in solution (see section 4.2.1).

In-plane GISAXS pattern was used to determine the most favourable conditions based on the diffraction patterns of the resulting films (see Fig. 50). The TiN showed no signs of degradation at these lower potentials all the way up to -2.4 V. The films darken the bronze colour of the substrate where it had been in contact with the solution. It was found that potentials between -1.8 V and −2.0 V for 5 s produced films with highest degree of ordering. Three peaks were witnessed in the scattering pattern at 2.40 °, 4.14 ° and 4.80 ° for films generated at -2.0 V. Then 2.44 °, 4.18 ° and 4.86 ° were observed when -1.8 V was applied. These peaks were related to the hexagonal ordering of the pores,

denoting the 10, 11 and 20 lattice planes. At potentials outside the optimum potential window, GISAXS patterns of the films began to decay, with no peak observed when -1.4 V was applied. Whilst -2.4 V generated bubbles were at the electrodes surface.

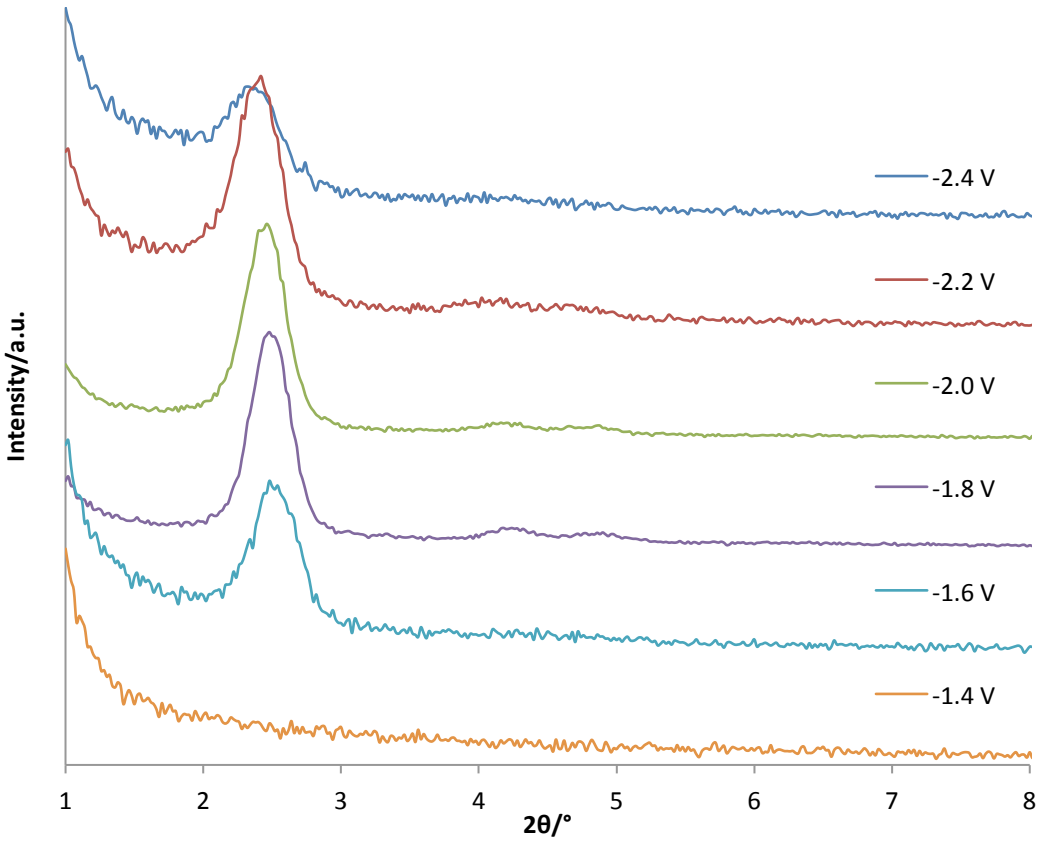

Figure 50 -GISAXS pattern of EASA film generated using various potentials applied for 5 s

Table 26 - Summary of the data obtained from the in-plane GISAXS patterns of EASA films generated using potentials for the same deposition time (5 s)

Applied potentials (V)	Peak posn. (2θ/°)			d_{10} (nm)	a_0 (nm)
	10	11	20		
-2.4	2.32	/	/	3.80	4.39
-2.2	2.34	4.08	4.68	3.77	4.35
-2.0	2.40	4.14	4.80	3.68	4.25
-1.8	2.44	4.18	4.86	3.62	4.18
-1.6	2.46	/	/	3.59	4.15
-1.4	/	/	/	/	/

TEM imaging was performed on the films generated on TiN (-2.0 V, 5 s) to confirm the size and ordering of the pores within the films (see Fig. 51 Inset). The effective diameter of the pores was measured at 1.6 nm. These images clearly match the results obtained from the in-plane GISAXS patterns, which clearly displays the formation of hexagonally ordered pore structure across the surface of the film. The cross-sectional image of the EASA (Fig. 51) shows the pore orientation to be perpendicular with the electrode on TiN-coated silicon. The pores visibly run from top to bottom, which is very important for the SCFED project. This is because it ensures that the deposited material will have access to the electrode surface beneath the film during deposition, therefore encouraging bottom-upward of potential nanowires within the pore channels.

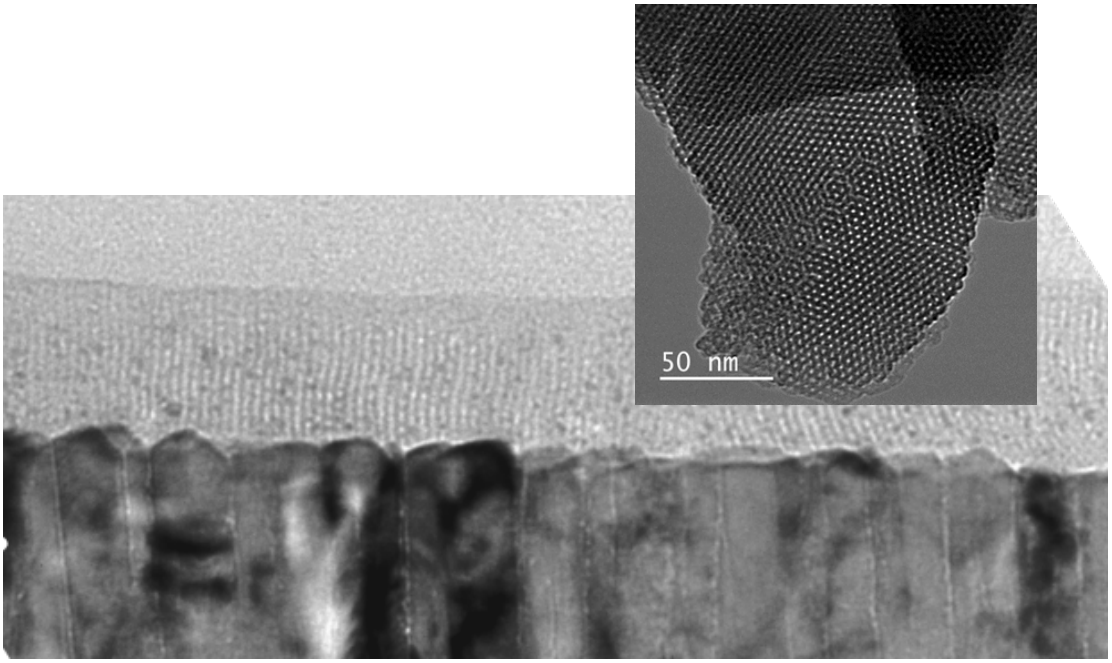

Figure 51 - TEM images of EASA mesoporous silica films. Inset – Top down TEM image of the scraped EASA film in lacey carbon grid. Bottom: TEM cross-sectional image of an EASA film on TiN showing the growth of perpendicular pores running through the sample. Reproduced from Ref. 97 with permission from the PCCP Owner Societies (http://dx.doi.org/10.1039/C4CP05730A).

He-ion microscopy (HIM) produces images with higher surface sensitivity than electron microscopy. This is important to ensure that the pores are open at the surface of film, as techniques like TEM can be misleading about the number of accessible pores. It has previously been shown to work well imaging the surface of insulating materials, such as silica.[88] Images of the surface of an EASA film were taken, which reveal the pores to be open (see Fig. 52). It should be noted that very few silica aggregates were found on the surface of the film, by-products of TEOS reacting in solution during deposition. Walcarius *et al* witnessed a large amount of silica particles collecting on the surface of their films, which were positioned horizontally at the bottom of the solution during deposition.[78] As these electrodes are submerged vertically in solution, it is believed that silica aggregates simply fall off the surface of the film. Any left were readily washed off with the distilled from the surface of the film.

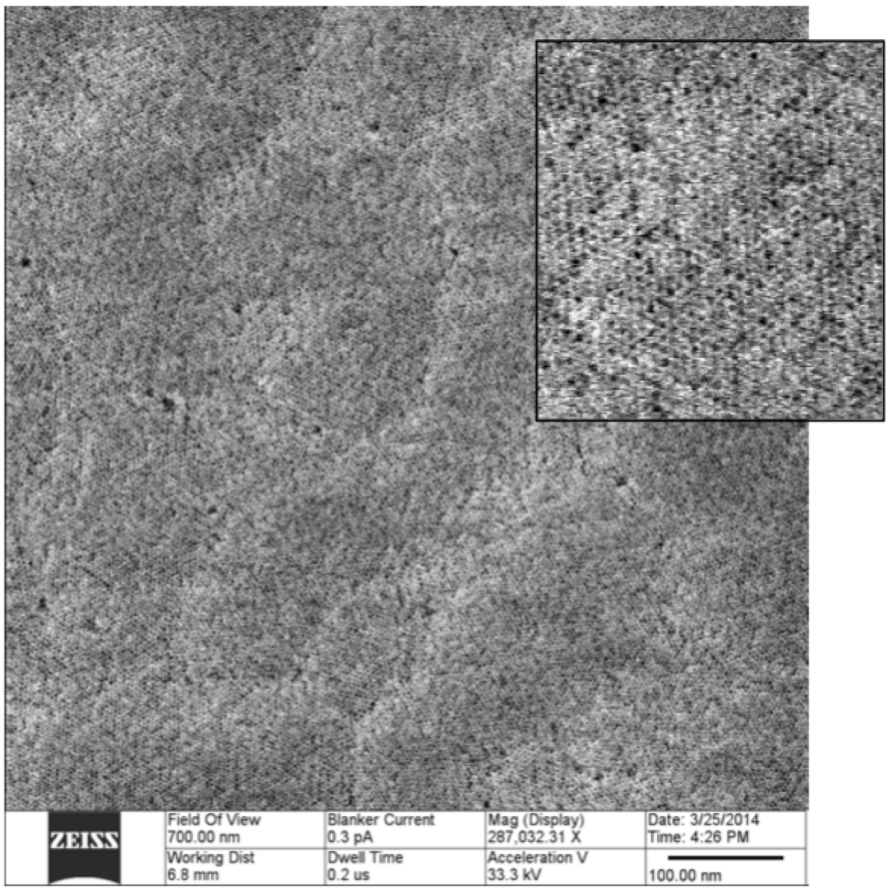

Figure 52 - He-ion Microscope image of surface of EASA mesoporous silica film. Reproduced from Ref. 97 with permission from the PCCP Owner Societies (http://dx.doi.org/10.1039/C4CP05730A).

4.3.3.1 Effect of the concentration of sodium nitrate on electrochemically-assisted self-assembled mesoporous silica

The effect of varying concentration of sodium nitrate on the EASA films was investigated. This was achieved by examining changes in the in-plane GISAXS patterns of the films, which related to variations in the pore ordering of the films. The sodium nitrate is an important component in the synthesis of the EASA films, as it is reduced at the electrode surface when a negative current is applied. This results in the release of hydroxyl ions, which increases the pH of the solution at the electrode's surface.

The concentration of $NaNO_3$ present in solution was initially halved (0.025 M), which led to no significant effect on the pore structure as witnessed in the

GISAXS pattern (see Fig. 53). The peak positions of the resulting features match closely with the results obtained using the standard solution, apart from being slightly noisier. The different potentials applied show little discrepancy between films. This effect may only influence the number of films produced from one batch of solution. In a sense, no extra hydroxyl ions would be released into solution, as $NaNO_3$ would be consumed quicker due to its lower concentration.

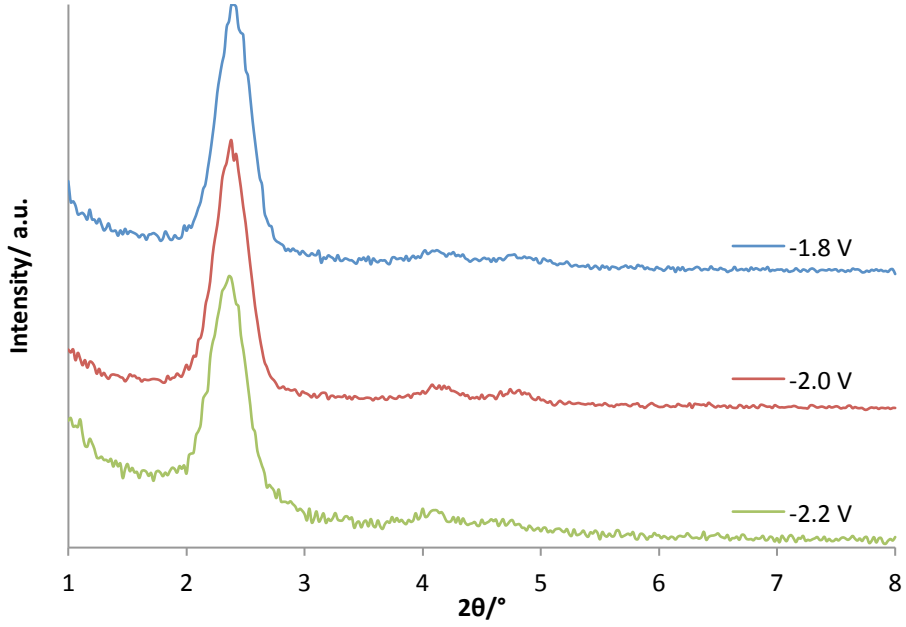

Figure 53 – GISAXS patterns of EASA mesoporous silica films produced with 0.025 M $NaNO_3$

Table 27 - Summary of the data obtained form the in-plane GISAXS patterns of EASA with 0.025 M $NaNO_3$

Applied potentials (V)	Peak posn. (2θ/˚)			d_{10} (nm)	a_0 (nm)
	10	11	20		
-1.8	2.38	4.22	4.80	3.71	4.28
-2.0	2.38	4.14	4.74	3.71	4.28
-2.2	2.36	4.06	4.70	3.74	4.32

However, doubling the concentration of $NaNO_3$ (0.2 M) led to a significant disruption to the pore structure. This is clearly visible in the in-plane GISAXS pattern (see Fig. 54), where the pore structure collapses as the potential is lowered from -2.0 V to -2.2 V. The film produced at -1.8 V appears to be the best, though its peaks are broader and the 11 and 20 features are less pronounced when compared with a standard EASA film. This may be the result of a higher concentration of hydroxide ions released in solutions, as there would be an elevated amount of NO_3^- ions at the electrode surfaces. With more hydroxide ions released, a larger change in pH would be expected resulting in a larger precipitation of silica. Consequently, this could disrupt the self-assembly occurring between the silica oligomers and CTAB micelle. This was seen when EASA was attempted in glass vessel. No visible features in the diffraction patterns due to CTA^+ coordinating with the $Si\text{-}O^-$ at the surface of the vessel. Therefore, an influx of silica is highly likely to disrupt the formation of pores. Nevertheless, the concentration of $NaNO_3$ in solution has directly influenced the formation of pore channels within there films.

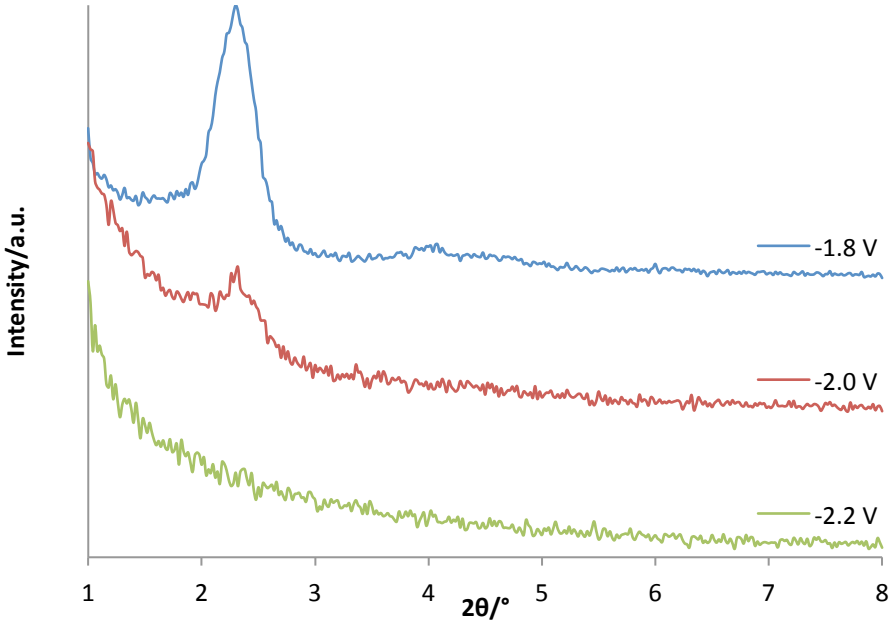

Figure 54 - GISAXS pattern of EASA mesoporous silica film with 0.2 M $NaNO_3$

Table 28 - Summary of the data obtained from the in-plane GISAXS patterns of EASA with 0.2 M $NaNO_3$

Applied potentials (V)	Peak posn. (2θ/°)			d_{10} (nm)	a_0 (nm)
	10	11	20		
-1.8	2.30	4.04	4.60	3.84	4.43
-2.0	2.34	/	/	3.77	4.35
-2.2	/	/	/	/	/

4.3.3.2 Effect of the concentration of potassium chloride on electrochemically-assisted self-assembled mesoporous silica on TiN

To test the role of $NaNO_3$ and ensure that the formation of the EASA films was the result of its reduction, potassium chloride was used in its place. Hence, if the pore structures were still found in the diffraction patterns of the resulting films, this would be a strong indication that the EASA process was not the result of electrochemical decomposition of NO_3^- ions. Instead it would be the result of electrolyte dissociation of water at the electrodes surface:[53]

$$2H_2O + 2e^- \rightarrow H_2 + 2OH^- \qquad E^\circ = -0.828\ V$$

However, if that is the case and a disruption to the pore structure is observed, then it would confirm that it is the reduction of NO_3^- to release OH^- ions:

$$NO_3^- + H_2O + 2e^- \rightarrow NO_2^- + 2OH^- \qquad E^\circ = +0.01\ V$$

The same molar concentration of $KCl_{(aq)}$ was added to solution as $NaNO_3$ (0.05 M). The films were produced on TiN with potentials between -1.8 V and -2.2 V for the same deposition time (5 s). The effect of replacing the electrolyte led to a significant deterioration in the pore structure, as established in the in-plane

GISAXS pattern (see Fig. 55). The only potential that produced ordered mesopores was -1.8 V (5 s), producing a single visible peaks at 2.18 ° and 4.28 °. Decreasing the potential to -2.0 V lead to a further reduction in the peak intensity. When -2.2 V was applied; no feature was witnessed in the scattering pattern.

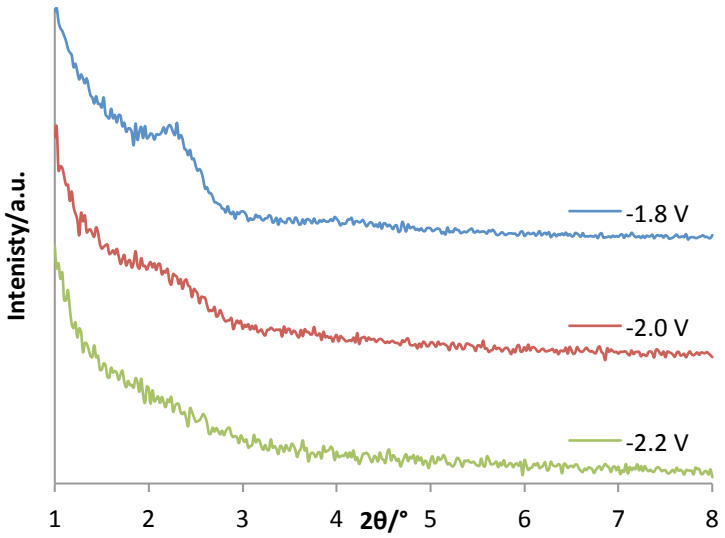

Figure 55 - GISAXS pattern of EASA mesoporous silica film with $KCl_{(aq)}$ (0.05 M) used to replace $NaNO_3$.

Table 29 - Summary of the data obtained from the in-plane GISAXS pattern of EASA with the addition KCl used to replace $NaNO_3$

Applied potentials (V)	Peak posn. (2θ/°)	d_{10} (nm)	a_0 (nm)
-1.8	2.18	4.05	4.68
-2.0	2.14	4.13	4.77
-2.2	/	/	/

Based on the replacement of $NaNO_3$ with KCl in solution has resulted in a significant disruption to the pore structure of the EASA films. It can be concluded that electrolytic reductive of $NaNO_3$ is pivotal in the formation of

hexagonally ordered mesopores. The controlled release of hydroxyl ions at the electrode surface induces sufficient conditions to allow for both the self-assembly of surfactants and formation of silica oligomers at the electrode's surface. As a result, the replacement of nitrate with an alternate counter anion leads to a significant reduction in the pore ordering.

Leading on from this work, ideally investigating films produced at higher potentials (i.e. > -1.8 V) should be explored to ensure, as there are small indications of an improvement in the pore structure. KBr is a better conductor of current than $NaNO_3$, so the potentials applied may result in similar results obtained as seen in section 4.3.1.1. Nevertheless, decreasing the current would result in a smaller amount of OH^- released.

4.4 The effect of swelling agents on EASA silica films

As discussed, control over the pore diameter of the films is important as it directly affects the size of the nanowire grown within the template. Producing templates of different size would provide SCFED with the ability to alter the shape and size of the nanowires. In Chapter 3, the addition of a swelling agent (trialkybenzene molecules) to Stöber films resulted in an increase in the lattice spacing, as shown in the resulting diffraction patterns of the films. This was related to an expansion in the interpore distance due to an enlargement of the pores. As the organic molecules are absorbed, their steric bulk causes the micelle to swell. Therefore a higher degree of control can be achieved over the size of nanowires in the pores.

4.4.1 1,3,5-trimethylbenzene (TMB)

Various molar equivalent amounts of TMB (0.1, 0.5 and 1) relative to CTAB (1.3 mmol) were added to EASA solutions after the addition of CTAB, once it had been dissolved. Variations in the pore spacing were measured based on the in-plane GISAXS patterns, based on shifts in the d-spacing (see Fig. 56). The

addition of a 0.1 molar eq. of TMB results in a clear shift in the 10 peak position from 2.40 ˚ to 2.28 ˚ (see Table 30). This was also mirrored in the other features present in the scattering pattern. Increasing the concentration of TMB to 0.5 molar eq led to further shift 2.26 ˚. Again this is reflected in both the 11 and 20 peaks. With the addition of 1 molar eq of TMB resulted in a significant degradation in the in-plane scattering pattern, denoting the collapse of the pore structure. Comparing the d_{10} spacing of 0.5 molar eq., there is an increase in the distance lattice planes from 3.71 to 3.91 nm relating to an extension in the interpore distance of 0.27 nm.

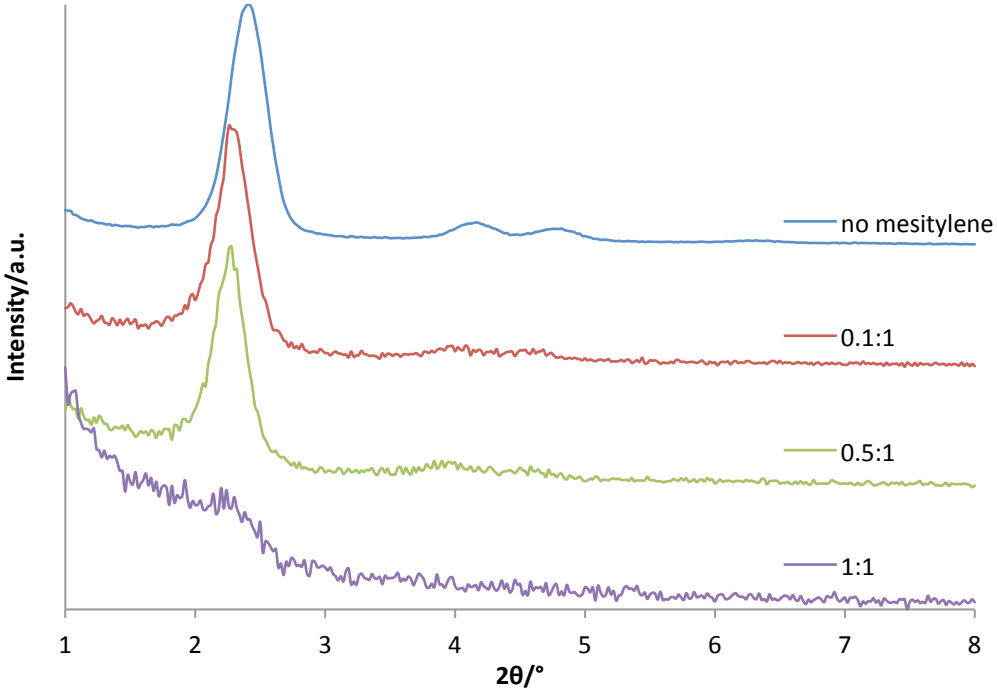

Figure 56 - GISAXS pattern of EASA mesoporous silica films with the addition of molar eq. of TMB/CTAB (0.1, 0.5 and 1 molar eq). Reproduced from Ref. 97 with permission from the PCCP Owner Societies (http://dx.doi.org/10.1039/C4CP05730A).

Table 30 - Summary of the data obtained from the in-plane GISAXS pattern of EASA films with the addition TMB

Molar eq. (TMB/CTAB)	TMB (μL)	Peak posn. (2θ/°)			d_{100} (nm)	a_o (nm)
		10	11	20		
No TMB	0	2.38	4.08	4.72	3.71	4.28
0.1	17.9	2.28	3.98	4.56	3.87	4.47
0.5	89.7	2.26	3.92	4.54	3.91	4.51
1	179.4	2.24	/	/	3.94	4.55

As shown in Figure 57, the pore width of a standard EASA film is 1.6 nm. The addition of TMB has led to an increase in pore width by 0.8 nm to ~2.4 nm with the addition of 0.5 molar eq. As a result, the uptake of swelling agent has led to a significant increase in the diameter of the pores. Based on the image of the surface of the EASA film, the pore size distribution (PSD) appears very narrow. The diffraction pattern of the film shows a shift relating to an increase in the interpore distance of 0.27 nm. Therefore it can be concluded that the expansion of the pore is reducing the thickness of the walls by as much as ~ 0.37 nm. The addition of 1 molar equivalence may leave the walls too weak to support the pore structure.

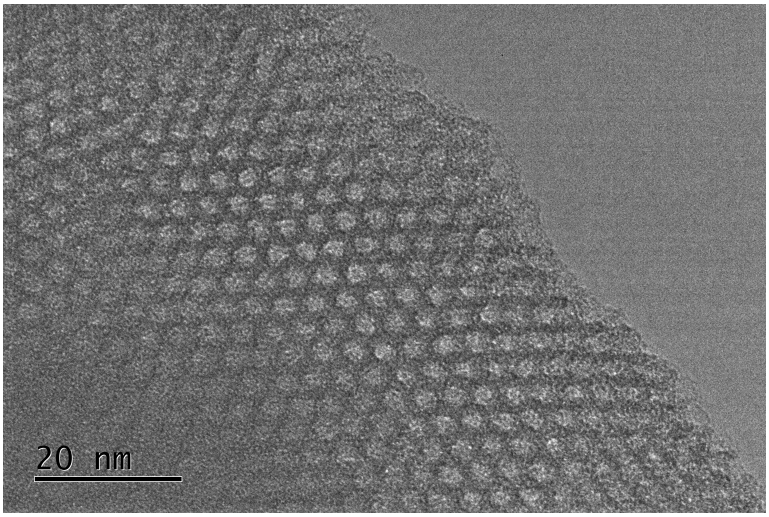

Figure 57 - TEM image of a scraped EASA film with the addition of TMB (0.5 molar eq) has led to an increase in the pore diameter from 1.6 nm to 2.4 nm. Reproduced from Ref. 97 with permission from the PCCP Owner Societies (http://dx.doi.org/10.1039/C4CP05730A).

4.4.2 1,3,5-triisopropylbenzene (TIPB)

An alternative swelling agent used instead of TMB was 1,3,5-triisopropylbenzene (TIPB). The larger terminal groups surrounding the aromatic benzene ring give the molecule more steric bulk and decrease the influence of the benzene ring. TIPB was added to solution (based on molar equivalents relative to CTAB). The films were deposited onto TiN-coated silicon (-2.0 V, 5 s). This was previously used in Chapter 3 on Stöber-derived films, which led to an increase in the pore size. However, in that system ageing the film at 130 ˚C resulted in the film cracking.

In-plane GISAXS patterns of EASA films with TIPB additions showed an increase in the lattice parameter for all films (see Fig. 58). 0.1 molar eq. of swelling agent (TIPB/CTAB) resulted in a larger shift in peak position (from 2.38 ˚ to 2.16 ˚), when compared against a standard EASA film, than with TMB (2.38 ˚ to 2.28 ˚). Increasing the amount of TIPB to 0.5 and 1 molar eq. led to some movement in the peak to 2.08 ˚ for both films. However, both samples showed signs of significant decay to the pore ordering present in the films. Using the d_{10} lattice planes to calculate the interpore distance, an expansion of 0.44 nm was calculated for 0.1 molar eq. (see Table 31).

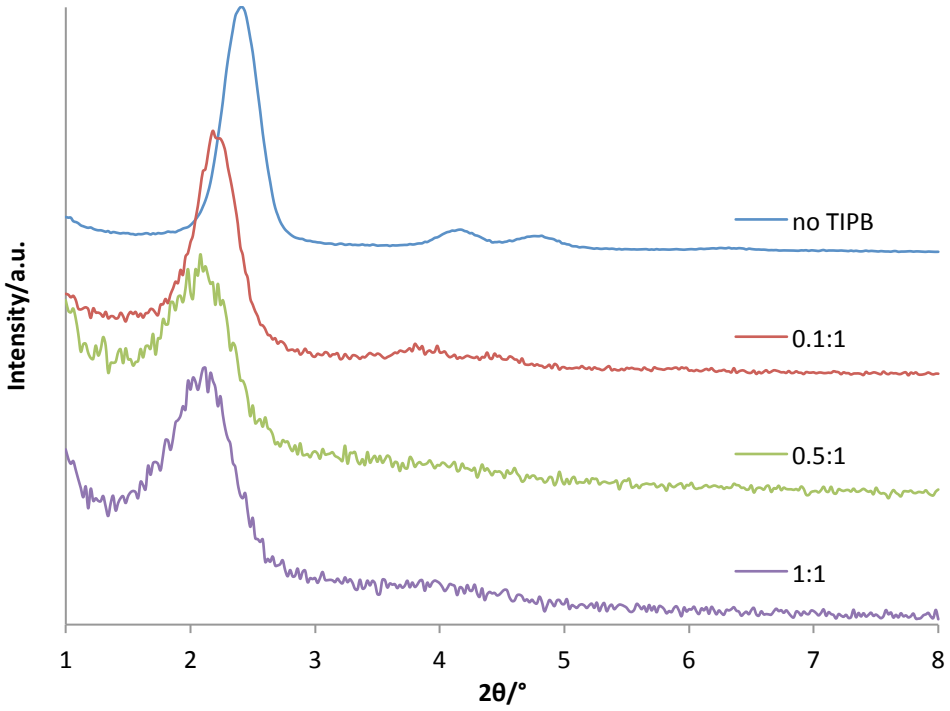

Figure 58- GISAXS pattern of EASA mesoporous silica films with the addition of molar amount of TIPB (where TIPB/CTAB).

Table 31 - Summary of the data obtained from the in-plane GISAXS pattern of EASA with the addition of swelling agent TIPB

Molar eq. (TIPB:CTAB)	TIPB (µL)	Peak posn. (2θ/˚)			d_{10} (nm)	a_0 (nm)
		10	11	20		
No TIPB	0	2.38	4.13	4.7	3.71	4.28
0.1	31	2.16	3.86	4.46	4.09	4.72
0.5	156	2.08	/	/	4.24	4.90
1	312	2.08	/	/	4.24	4.90

SEM images of the surface indicate the formation of cracks, flakes and pinholes, which develop across the surface of the TIPB EASA films (see Fig. 59 Left). This mirrors the results obtained when TIPB was added to Stöber films in Chapter 3. Whilst the TEM images of the films indict there is no visible

ordering pore, it is also hard to quantify how much they have expanded (see Fig. 59 Right). As shown with the addition of TMB, this partly sacrifices the thickness of the pore walls when comparing the TEM and XRD results. Due to the larger expansion pore size and weaker walls may exert too much strain on the film as it dries, resulting in the formation of cracks and other artefacts.

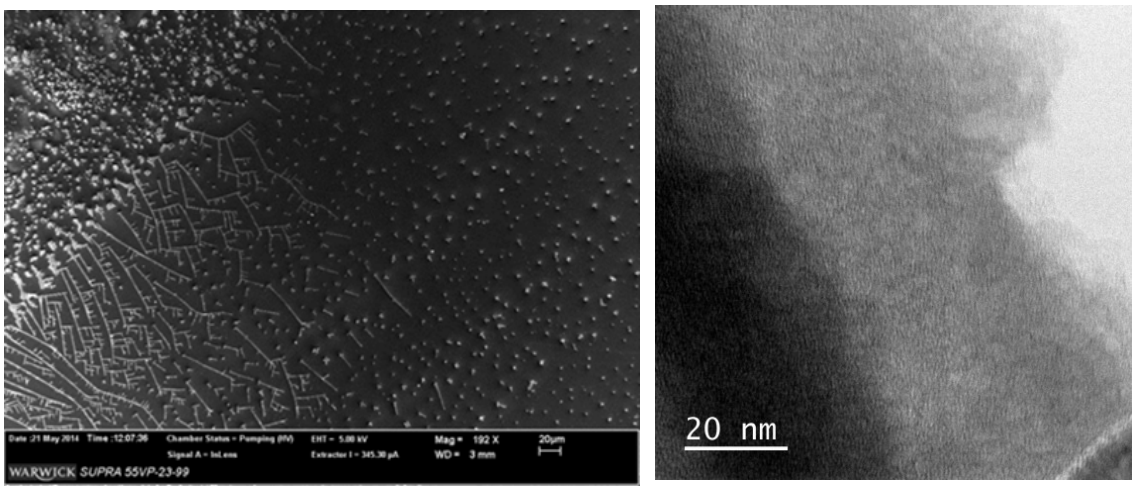

Figure 59 - (Left) SEM image of the surface of EASA film with the addition of TIPB (1 molar eq). (Right) TEM image of scraped EASA film with the addition of TIPB (1 molar eq)

4.4.3 Summary

The data obtained from the addition of a swelling agent to the EASA films directly leads to an expansion of the pores. This was confirmed for both TMB and TIPB using the diffraction patterns and TEM imaging. Due to the clarity of the images produced, the pores of samples could be measured, showing that the addition of 0.5 molar eq. of TMB increased the pore diameter by 1 nm. However, this was not seen in the expansion in the lattice planes, which only increased by 0.23 nm. Therefore the pore walls were reduced in thickness by about 0.37 nm. In the case of TIPB, a larger increase in the interpore distance was witnessed, expanding to 0.44 nm (both 0.5 and 1 molar eq.). This was twice that of TMB and cracks, flakes and potholes appeared on the surface of the film. It was also hard to verify the exact increase in pore diameter of the films through TEM. It is not hard to imagine that this additional increase in

interpore distance may have reduced the breadth of the pore walls to the point of collapse. These results also show that changes in the interpore distance do not directly relate to an increase in pore diameter.

4.5 Varying tail length of alkyltrimethylammonium bromide surfactants

As shown with the Stöber films, varying the tail length of the surfactant used directly affects the resulting pore diameter. Some control over the pore size can be achieved based on the number of carbon atoms within the surfactant tail. As previously discussed, this is of particular interest to the SCFED project, as it allows for better control of the nanowire diameter based on the pore width of the template. In the course of this investigation, the tail length of alkytrimethylammonium surfactant was reduced relative to the standard CTAB (C_{16}TAB) surfactant. The surfactants studied have included tetradecyltrimethylammonium bromide (MyTAB, C_{14}TAB), dodecyltrimethylammonium (DoTAB, C_{12}TAB) and decyltrimethylammonium bromide (DeTAB, C_{10}TAB). Walcarius *et al* demonstrated that reducing the surfactant chain length led to a smaller response from the current when analysed with a redox probe.[78] Films electrodeposited on sputtered TiN using same conditions (-2.0 V, 5 s)

Initially the same molar amounts of surfactant as in the standard EASA solution (section 4.2.1) were used to replace CTAB in solution (1.29 mmols). This resulted in peak positions shifting towards a lower d-spacing as the length of the surfactant was decreased in the in-plane GISAXS patterns (see Fig. 60). When compared against CTAB (2.38 °), a feature was witnessed at 2.52 ° for MyTAB and 2.70 ° for DoTAB. However, a reduction in the pore ordering was also observed, mimicking the results obtained from the Stöber-derived films. Increasing the concentration of the shorter surfactant in the Stöber film improved the diffraction pattern (see Section 3.9.2). However this was not observed when the molar amount of DoTAB was increased by four times. Therefore, it can be concluded that the EASA method is less sensitive to the bulk concentration of surfactant in solution, which is in contrast to Walcarius

and co-worker when using DoTAB. They witnessed an larger response in the current from the redox probe, which was concluded to be an improvement in the structure ordering of the pores enhancing it diffusion through the film.[78] Due to the potential applied to the substrate, it is capable of attracting the appropriate of surfactant from solution and it is less responsive to variations in concentrations. However, with lower concentrations of surfactant may result in a solution producing fewer films from a single batch.

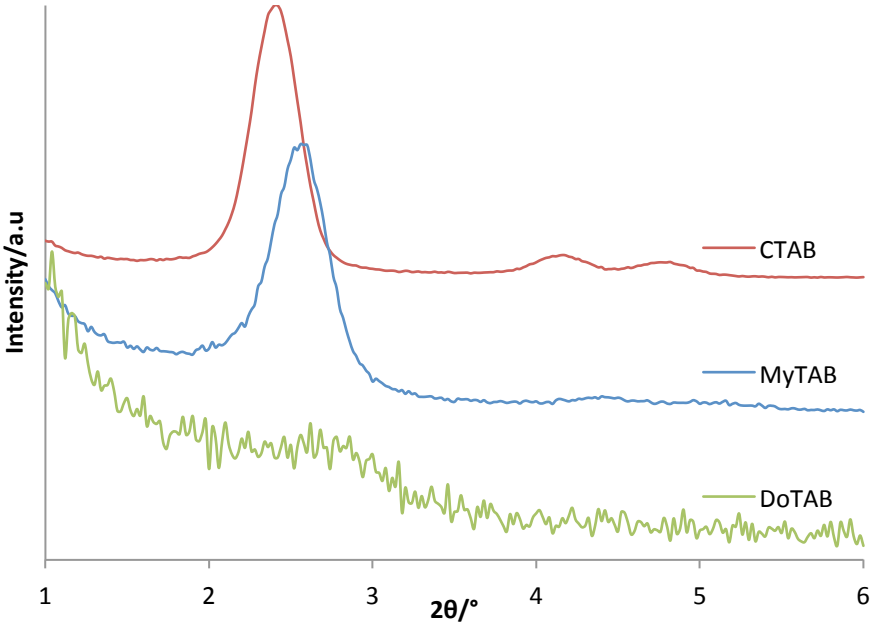

Figure 60 - GISAXS pattern of EASA films with surfactants with varying chain lengths on sputtered TiN-coated silicon

Table 32 - Summary of the data obtained from the in-plane GISAXS pattern of EASA films synthesized using different alkyltrimethylammonium surfactants with different tail lengths.

Surfactant	Peak posn. (2θ/°)			d_{10} (nm)	a_0 (nm)
	10	11	20		
CTAB	2.38	4.10	4.74	3.71	4.28
MyTAB	2.52	4.40	5.10	3.45	3.98
DoTAB	2.70	/	/	3.27	3.77

4.6 EASA films with cetylpyridinium bromide

Alterations were made to the polar head of the surfactant used during EASA in order to investigate the effects on pore structure of the resulting films. CTAB was replaced with cetylpyridinium bromide (CPyB) to determine the effect of an alternate cationic surfactant head on EASA. When this was attempted on Stöber-derived films, it resulted in a shift in the peak position denoting an increase in the lattice planes. Therefore, the same molar equivalent quantity of CPyB was used instead of CTAB in solution. The electrodeposition was done using potentials between -1.8 to -2.4 V and was applied for 5 s. This resulted in a thick waxy film covering the electrode, which when washed off with ethanol revealed a similar film that those fabricated using CTAB, though somewhat sparser.

The films produced a feature around 2.3 ˚ in the in-plane GISAXS pattern (see Fig. 61). As the potential was increased to -2.4 V, the peak intensity was noted to improve. However, at this potential bubbles were emitted from the surface of the electrode during depositions. Films generated closer to -1.8 V resulted in little to no film formation beneath the waxy layer. This was determined to be due to a build up of surfactant on the silica film beneath. When compared against CTAB films, was significantly less pore ordering in the CPyB films, though there was an expansion in the lattice planes. Therefore, the replacement of CTAB with CPyB proved to produce films with disordered pore structures. As a result the addition of TMB proved a more successful method of increasing the pore diameter of the film.

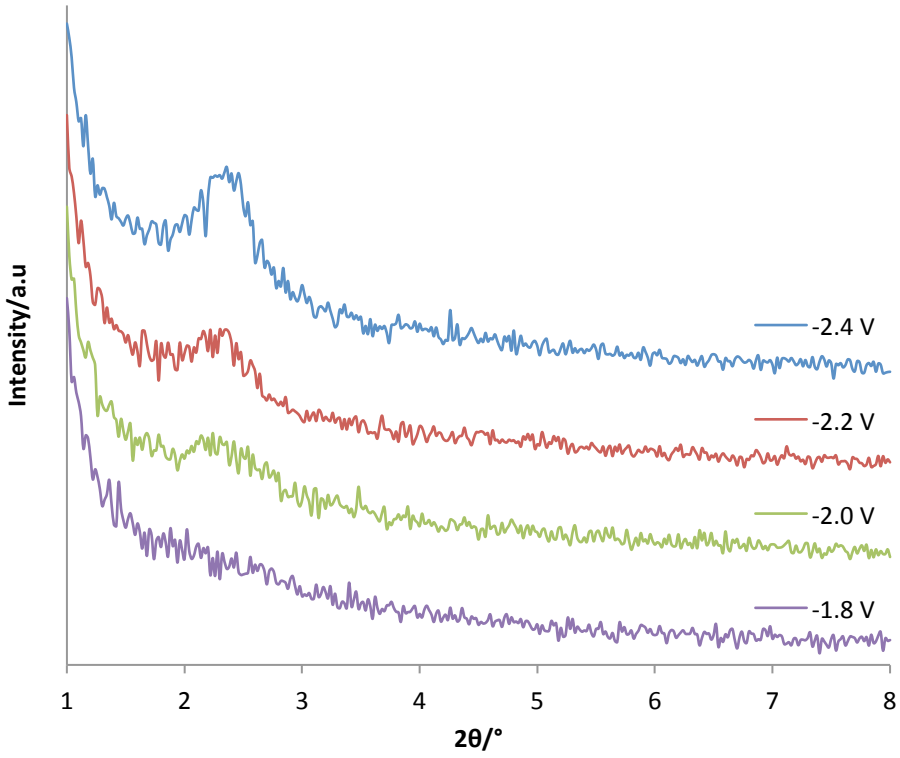

Figure 61 - GISAXS pattern of EASA film generated under various potentials using CPyB surfactant on TiN

Table 33 - Summary of the data obtained from the in-plane GISAXS pattern of EASA films synthesized using CPyB.

Applied potential (V)	Peak posn. (2θ/˚)	d_{10} (nm)	a_0 (nm)
-2.4	2.28	3.87	4.47
-2.2	2.32	3.81	4.40
-2.0	2.22	3.98	4.60
-1.8	/	/	/

4.7 EASA film on Si-Mat TiN

The supply of TiN changed during the SCFED project to Si-Mat (Silicon Materials), which was deposited on the silicon by physical vapour deposition (PVD) with a thickness of 300 nm. This alteration to the TiN meant that the potential window used to generate the EASA films changed. Therefore, the fabrication of the EASA film needed to be re-optimised in order to produce suitable templates on the new electrodes. This was achieved by varying the potentials and times they were applied to the electrode.

Films grown at -1.8 V (5 s) showed a reduction in the pore ordering based on broader peaks in the in-plane GISAXS pattern, producing features at 2.24 °, 4.03 ° and 4.67 ° (see Fig. 62). When the potential was decreased to -1.6 V (10 s), the films exhibited an improvement, generating reflections in the scattering pattern with notably less noise. The scattering pattern produced peaks at 2.34 °, 4.05 ° and 4.70 °. An additional peak was witnessed in at 6.13 ° denoting an enhancement in the pore organisation. Mimicking the same conditions used for ITO (-1.3 V, 20 s), the films generated on Si-Mat TiN proving to be the optimum conditions as they produced a scattering pattern with the least amount of noise.

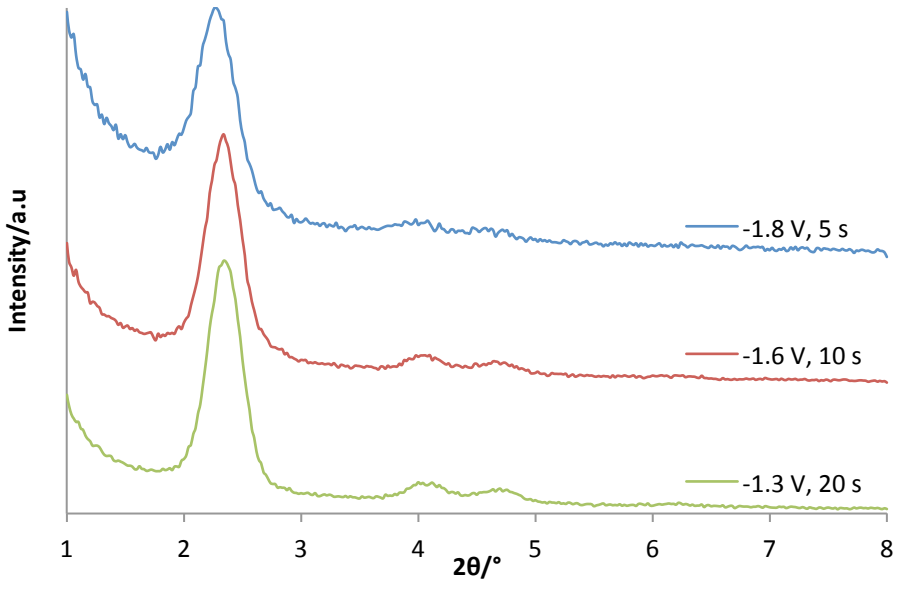

Figure 62 - GISAXS patterns of EASA silica films grown on Si-Mat TiN

Table 34 - Summary of the data obtained from the in-plane GISAXS pattern of EASA films deposited on Si-Mat TiN

Conditions	Peak posn. (2θ/°)				d_{10} (nm)	a_0 (nm)
	10	11	20	21		
-1.8 V, 5 s	2.24	4.03	4.67		3.94	4.55
-1.6 V, 10 s	2.34	4.02	4.70	6.13	3.77	4.35
-1.3 V, 20 s	2.34	4.02	4.62	6.12	3.77	4.35

The pore structure of an EASA film was determined using ellipsometric porosimetry. The adsorption/desorption isotherm, pore size distribution and thickness are resolved based on the reflective index of the film as the partial pressure of a volatile solvent was varied.[93] The adsorption/desorption isotherms differ depending on the solvent used for the ellipsometric porosimetry (see Fig. 62). The organic solvents (toluene, IPA and methanol) have good wetting properties on silica allowing good adsorption and desorption.[113]

Though the different organic solvents produce similar isotherms, a trend becomes pronounced when the polarity of the solvent molecules are taken into account. Toluene, having the highest boiling point would condense in the pores more readily they the other solvents. Therefore reducing the partial pressure necessary for the solvent to undergo capillary condensation in order to fill the pores. It produced a Type I isotherm (see Fig. 63A). IPA needed a higher partial pressure than toluene to level the curvature of the Type IV isotherm (see Fig. 63 C). As an alcohol, the hydroxyl group would be attracted to the silica pore walls, forming a monolayer before forming a meniscus. The larger attraction with the silica walls means more IPA molecules can collect in the pores of the film. Methanol was the most polar organic solvent used and its isotherm was the closest to water (see Fig. 63 D). A larger partial pressure was required to level out the curvature of the isotherm and fill the pore channels. Water required the highest partial pressure to flatten the isotherm curve, which follows the trend, as it is the most polar solvent used (see Fig. 63 B). The isotherm is indicative of non-porous material (Type III). A shift occurs

between the adsorbed and desorbed isotherms representing strong interaction between water and pore walls, as expected. The BET surface area of the film was found to be ~1100 $m^2 g^{-1}$ using toluene.

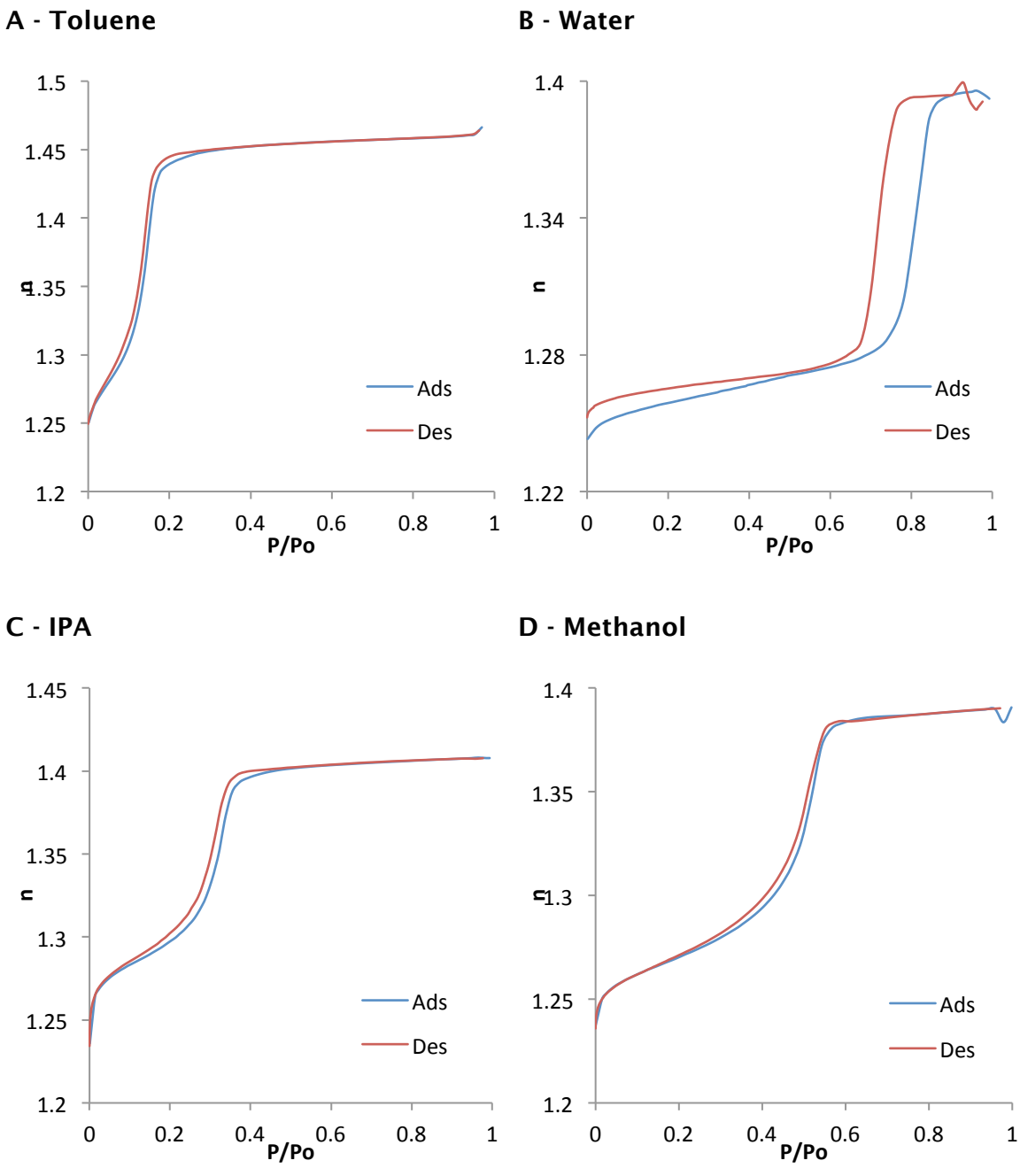

Figure 63 - Sorption isotherms of the EASA silica film on new TiN: (A) Toluene, (B) Water, (C) IPA, (D) Methanol (n = reflective index)

Table 35 - Summary of the data obtained from the ellipsometric porosimetry of standard EASA film determine using different solvents.

Solvent	Porosity (%)	Mesopore radius (nm)	Micropore radius (nm)
Toluene	38.2	$1.36_{abs}/1.37_{des}$	$0.72_{abs}/0.74_{des}$
Water	40.1	/	/
IPA	42.6	$1.37_{abs}/1.34_{des}$	$0.57_{abs}/0.60_{des}$
Methanol	42.5	/	/

Comparing each of the solvent isotherms, toluene was deemed to be the best solvent for determining the porosity of the EASA films. This was also centred on higher levels of polarisability as seen with the polar solvent occurring between adsorbate and surface, which leads to greater distortion of results prompted by porous confinement.[114] Figures 64 and 65 show size distributions calculated from the toluene isotherms. Pore size distribution using the Dubinin-Radushkevich (DR) model (see Fig. 63A) based on toluene sorption agrees closely with the 1.6 nm pore diameter established using TEM (see Fig. 51). Conversely this does not agree with the modified Kelvin equation, which measures the pore diameter to be 2.72 nm (see Fig. 65). However, it has widely been noted that this is outside the parameters of the equation, which overestimates the pressures required to wet micropores.[115] The size of the micropores enhances the importance of molecules initially adsorbed on the surface of the pore walls, as the channels can be several molecules in width.

As there is a stronger interaction occurring between the molecules held at the pore walls, the Kelvin equation fails to account for its influence, becoming more irrelevant as pore diameter decreases. The modified Kelvin equation accounts for some of this by introducing a correction based on lowering the filling pressure. This was achieved by including the thickness of molecules already adsorbed on the pore walls before the condensation of adsorbate. However, this only partly resolves this issue and does not fully account for the error. The DB model on the other hand assumes that liquid in the pore

channels is homogenously filled and has bulk-like properties.[116] Therefore, the molecules adsorbed on the pore walls become more dominant as the pore channel decreases, becoming more accurate for the micropore region (i.e. < 2 nm).

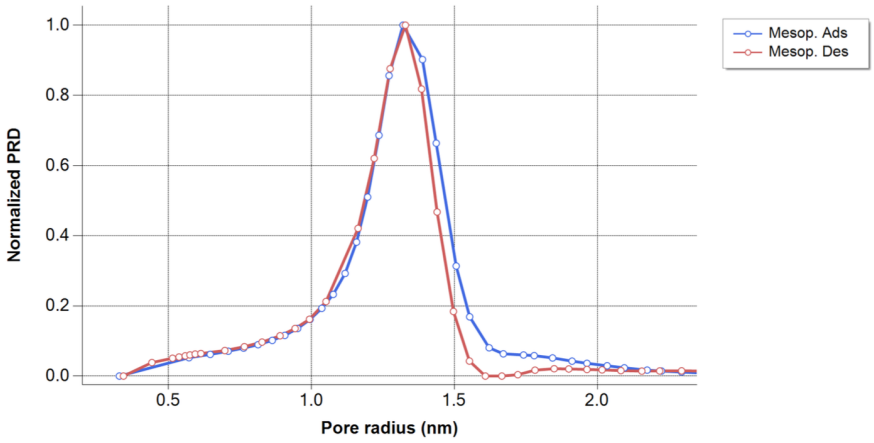

6ure 64 - Pore size distribution of EASA silica film using modified Kelvin equation (Toluene)

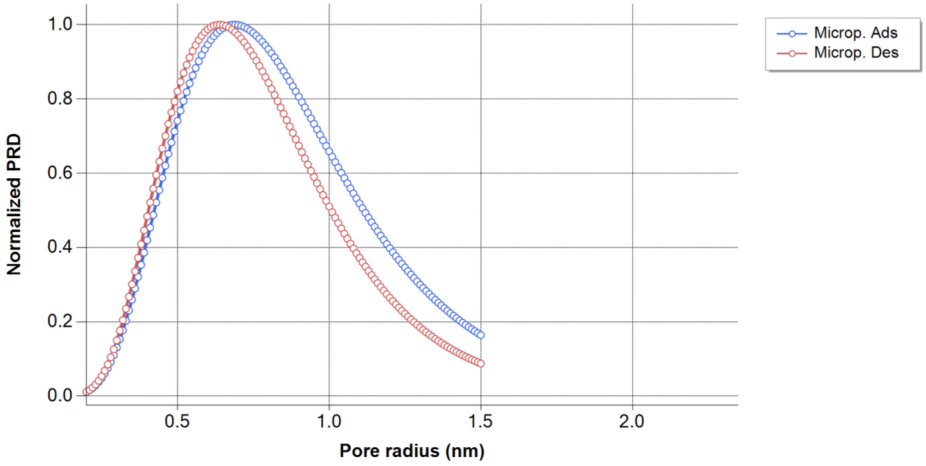

Figure 65 - Pore size distribution of EASA silica film (Toluene) using the Dubinin-Radushkevich model

4.8 Supercritical fluid electrodeposition of Sn in EASA films

As has been demonstrated in this chapter, EASA films provide nanoporous templates that meet all the criteria needed in order to grow nanowires using SCFED. The in-plane GISAXS patterns and cross sectional TEM images show that the pores are orientated perpendicular to the substrate. Imaging of the pores and EP measure the pore diameters to be 1.5-1.6 nm in standard EASA. Transferring the films onto TiN has been important in resolving these measurements, as well as increasing the potential window in order to allow for a greater range of material to be deposited into the films. Due to the better ordering of the pores, EASA was chosen over the Stöber films for SCFED. As a result, films were produced on appropriately sized piece of TiN (8 × 8 mm), so that it could fit within the supercritical cell. This was pre-contacted to an insulated wire before growth of the EASA film (see Fig 66). The quality of the films was confirmed using the in-plane GISAXS pattern, than passed onto a member of the electrochemical group of the SCFED project in order to perform the deposition. In the case of depositing Sn, it was passed on Dr. Peter Richardson.

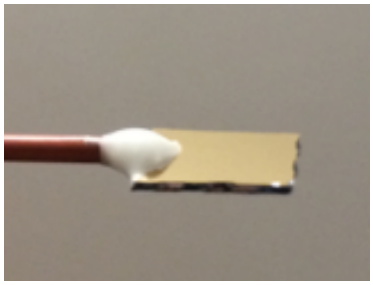

Figure 66 - Image of an EASA film grown on a TiN (8 × 8 mm) substrate of appropriate size to fit in the supercritical cell. This consisted of a steel wire contacted to TiN using Ag epoxy resin, and insulated.

Initially, cyclic voltammetry was performed on plain electrodes of both Au and TiN using conditions seen in section 4.2.3. In both cases a nucleation loop was observed occurring at ~-0.8 V, denoting the successful deposition of metal onto the surface of the electrode. This was related to the conversion of Sn^{2+} → Sn^{0} due to the application of an overpotential in order to induce nucleation and overcome small nuclei, which dissolve back into solution (see Fig. 67 left for

CV on TiN). The voltammogram also became very noisy past ~ -1.0 V, which was attributed to the convection of the supercritical solvent.

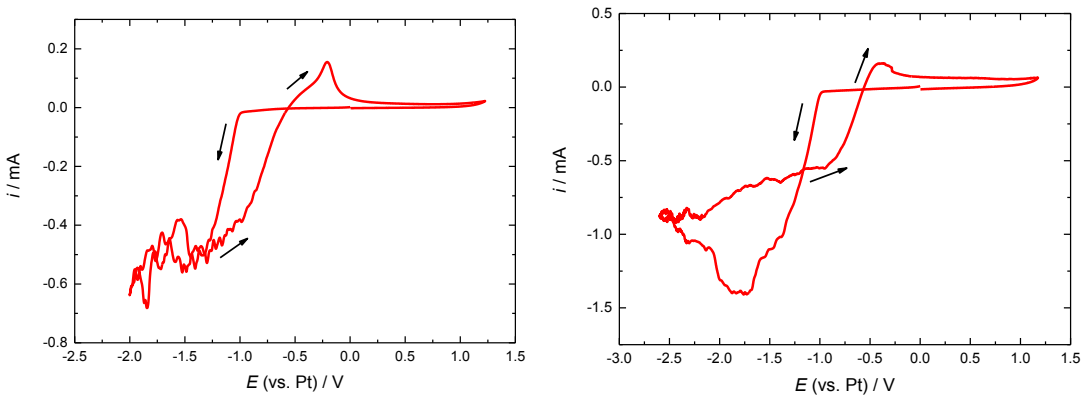

Figure 67 - Cyclic voltammetry of 2 mM [N^nBu_4][$SnCl_3$] in sc-CH_2F_2 (17.2 MPa and 358 K) measured at a TiN slide electrode and referenced to a Pt pseudo-reference electrode. 50 mM [N^nBu_4]Cl was used as the supporting electrolyte. Arrows indicate potential scan direction. (Left) Plain TiN, (Right) EASA film on TiN

When a CV was performed on an EASA film on TiN, a nucleation loop was observed and the noise of the voltammogram reduced. This was attributed to the film acting as a baffle and reducing the convection of the solvent as it entered the pore channels. It was investigated by the SCFED group by performing CVs on both macro and microelectrodes with and without baffles.[13] All indications from the electrochemistry show that Sn was being deposited into the films as the result mimicked those seen on the planar electrodes.

Two films were exposed to the deposition conditions. One film had -1.5 V at 3600 s applied and the other a control sample. Samples were sent to the electron microscopy group at Warwick University for analysis by the. EDX mapping of the cross section of a film was performed in order to determine whether Sn was present within the films (see Fig. 68). This revealed the presence of Sn within the structure of the film, though TEM imaging could not find any discrete nanowires present. HIM imaging of the surface of the films showed the formation of small deposits of Sn across the surface of the film (See Fig. 69).

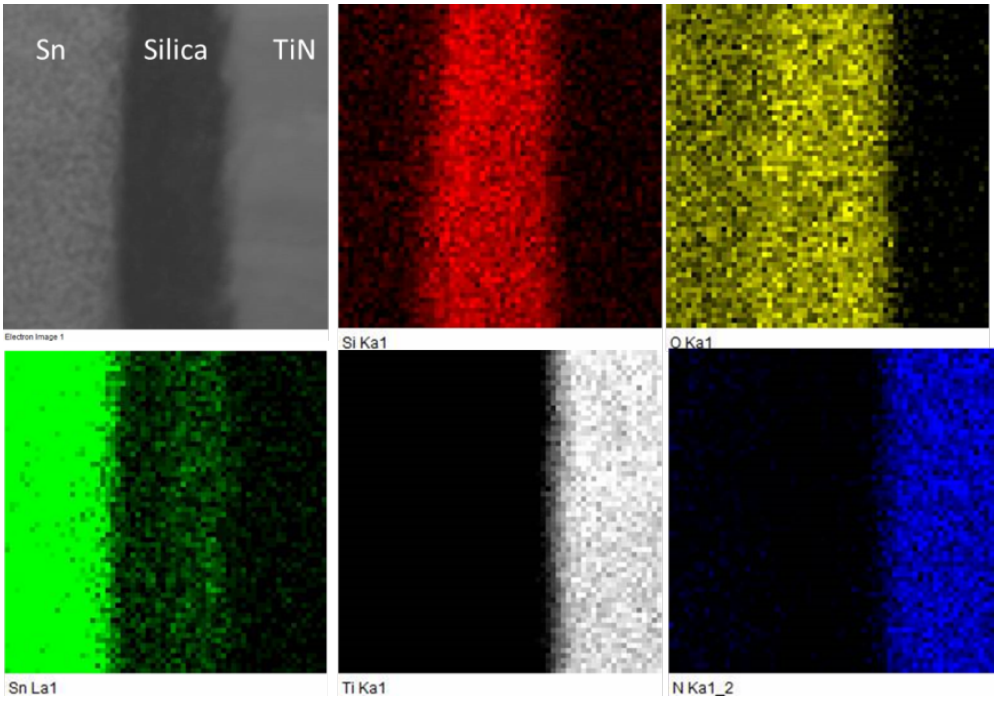

Figure 68 - EDX mapping of a cross section of an EASA film with Sn deposited via SCFED (bottom left image).

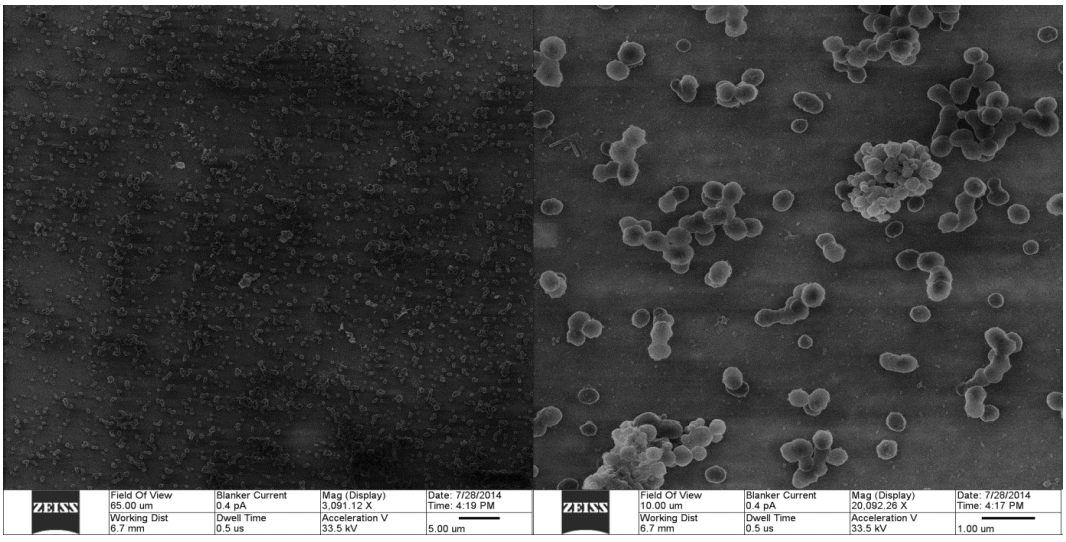

Figure 69 - HIM images of the surface of EASA with Sn deposited via SCFED indicating individual nucleation sites

Based on the data obtained, it can be concluded that Sn enters the pores of the film and was being deposited via SCFED. The conversion of Sn^{2+} → Sn^{0} in the CV and the presence of tin within the film have clearly been indicated by EDX mapping of its cross-section. However, it appears that deposition is only occurring in a small number of the pores. Even with the high degree of ordering seen in the EASA, if nucleation were to occur more readily in one pore over another. Subsequently this would lead to the formation of single nanowires growing to the surface quicker than those around them. The consequence being that it would disrupt the growth of other nanowires nearby, as the diffusion distance would decrease the longer the single nanowire gets. It would also provide a path for the current to reach the surface without making the reagents travel down the pore channels. Hence producing the mushrooming effect, as seen in the HIM images (see Fig. 69). This is because the growth of the nanowire is no longer restricted to the pore channel as it breaches the surface. Imaging a single wire proves challenging at best when considering the average diameter of the tin mushrooms is around 100 nm and width of the nanowire would be 1.6 nm. A potential solution to this problem would be pulsing the current applied to deposit the Sn. This would enable the concentrations of reagents to equalising within the pores and limit the effect of a faster growing nanowire.

4.9 EASA deposition from titanate precursors

Titanium dioxide (titania) is a material of great interest with a range of unique and far-reaching properties, such as its photoactive abilities.[117] Control over the structure of materials is important in order to enhance these properties as they can be dependent on factors such as surface area. Manipulating structural properties, such as particle size, porosity and pore diameter/volume can enhance these abilities.

The synthesis routes used to produce mesoporous titania are very similar to those used for silica (see Section 1.3.2), where mesopores can be fabricated

through soft-templating methods using sol-gel chemistry.[118] However titanate species will react far more vigorously than the silicate, due to higher reactivity of the metal centre. As a result, stabilising agents are often needed in order to prevent rapid precipitation, particularly in aqueous solutions. These stabilising agents may comprise of low pH solutions to prevent the condensation reaction. Others use ligands to increase the coordination number of the titanium, blocking the molecule from accepting water and slowing the rate of reaction, such as acetylacetone (Acac) or acetic acid.[119] A common method used for growing of mesoporous titania films is the evaporation-induced self-assembly (EISA) method, which leads to the formation of pore channels that generally run parallel to their support (see Section 1.3.3).[107,120]

Electrodeposition has been used to generate a number of different metal oxide films, including silica,[52] titania,[121,122] zinc oxide[123] and other metal oxides.[53] As shown in this chapter electrochemically-assisted self-assembly (EASA) can produce silica films with pore channels running perpendicular to its substrate. Applying similar conditions to titania film may produce similar results with a number of small changes. The advantage that EASA has over other fabrication methods is that the reaction is controlled by the application of a current through an electrode. This current triggers the reduction of nitrates present in solution, which releases hydroxide ions at the surface of the electrode:

$$NO_3^- + H_2O + 2e^- \rightarrow NO_2^- + 2OH^- \quad E^\circ = 0.01\ V$$

The negative potential applied to the electrode also attracts cationic surfactant molecules in solution, which organise on its surface. In order to control the migration of hydroxide ions, the solution is made acidic with the addition of HCl, hence neutralising the base away from the electrode surface, as well as hydrolysing the inorganic precursor.

It should be noted that the addition of cationic surfactants (e.g. CTAB) have shown to have destabilising effect on titania sols.[124] In the first reported

example of hexagonal packed mesoporous titania, Antonelli and Ying found only negatively charged surfactants produced ordered mesopores.[119] Low pH was used to stabilise the titanate precursors in solution, which resulted in positively charged titania oligomers.

This work was performed with the aid of a project student, Alex Pateman, during a three-month summer studentship.

4.9.1 Effect of stabilising agents on silica EASA films

Due to the higher rate of hydrolysis of alkoxide titanate species, the effects of stabilising agents commonly used in TiO_2 sol-gel chemistry, acetyl acetone (Acac) and diethanolamine (DEA), on the formation of EASA silica films were investigated. The purpose of these stabilising agents (or moderator) is to bind to the metal centre and increase its coordination number and reduce its reactivity. Their effects were investigated on silicate species to see if they might disrupt the self-assembly of CTAB. Acac and DEA were added to standard sol for the synthesis of EASA silica films based on a 1:1 molar ratio with TEOS (see Section 4.2.4). The moderators gave no indication of any further reactions with reagents present in solution. Electrodeposition was then performed using the custom cell against a pseudo Ag reference electrode and stainless steel counter electrode. The films were deposited by applying a potential of -2.0 V for 5 s on TiN-coated silicon using the custom cell described in section 4.3.1.

The in-plane GISAXS patterns of EASA films with addition of either Acac or DEA showed that they maintain vertically aligned hexagonal pore arrangements (see Fig. 70). The features in the scattering patterns represent the hexagonal arrangement of pores orientated perpendicular to their support at ~2.26˚, 3.9˚ and 4.7˚. The shift in peak position is comparable to the addition of swelling agent, as they increased the interpore distance by 0.2 nm (see Section 4.4). DEA shows an increase in the noise of the diffraction pattern more than that of Acac. The sharpness of the reflections observed does decrease in a similar manner to that of the swelling agents (see section 4.4).

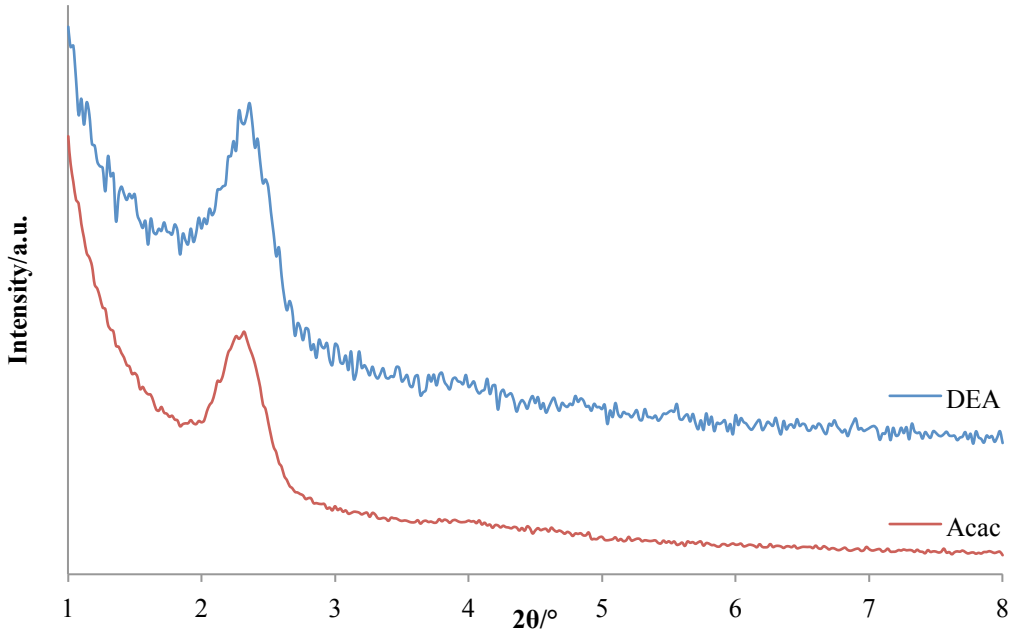

Figure 70 - In-plane GISAXS pattern of EASA silica film with the addition either Acac or DEA

Table 36 - Summary of the XRD data of silica EASA films with the addition the of moderators Acac and DEA

Moderators	Peaks posn. (2θ/°)			d_{10} (nm)	a_o (nm)
	10	11	20		
Acac	2.24	3.94	4.62	3.94	4.55
DEA	2.28	3.92	4.78	3.87	4.47

4.9.2 Effect of varying the ratio of titanium isopropoxide and tetraethyl orthosilicate on EASA films

Mixed silica-titania films have been shown to form with mesopores using alkyltrimethylammonium and oligo(ethylene oxide) alkyl ether surfactants.[125,126] Hence the addition of $Ti(O^iPr)_4$ to a silicate sol was investigated to determine the effect of this alkoxide on the EASA film generation mechanism. $Ti(O^iPr)_4$ with Acac (4.66 mmol) was added to a standard EASA sol, replacing molar amounts of TEOS in solution (see section 4.2.5). The amount of $Ti(O^iPr)_4$ was varied between 20 %, 50 %, 80 % and 100 %, with TEOS added to ensure that the combined quantity of both reagents reached a total of 4.66 mmol.

All resulting films appeared white and patchy on the TiN with the addition of $Ti(O^iPr)_4$. The in-plane GISAXS patterns show that its presence in solution resulted in a dramatic reduction in observable features (see Fig. 71). The only film to show any signs of retaining some pore ordering was that of 80/20 (TEOS/ $Ti(O^iPr)_4$). However, the feature at 2.06 ° is both broad and noisy, suggesting that the $Ti(O^iPr)_4$ disrupted the pore formation of EASA films. CVs were performed showing that as the ratio of $Ti(O^iPr)_4$ increased in solution, the number of reduction peaks decreased from two to one (see Fig. 72). Instead of cooperative self-assembly as seen between CTAB and silica, the positive charge on the titania could be competing for space at the electrode's surface and aggregating. This has been seen using zeta potential measurements of the surface charge of titania particle, which was found to be positive in solutions of low pH 4,[127] whereas silica-coated titania particles acquired solutions with pH below 2 to become protonated.

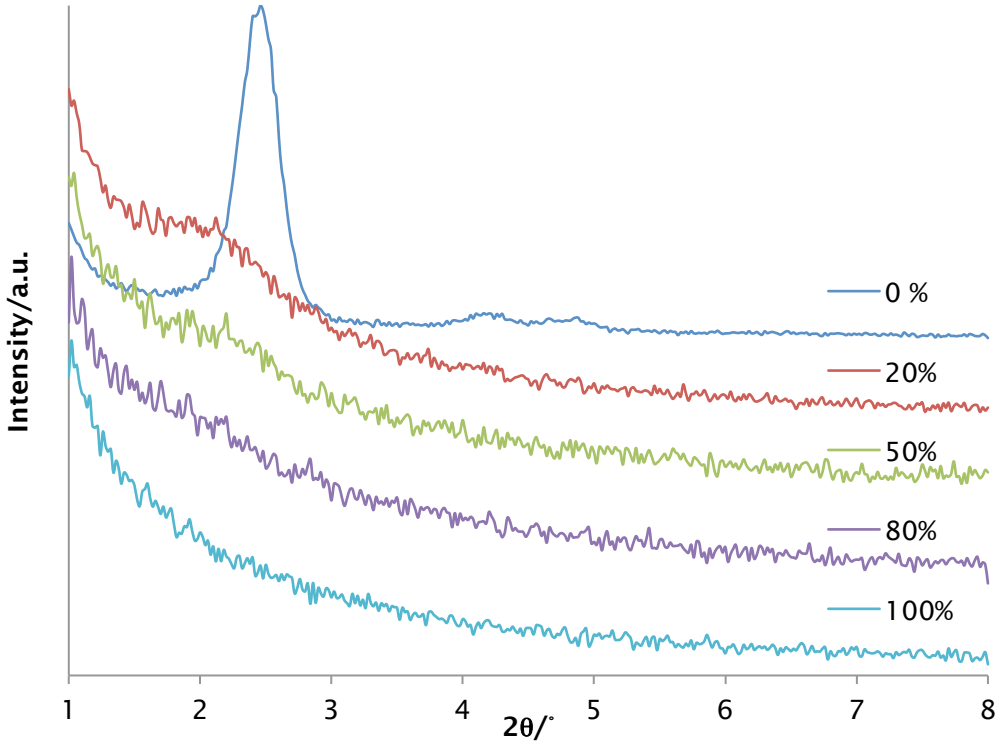

Figure 71 - In plane GISAXS patterns of EASA films with various Si:Ti ratios

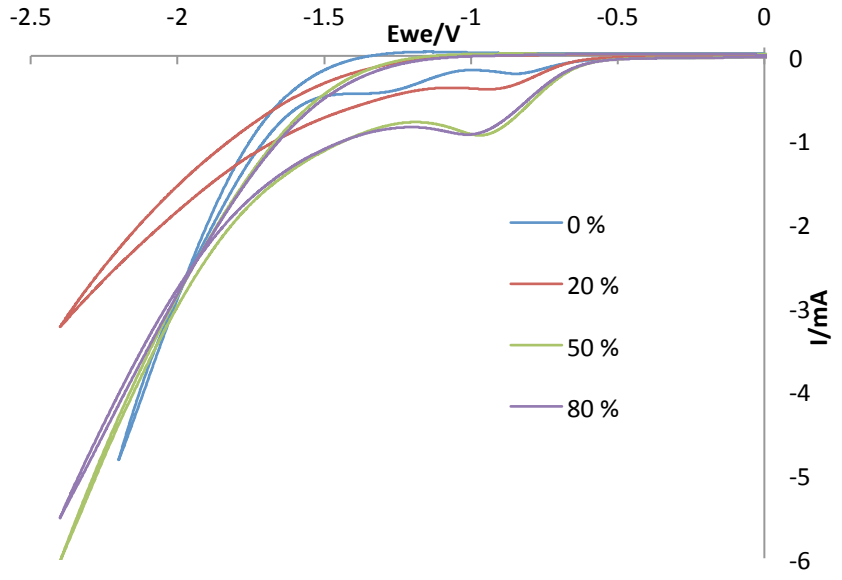

Figure 72 - Cyclic voltammogram of varying ratios of TEOS/ $Ti(O^iPr)_4$ performed on sputtered TiN in standard EASA solution (using pseudo Ag rod reference electrode and stainless steel cone counter electrode)

4.10 Summary

The synthesis of the EASA silica template films with pore channels running perpendicular to its substrate was achieved. This was confirmed using a range of techniques, including in-plane GISAXS, EP, TEM and HIM imaging. As a result, EASA films were produced with hexagonally organised pores with a narrow pore size distribution of 1.6 nm in diameter. Over the course of this investigation it was found that producing EASA film was more favourable on TiN. This increased the potential window of the template, enabling the deposition of more electropositive elements. It also allowed the porosity of the films to be determined using EP, as it provided a reflective surface beneath the film. Nitrate ions in solution were also shown to play a critical role in the film generation by releasing hydroxide ions at the electrode surfaces. Replacement with alternative electrolytes led to a significant reduction in the quality of the films.

The subsequent films were modified in order to control the pore width. This was achieved using with the addition of a swelling agent, which increased the diameter of the pores from 1.6 nm to 2.4 nm. The pore width was decreased by reducing of the tail length of the surfactant, resulting in narrower channels. Cationic ammonium surfactants were proven to be more effective then pyridinium in the formation of organised pore structures. The addition of molar ratios $Ti(O^iPr)_4$ to solution disrupted the pore formation when present. This was attributed to the formation of a positive charge on the titania due to the pH of the solution, which was used to prevent the bulk precipitation of aggregates. As a result, the inorganic species could not undergo cooperative self-assembly with cationic CTAB.

Sn was deposited into EASA films on TiN using SCFED. Indications from both the electrochemistry and EDX mapping of the film's cross section implied the deposition of Sn into the pores of the film. It was concluded that due to no discrete nanowires visible in the TEM and the presence of mushroom like structure on top of the film that single nanowires were growing through the template. Furthering this, EASA films were also taken forward for chemical

modification by reacting with the silica surface of the film with functionalised silane molecules (see Chapter 5).

Chapter 5 - Surface modification of mesoporous silica

5.1 Introduction

As shown in the two previous chapters, films with perpendicularly aligned pore channels can be grown onto TiN, ITO and silica. The methods investigated were a Stöber-derived hydrothermal process (Chapter 3) and electrochemically-assisted self-assembly (EASA) method (Chapter 4). EASA was determined as the most suitable method for the SCFED project, as it produced a hexagonally ordered pore rearrangement directly on an electrode's surface. The pore size can be altered by the addition of swelling agents or made smaller by decreasing the length of the surfactant tail. However, these processes are limited, as reducing the tail length of the surfactant led to a reduction in the quality of the pore structure. There are a number of advantages to post-synthesis grafting of the functionalised molecules to the surface of the templates, which are particularly attractive to the SCFED project. These include:

1) The ability to retain the pore ordering present in the film, whilst reducing the width of the pore channels present within template.

2) Chemically modifying the walls of the template to better suit the material deposited into the pores of the sample.

3) Chemically modifying the walls to improve penetration by certain fluids.

The chemical modification of mesoporous silica has widely been investigated for application, such as catalysis[128] and filtration.[129] This can be achieved by reacting functionalised silane molecules with silanol groups (Si-OH) present at the surface of the silica, leaving the grafting agent anchored in place. As a result, control over pore diameter is based on the steric bulk of the grafting agent. This process is a post-synthesis procedure that requires the support to be stable during anchoring process, to avoid compromising the structural rigidity of the pore walls. The initial stages of investigation have involved using mesoporous silica powders to determine the changes in the pore size with addition of a grafting agent. Nitrogen sorption is a well-established method of determining porosity of powders, but due to the limited sample volume is not feasible in the mesoporous silica films. Therefore, mesoporous silica powders have been used to gauge changes in pore size after the addition of a grafting agent. Once this change has been established, it can then be applied to the

mesoporous silica films, as their surface chemistry is very similar. For a limited number of films, the porosity was determined using ellipsometric porosity.

The grafting agents chosen were trimethylchlorosilane (TMCS), phenyldimethylchlorosilane (PDCS), tert-butyldimethylchlorosilane (tBDCS) and hexamethyldisilazane (HMDS). The monochlorosilane grafting agents were chosen as they can produce various changes in pore size, but undergo similar reactions with the walls of the pore:

$$Si\text{-}OH + (R)_3Si\text{-}Cl \rightarrow Si\text{-}O\text{-}Si(R)_3 + HCl$$

The disilazane is another common surface treatment agent, so allowed us to evaluate which was the most effective grafting agent chemistry:

$$Si\text{-}OH + HN(Si(Me)_3)_2 \rightarrow Si\text{-}O\text{-}Si(Me)_3 + H_2NSi(Me)_3$$

$$Si\text{-}OH + H_2NSi(Me)_3 \rightarrow Si\text{-}O\text{-}Si(Me)_3 + NH_3$$

5.2 Experimental detail

5.2.1 Mesoporous silica powder

This synthesis route was taken from Nooney *et al.*[100] Water (442 mL) was mixed with ammonia solution (35 wt %, 40.7 mL, Fisher) and heated to 50 ˚C under stirring. Hexadecyltrimethylammonium bromide (1.1 g, Sigma Aldrich), applied with rapid stirring to ensure it completely dissolved. The sol was taken off the heat and tetraethyl orthosilicate (5.6 mL, 98 %, Sigma Aldrich) was added immediately. The mixture was stirred and allowed to cool to room temperature over 2 hr. The resulting precipitate was filtered by suction. The powder was dried at 60 ˚C overnight before Soxhlet extraction.

5.2.2 Removal of surfactant by Soxhlet extraction

Soxhlet extraction was used to remove the surfactant from the pore of both the films and powders. This involved washing the powders/films (contained within extraction thimble) with 0.1 M HCl in ethanol for 6 hrs.

5.2.3 Grafting in dry basic toluene

This method was modified based on work by Deschner and co-workers.[130] Mesoporous silica powder (0.5 g) or films were dehydrated by heating under vacuum in an oil bath at 110 ˚C for 6 hrs after the surfactant had been removed. Dry toluene (5 mL, Fisher) containing triethylamine (550 μL, 98 %, Sigma Aldrich) was added, followed by the grafting agent (3.9 mmol) in toluene (5 mL). The mixture was heated with stirring at 60 ˚C for 24 hrs under nitrogen. The mixture was filtered under suction and washed with toluene (25 mL ×3) and THF (25 mL ×3). The powder was Soxhlet washed with THF (50 mL) for 24 hrs and dried under vacuum at 110 ˚C to remove any remaining solvent.

5.2.4 Grafting via refluxing in dry THF

Mesoporous silica powder (0.5 g) or film was dehydrated by heating under vacuum in an oil bath at 110 ˚C for 6 hrs after the surfactant had been removed. Dry THF (10 mL, Fisher) was added to the sample, followed by grafting agent (3.9 mmol). The solution was refluxed for 24 hrs under nitrogen then collected by filteration under suction. The sample was washed with THF (20 mL ×5) and diethyl ether (20 mL ×5). Soxhlet washing using wet diethyl ether was performed on the sample to remove any remaining grafting agent. Any remaining solvent was removed by heating under vacuum at 110 ˚C.

5.3. Characterisation of functionalised mesoporous silica materials

5.3.1 Small angle X-ray scattering (SAXS)

Powder was mounted within a 0.7 mm borosilicate glass capillary tubes. SAXS was performed using Rigaku Smartlab system with a 9 kW Cu-Ka source, parallel line beam optics and a DTex250 1D detector. Scans were performed across 1-10 ° 2θ. See section 4.2.2 for GISXAS of films.

5.3.2 Nitrogen adsorption-desorption measurements

The porosity and surface area of the powders were determined using nitrogen adsorption. The measurements were performed on a Micromeritic 3Flex Surface Characterisation Analyser. Samples were dehydrated under vacuum at 110 °C overnight to remove any water/solvent from the pores. N_2 adsorption-desorption isotherms collected at 77 K. Pore size distribution obtained using original density functional theory method.

5.3.3 Solid State ^{29}Si NMR

Silicon solid state NMR was performed Dr Marina Carravetta using a Bruker Avance II spectrometer. Samples were recorded using ramped cross-polarization with 4.5 ms contact time under MAS (8 kHz) and spinal64 decoupling using 80 kHz nutation frequency.

5.3.4 CHN Analysis

Samples outsourced to MEDAC Ltd in order to perform CHN analysis. Samples were analysed using a Thermo FlashEA®1112 elemental analyser.

5.3.5 Ellipsometric porosimetry

Measurements were performed using a PS-2000 ellipsometric porosimeter by Dr Peter Basa at Semilab headquarters in Budapest. Samples were exposed to water, toluene, IPA and methanol and based on the optical modelling of a plain piece of MOCVD TiN-coated silicon. The pressure was altered based on 5 s intervals with the incidence angle readings taken at 60 °.

5.4 Results and discussion

5.4.1 Mesoporous silica powder

The method chosen for the synthesis of mesoporous silica powders was taken from Nooney and co-workers.[100] This is based on a simple one-pot synthesis of mesoporous silica powder, where TEOS is exposed to ammonia in the presence of CTAB. The TEOS undergoes hydrolysis at an elevated temperature (50 °C) in water. The elevated temperature increases the solubility of CTAB within the water and forms the pore structure based on cooperative self-assembly with TEOS oligomers. The ammonia dramatically increases the rate of hydrolysis. The advantage of this method is that it is quick and scaling up the reaction is simple. The powder was dried and the surfactant was removed through Soxhlet washing in acidified ethanol (0.1 M HCl), in order to displace the surfactant from the pore channels. The surfactant was not burnt out of the pores to ensure comparability with films grown on TiN. High temperature also favours the formation of Si-O-Si at the surface of the powder, due to dehydration.[95] This is detrimental to grafting as silanol groups (Si-OH) are used to bind the silane molecule to the walls of the silica. Therefore, ensuring high concentrations of silanol groups at the surface of the samples will increase the number of sites available for binding the grafting agent.

Small angle X-ray scattering (SAXS) was used to determine the pore organisation and lattice parameters of the powder. It shows that both the powder and the film have the same pore structures, resulting in the presence of 10, 11 and 20 peaks (see Fig. 73). The lattice parameters of the powders and the EASA films are within 0.13 nm of each other (see Table 37). Therefore, we can establish that both the powder and EASA film have similar structural properties.

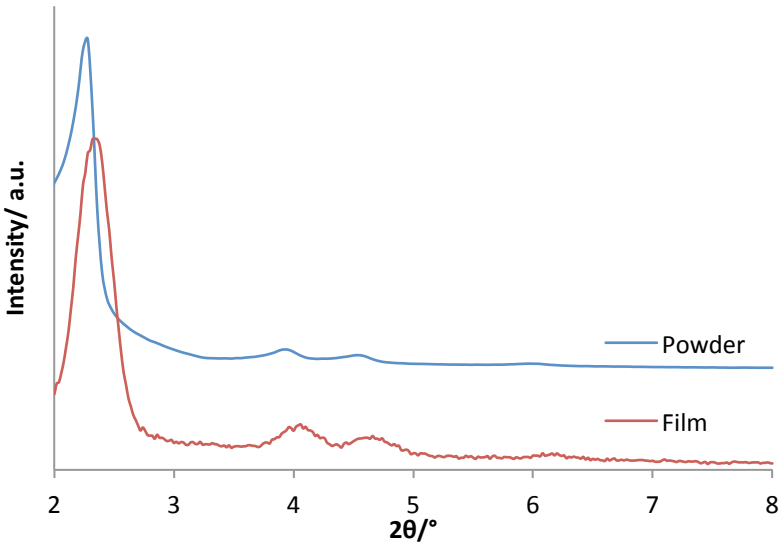

Figure 73 - XRD patterns comparing pore ordering present the mesoporous silica powder with EASA silica film grown as describe in section 4.2.1.

Table 37 - Comparison of lattice parameter of mesoporous silica powder and EASA silica film

Sample	Surface area (m^2/g)	Pore diameter (nm)	Peak posn. (2θ/°)	d_{100} (nm)
EASA film	~1100	1.60	2.32	3.87
Powder	1093	2.95	2.28	3.77

Nitrogen sorption was used to determine porosity of the mesoporous silica powders, with the BET surface area measured as 1093 m^2/g. The nitrogen isotherm of the powder is Type IV (Fig. 74). This similar to the results obtained by Nooney *et al*, who state that this is typical of MCM 41 samples.[100] The pore size distribution was measured the pore diameter of the powder to be about ~2.95 nm modelled using original density functional theory. It was found that BJH modelling of pore size was inconsistent at this scale. This has been backed up by a number of different groups aim to improve the modelling of capillary condensation in the pores of MCM 41 as reviewed by Landers *et al*.[131] The pore size of the powder is just over twice the size in the EASA films measured in Chapter 4. However, establishing the change in pore size on grafting will still

provide useful information on the effectiveness of the grafting agents for the EASA silica films.

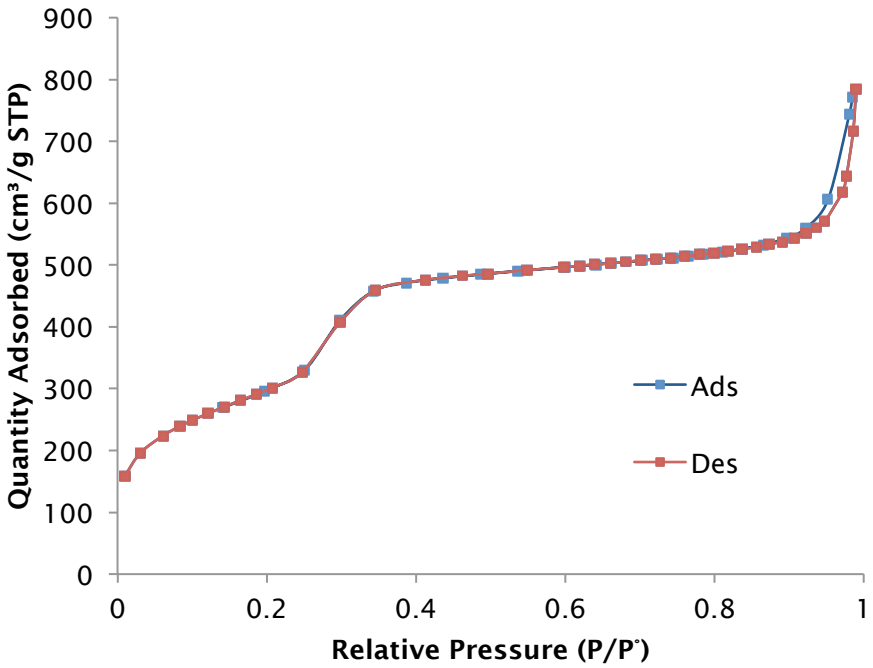

Figure 74 –Nitrogen adsorption/desorption isotherm of mesoporous silica powder washed via Soxhlet extraction.

5.4.2 Grafting in dry basic toluene

In order to graft functional groups onto the walls of mesoporous silica, the powder was dehydrated to prevent the grafting agent from reacting with the water instead of silanol groups covering the surface of the powder. Triethylamine (Et_3N) was used to deprotonate the silanol groups to encourage nucleophilic substitution with the grafting agent. This was done in dry toluene at 60 ˚C under stirring with molar equivalents (3.9 mmols) of grafting agent and Et_3N (see section 5.2.3). This was based on a method by Deschner *et al.*[130] Three functionalised monochlorosilanes were used to ensure the grafting agent did not polymerise. These were trimethylchlorosilane (TMCS, Me_3SiCl), phenyldimethylchlorosilane (PDCS, $(Me)_2Si(Ph)Cl$) and tert-butyldimethylchlorosilane (tBDCS, $(Me)_2Si(C_4H_9)Cl$). Hexamethyldisilazane (HMDS, $HN(SiMe_3)_2$) was also trialled to provide an alterative to the

monochlorosilane, which anchors to the pore walls through a via self-catalysing mechanism.

Initial results showed all the grafted samples to have very low surface areas. The powders were Soxhlet washed and dried under vacuum at 130 °C, in order to remove as much of the solvent from the pores as possible. The resulting isotherms of the grafted powders were compared against an untreated sample (see Fig. 75). A significant drop in the volume of adsorbed nitrogen was observed in the isotherms of all the grafted samples, which correlated to the reduction in the surface area of powders (see Table 38). A shift in the pore size distribution (PSD) from 2.9 to ~2.2 nm was observed for all grafted powders determined using original DFT modelling (see Fig. 76). tBDCS produced a peak at 2.16 nm, whereas the other grafted samples it is hard to quantify. HMDS resulted in powders with a pore diameter of 2.34 nm and a surface area of 180 m^2/g. Powders grafted with PDCS had a surface area of 77 m^2/g with the pore diameter of 2.34 nm. However, it can be imagined that π-stacking between the aromatic rings of the phenyl group and the toluene prevented the solvent from leaving the pore. The porosity of TMCS sample was not determine due to the powder being so light, it would enter the BET machine on degassing. Therefore to avoid damaging the machine, no further measurements were made on the sample. SAXS patterns of the treated powder samples show pore structure within the powders to have survived the grafting process in the presence of Et_3N (see Fig. 77). All samples show a reduction in the peak intensity within the scattering pattern, except for TMCS which mirrors the results obtained for the ungrafted powder. This reduction in peak intensity can be attributed to larger amounts of solvent remaining within the pores, which could reduce X-ray scattering contrast between and the pore walls of the powder.

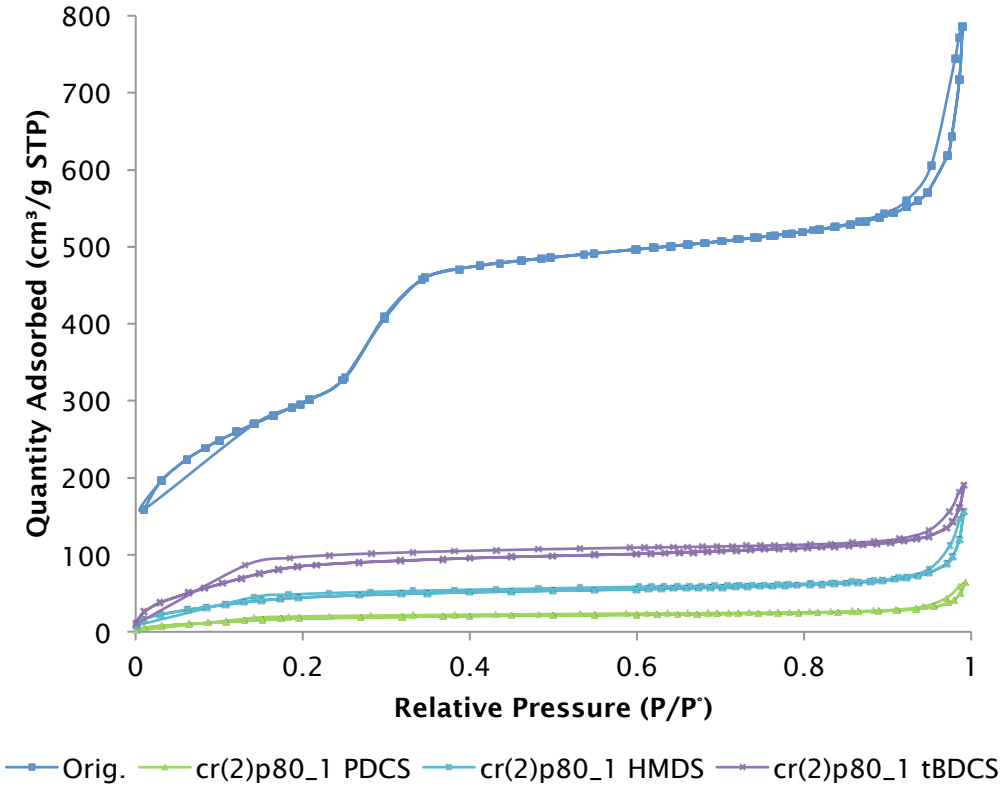

Figure 75 - Liquid Nitrogen Isotherm comparing the ungrafted and grafted powders in basic toluene

Table 38 - Summary of the data collected on mesoporous silica powders grafted in the presence of Et_3N

Grafting agent	d_{100} (nm)	Pore diameter (nm)	s_t (m^2/g)
Orig.	3.87	2.95	1,093
PDCS	3.94	2.16	77
HMDS	3.80	2.34	183
tBDCS	3.87	2.16	371
TMCS	3.94	/	/

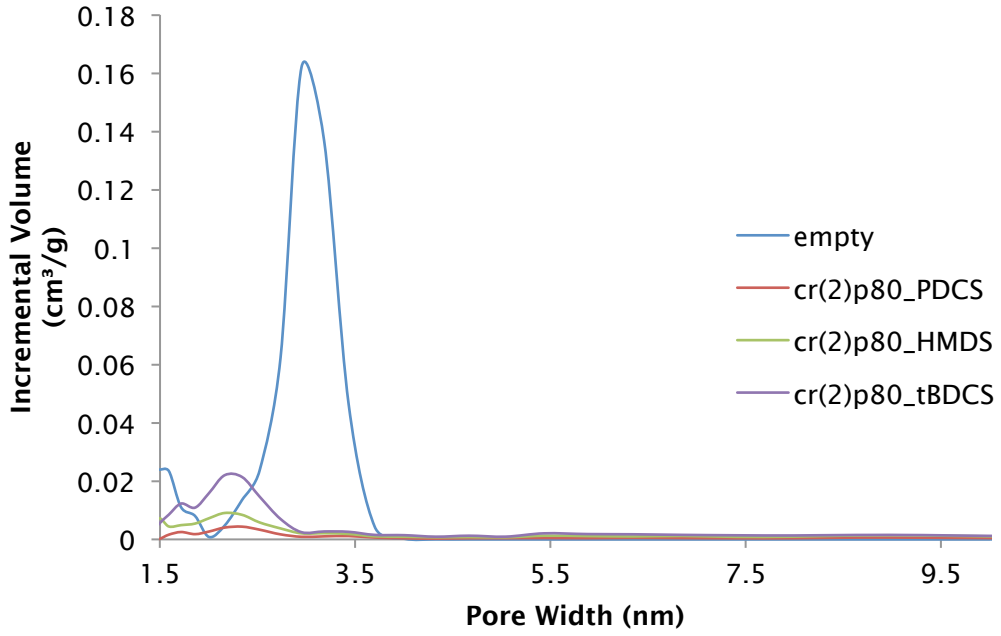

Figure 76 - Pore size distribution of mesoporous silica powder grafted in basic toluene

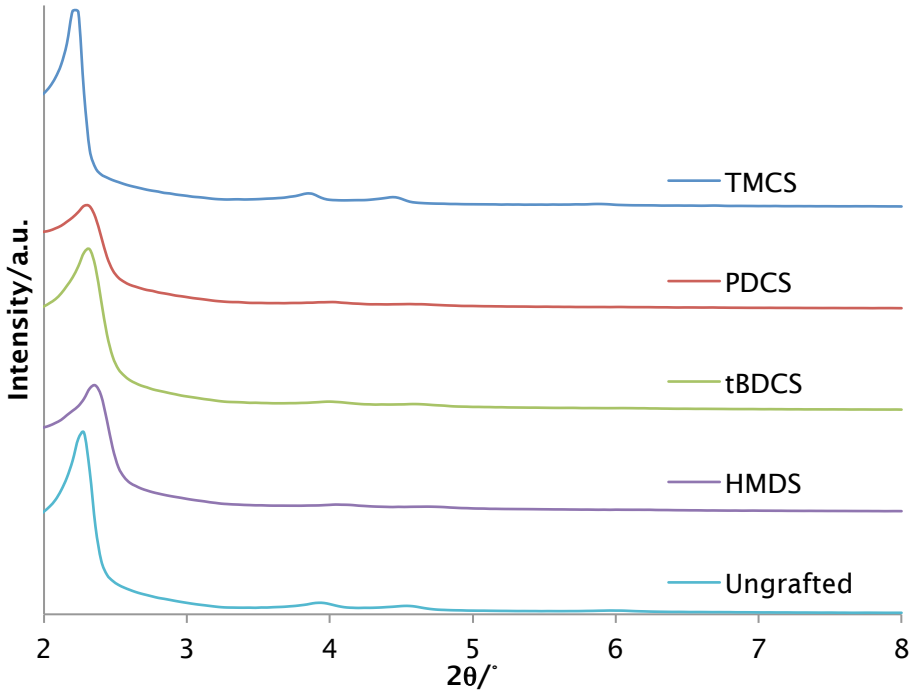

Figure 77 - SAXS pattern of grafted mesoporous silica powders in basic toluene

The pores remained and grafting occurred as planned. However, as the pore walls become lined with alkyl groups, they become increasingly lipophilic.

Hence, the pore becomes increasingly favourable to organic solvent. Combined with the high boiling point of toluene (110.6 ˚C), this leads to the solvent becoming harder to remove from the powder. As a result, it effectively blocked nitrogen from entering the pore structure, which caused the significant drop witnessed in the surface area of the powders. Harsher methods of removing organic material (e.g. high temperature or plasma ashing) would risk removing grafted alkyl groups.

Using both the sorption data and XRD patterns, it can be concluded that the pores of the grafted powders are not collapsing in the presence of Et_3N. The diffraction patterns clearly indicate that the pore structure survives the grafting process (see Fig.77). Therefore nitrogen is simply unable to condense in the pores of the powder due to the presence of toluene. If the pores had remained hydrophilic then it can be expected that the solvent could be removed far more easily. As a result, the grafted pores provide more favourable environment for the toluene, particularly PDCS where the largest reduction in surface area was witnessed. Consequently, a lighter solvent is required to ensure that it can be removed from the sample structure, and no base to reduce the chances of pore collapse.

5.4.3 EASA grafted in basic toluene

The EASA films were exposed to exactly the same conditions as those performed on the powders. As seen from the in-plane GISAXS pattern a significant reduction in the intensity of features was observed (see Fig. 78). This is made clear in the control sample, which clearly displays a collapse in the pore structure. Due to the reduced mass of the film, the Et_3N is effectively dissolving the silica walls of the pore before the grafting can take place. This is less of a problem for the powder, which can afford the loss of small amounts of silica without pore collapse, whereas the film cannot. Alternately it can be concluded that grafting in toluene in the presence of Et_3N has increased the lipophilicity of the pore channels. This would be favourable for toluene to collect in the pores, which was seen in the powder as nitrogen sorption. It showed that after grafting the powders have considerably lower surface area,

yet the SAXS pattern showed the pore structure had remained constant. Due to the thickness and reduced amount of material the collection of solvent within the pore may be enough to reduce the contrast in density between the pore walls and void. This would decrease the amount of coherent scattering of X-rays, reducing the intensity of the feature seen in the diffraction.

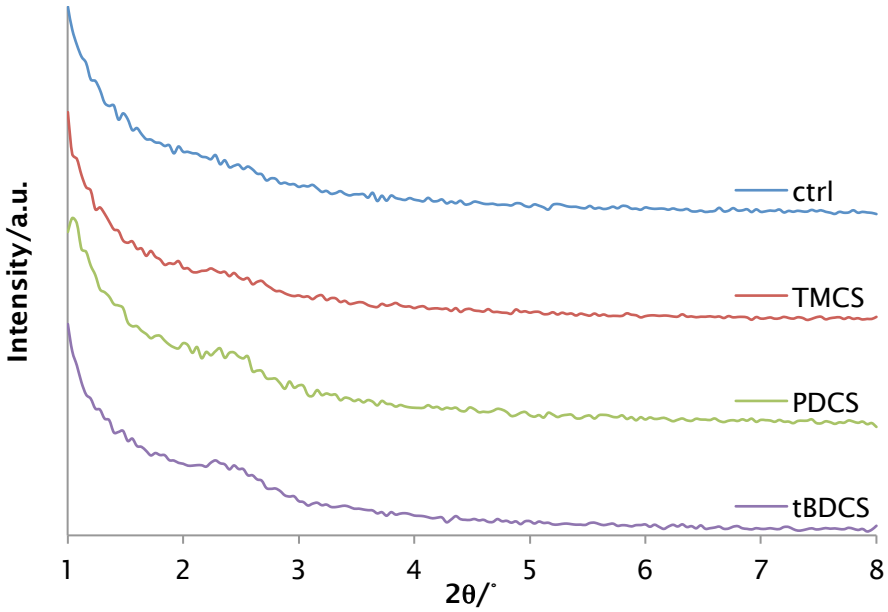

Figure 78 - In-plane GISAXS pattern of EASA mesoporous silica films grafted in basic toluene

5.4.4 Grafting functionalised silanes in refluxing THF

In order to avoid pore blocking of the pore walls of mesoporous silica powder, the reaction conditions were altered. Tetrahydrofuran (THF) replaced toluene as the reaction solvent, as it has a lower boiling point (66 ˚C) and is therefore easier to remove. As a polar aprotic solvent, this allows THF to accept hydrogen bonds and the basic nature of the oxygen can be used to deprotonate the silanol groups. This was based on work Brown *et al.*[132] As a result, no base was required to encourage the reaction between the functionalised silanes with the pore walls. The grafting was performed via refluxing at a higher temperature to encourage penetration in to the pores of the powder and improve the rate of reaction.

The powders were refluxed in dry THF in the presence of the grafting agents using an oil bath heated to 110 ˚C, after being dried at 130 ˚C under vacuum for 6 hrs (see section 5.2.4). The samples were then washed with THF to help remove any excess grafting agent, followed by diethyl ether all under suction filtration. Soxhlet washing with diethyl ether was used to displace as much as possible of the remaining grafting agent and the THF with a lighter solvent (bp = 35 ˚C). The powders were dried under vacuum at 130 ˚C to remove any solvent that was left.

Nitrogen isotherms of the refluxed samples show significantly larger surface area and pore volume than observed in the data obtained when grafting in the presence of Et_3N (see Fig. 79) in all samples apart from that with HMDS (see Table 39). When compared against the ungrafted powder, the sample's surface area gradually decreases with the increasing size of the grafting agent and the pore width and volume decrease (see Fig. 80). The addition of TMCS to the walls leads to a decrease in the pore diameter from 2.95 nm to 2.73 nm. Both PDCS and tBDCS decrease the pore diameter to 2.52 nm, whereas with HMDS is hard to resolve (~2.50 nm). The SAXS patterns shows that all the samples survive the refluxing process, with the observed features more defined than those grafted in basic toluene with minimal alterations to the pore ordering (see Fig. 81).

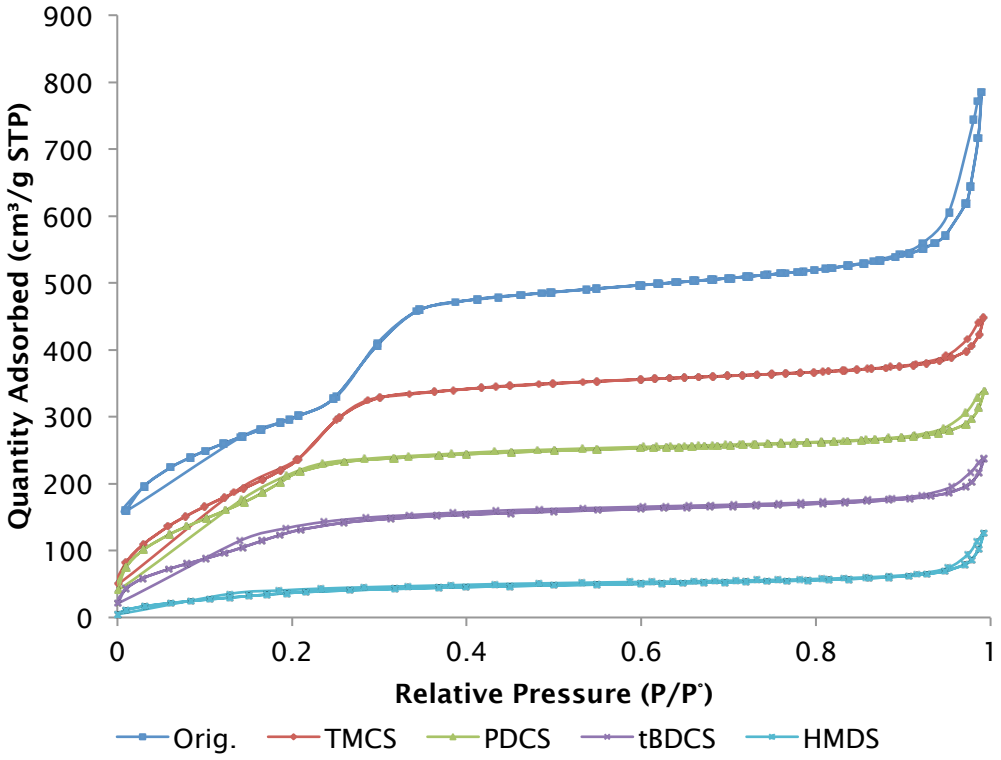

Figure 79 - Nitrogen isotherm comparing the ungrafted and grafted powders by refluxing in THF

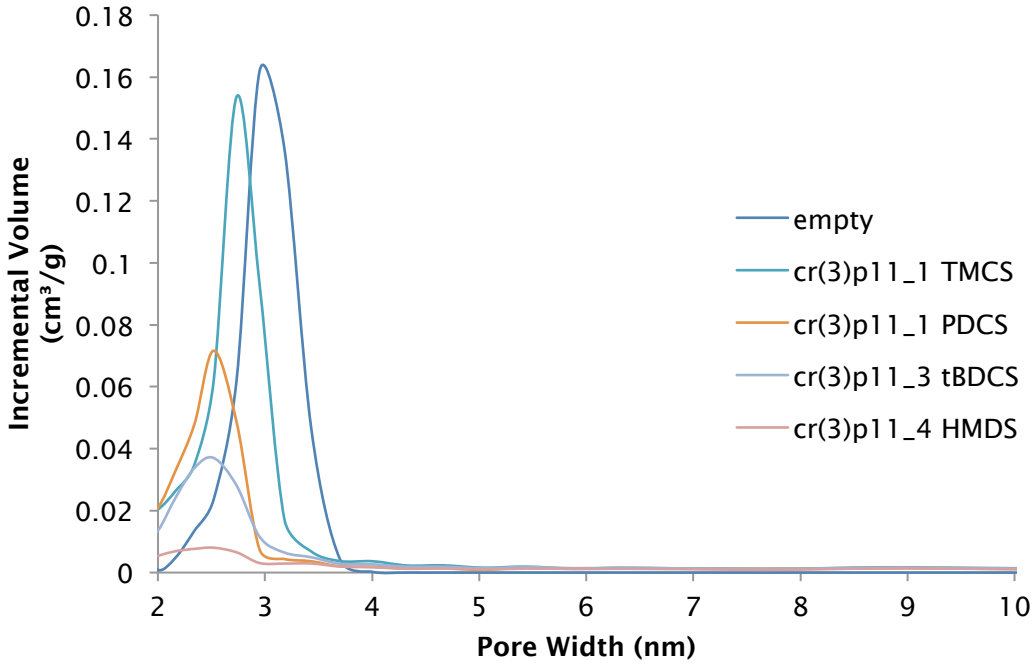

Figure 80 – Pore size distribution of mesoporous silica powder grafted and grafted with functionalised silanes using original DFT.

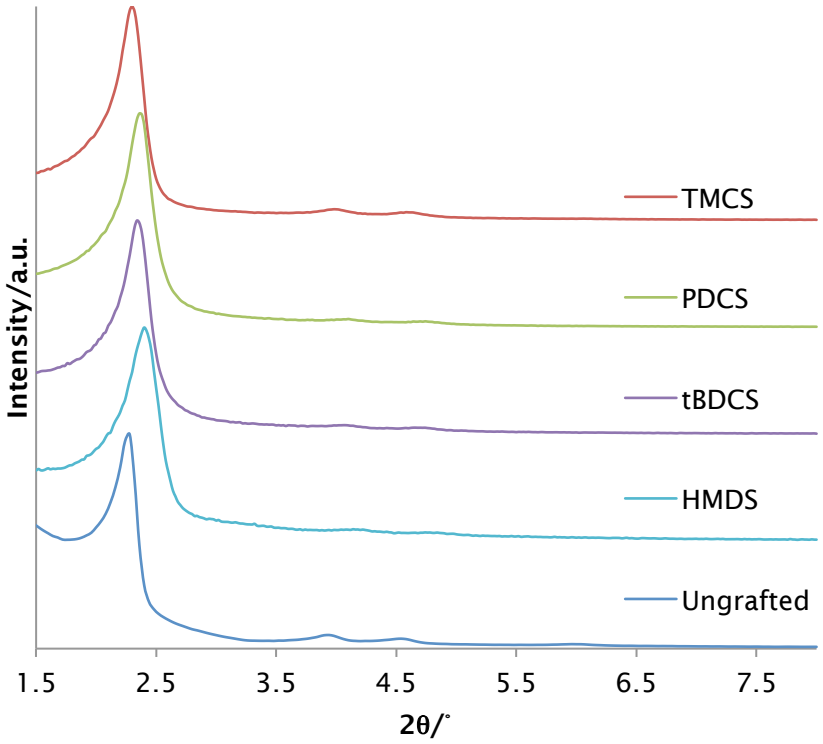

Figure 81 – SAXS pattern of grafted mesoporous silica by refluxing in THF

Table 39 – Summary of the data obtained from grafted mesoporous in THF silica powders compared against an ungrafted sample

Grafting agents	d_{100} *(nm)*	Pore diameter *(nm)*	BET surface area (m^2/g)
Ungrafted	3.87	2.95	1,093
TMCS	3.87	2.73	904
PDCS	3.78	2.52	729
tBDCS	3.78	2.52	538
HMDS	3.71	~2.50	161

CHN analysis was performed on the powders to gauge the amount of organic material present within the pores (see Table 40). Comparing the ratio of carbon, hydrogen and nitrogen before and after grafting, changes in the organic composition of the powder can be established. We can see a large ratio of carbon remaining within the ungrafted sample. The carbon percentage

could include a range of materials, such as the grafting agent, reaction solvent and surfactant. We also see nitrogen within the sample, suggesting that not all the surfactant (CTAB) was washed out of the pores of the sample. It is highly unlikely that of ammonia solution remains, in part due to its low vapour pressure and the subsequent washing in acidified ethanol. Therefore, it is more probable that any nitrogen present is due to the presence of the ammonium group of CTAB. The ratios of carbon and nitrogen (C/N) of the surfactant is 19:1. Hence, the closer the ratio of C/N to the ungrafted, the less likely the surfactant is being displaced from the pores of the sample as it grafts to the walls. TMCS and PDCS have the lowest ratio of nitrogen present in the sample with C/N ratios of 112.7 and 66.9 respectively. Consequently, this high ratio cannot be explained by the simple presence of CTAB (where C:N = 19), thus must be due to the existence of grafting agents attached to the pore walls. CHN analysis of both tBDCS and HMDS has revealed their ratios to be 20.3 and 19 respectively, which are very close to that of CTAB. Therefore, it can be assumed that they have displaced the least amount of surfactant and that the grafting was least successful.

Table 40 – CHN analysis of grafted and ungrafted mesoporous silica powder

Grafting agents	Carbon (%)	Hydrogen (%)	Nitrogen (%)	Ratio of C/N
Ungrafted	26.8	5.4	1.5	17.7
TMCS	11.3	2.7	< 0.1	112.7
PDCS	15.4	2.6	0.2	66.9
tBDCS	18.7	3.9	0.9	20.3
HMDS	24.8	5.0	1.3	19.0

^{29}Si Solid State NMR was used to determine the number of silicon environments, in order to gauge the success of the grafting. The different functional groups attached to the grafting agents contrasts with the environments the silicon is found in the walls of the powder. To ensure that any extra silicon environments are not the result of unreacted or hydrolysed

(due to the presence of water) grafting agents remaining within the pores, the powder were thoroughly washed and dried (see section 6.2.4). Therefore, it can be assumed that any additional silicon peaks witnessed in the ^{29}Si NMR originate from silane groups attached to the pore walls of the sample. Figure 82 demonstrates the various silicon environments found within TMCS grafted sample, which include Si-O-Si, Si-OH and Si-R bonds.

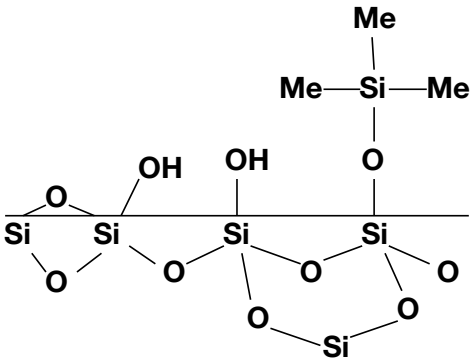

Figure 82 - Examples of likely silicon environments within mesoporous silica functionalised with TMCS, which include Si-O-Si, Si-OH and Si-(R)$_3$

As shown in Figure 83, the ^{29}Si MAS NMR spectra represent the different silicon environments within each sample. The ungrafted sample contains just two environments, with the peak at ~-98 ppm assigned to the (Si-O)$_3$Si-OH and the second at about -110 ppm allocated to (Si-O)$_4$Si.[94] Spectra of the grafted samples all show an additional third silicon environment, which occurs between 10-20 ppm and is indicative of grafted silane molecule.[133] TMCS produces a particularly intense peak, denoting large amounts of trimethysilane groups bound to the walls of the powder. Though HMDS has produced weak porosity, the ^{29}Si NMR does show bound trimethysilyl groups, which aligns with the Si peak found in TMCS at 15 ppm.[95] tBDCS also aligns up with similar grafting agents reported by Fukaya and co-workers, producing a slightly shifted peak at 19 ppm.[134] It can be noted that all grafted sample still retain the silanol peak in their spectra at -100 ppm. Though this is not preferable, it is highly unlikely that all silanol groups would undergo silylation. This would be down to the steric bulk of the grafting agents, particularly in samples such as PDCS and tBDCS. However, this would ensure that other molecules would not

have access to the pore walls. We can see this in the bound silane peak, which intensity is weaker than both the smaller grafting agents.

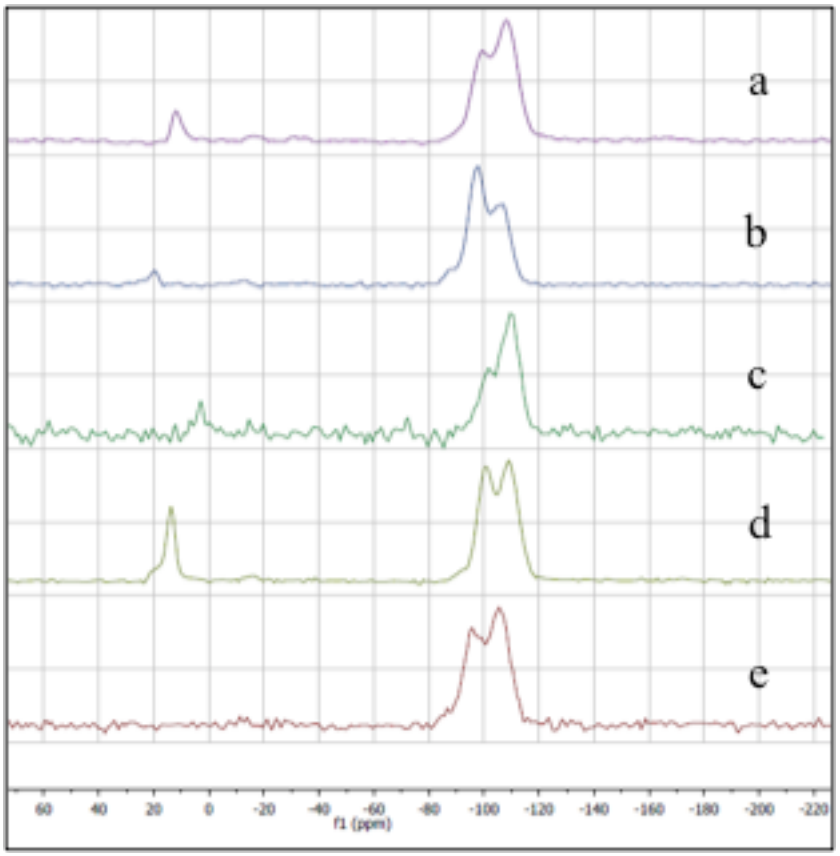

Figure 83 - ^{29}Si MAS-NMR of functionalised mesoporous silica powder samples (a) HMDS, (b) tBDCS, (c) PDCS, (d) TMCS, (e) Ungrafted

In summary, refluxing monochlorosilane molecules in the dry THF has resulted in the successful attachment of grafting agents to the surface of mesoporous silica powders. TMCS and PDCS were the grafting agents that were most successful. This was observed in the nitrogen sorption, showing a slight reduction in both pore volume and width, relative to the size of the grafting agent, whilst retaining large surface areas. Both the CHN analyses denoted the presence of additional amounts carbon present due to the grafting agent. tBDCS and HMDS appeared less successful, with both samples having significantly smaller surface areas. CHN analysis indicated high ratios of nitrogen present that were close in ratio to CTAB. ^{29}Si NMR confirmed the presence of an additional silicon environment for all samples after the grafting process. It possible that the larger steric bulk of HMDS prevent the grafting

agent from diffusing down the pores. The high reactivity of the trimethylsilane group probably reacts with the entrance to the pores as indicated in the ^{29}Si NMR, where a silicon group matching that of TMCS is observed at a lower intensity.

5.4.5 EASA films on sputtered TiN grafted by refluxing in THF

The EASA films were exposed to exactly the same conditions and reagents as the refluxed powders. Before grafting, the films were Soxhlet washed in ethanol (containing 0.1.M HCl) to remove the maximum amount of surfactant from the pores and dried at 130 ˚C (under vacuum). The GISAXS patterns (as shown in Fig. 84) show that they retain their pore structure and survive the refluxing process. All samples show the 10, 11 and 20 peaks, due to the hexagonal arrangement of the pores, at ~2.38 ˚, ~4.13 ˚ and ~4.80 ˚ respectively. However, the patterns are much noisier than the ungrafted film, which can be attributed to the reduction in electron density contrast between pore walls and pore void. The addition of the lighter elements to the pore walls reduced the contrast in electron density between the wall and void.

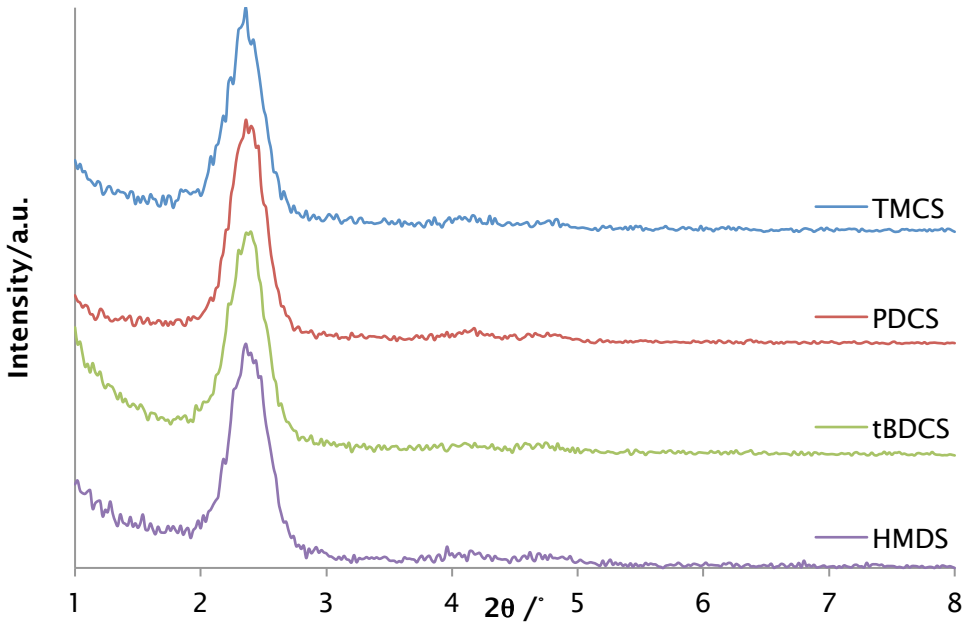

Figure 84 - GISAXS pattern of EASA films grafted with TMCS, PDCS, TBDCS and HMDC

Table 41 – Summary of the data obtained from the in-plane GISAXS patterns of grafted EASA films.

Grafting agents	Peak posn. (2θ/˚)			d_{10} (nm)	a_o (nm)
	10	11	20		
TMCS	2.38	4.13	4.80	3.74	4.32
PDCS	2.37	4.13	4.82	3.72	4.30
tBDCS	2.38	4.18	4.61	3.74	4.32
HMDS	2.37	4.19	4.76	3.72	4.30

Each of EASA films (both grafted and ungrafted) had a water droplet (1 μL) placed on its surface. This was to investigate the behaviour towards water, as the grafting would be expected to have turned the films hydrophobic. The ungrafted sample (see Fig. 85A) demonstrates the hydrophilic nature of the film's surface with the droplet producing a contact angle of 61 ˚. The water droplet shows a strong attraction to the surface of the film. All grafted sample undergo a hydrophobic response to the water droplet, with the largest contact angle of 97 ˚ from tBDCS (see Fig. 85E). This was because it was the most hydrophobic grafting agent, due to the tert-butyldimethylsilane groups. Though this does not indicate that grafting of the internal pore walls, it does indicate the grafting agent has successfully bound the exterior of the films.

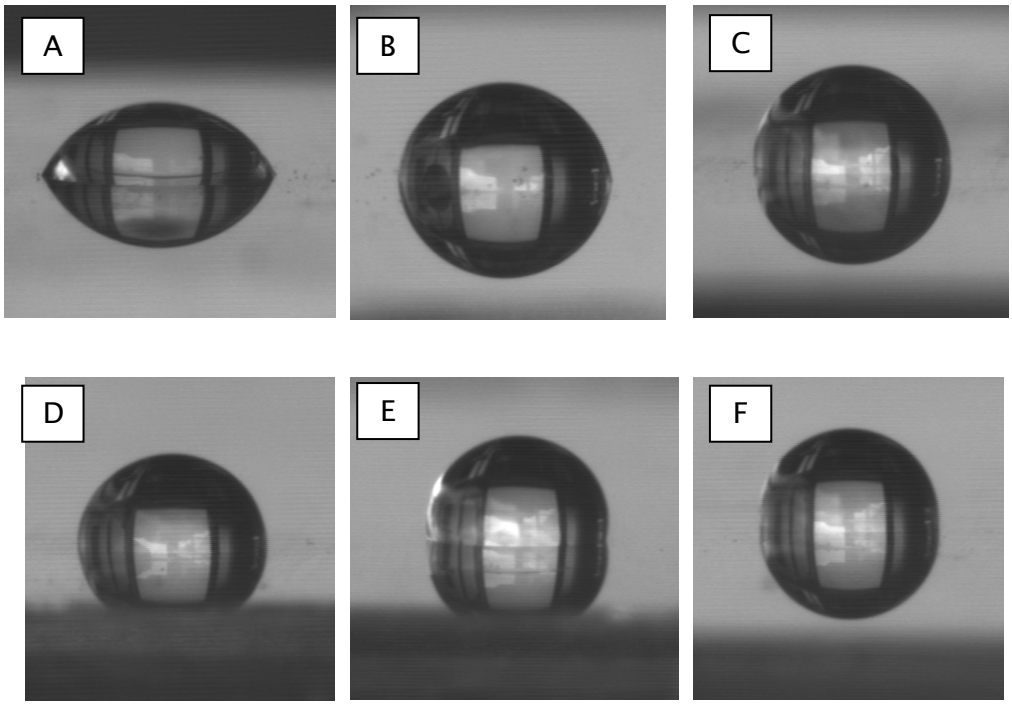

Figure 85 – Images of water droplets on the surface of EASA films: (A) EASA film, (B) TiN, (C) TMCS (D) PDCS (E) tBDCS (F) HMDS

Table 42 - Summary of contact angle results

Grafting agent	Contact angle (°)
Ungrafted	61
Plain TiN	79
TMCS	89
PDCS	84
tBDCS	97
HMDS	90

5.4.6 Grafting EASA films on Si-Mat TiN

The supply of TiN changed during the SCFED project to Si-Mat (Silicon Materials), who produced film of lower resistivity, which were deposited on the

silicon by Si-Mat with a thickness of 300 nm. This resulted in a change in the behaviour of the TiN film, requiring the reoptimisation of the conditions required to grow the template (see Section 4.7). The films on “new” produced identical in-plane GISAXS patterns as those produced on the sputtered TiN.

The films were fabricated on a masked electrode, which defined an exposed area of TiN surrounded by 200 nm thick silica film. This was to provide insulation to the surrounding electrode surface during electrodeposition. The EASA film is only deposited in this area. The films altered the colour of the new TiN from grey to dark purple (shown in Fig. 86). Using the synthesis conditions established in section 5.4.4, the films were refluxed in their respected grafting agents whilst suspended in THF under inert atmosphere. The films were repeatedly washed with THF (3*x*20 mL) and Et_2O (3*x*20 mL) to remove any remaining reagents from the film. This included Soxhlet washing each film with Et_2O, followed by drying under vacuum at 130 ˚C. In-plane GISAXS showed a slight reduction in the 11 and 20 feature in the scattering patterns when compared with an untreated film (see Fig. 87). This was expected due to the grafted molecule reducing the contrast between the pore void and wall. As a result, this reduced the amount of coherent X-ray scattering given off by the films. No degradation was witnessed in the diffraction pattern after the films were exposed to the Soxhlet washings.

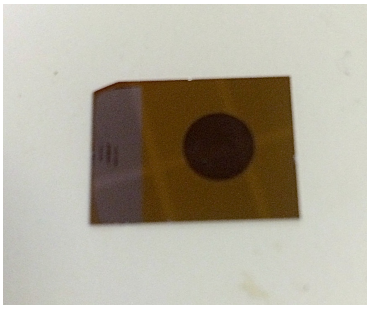

Figure 86 - Image of the masked TiN electrode

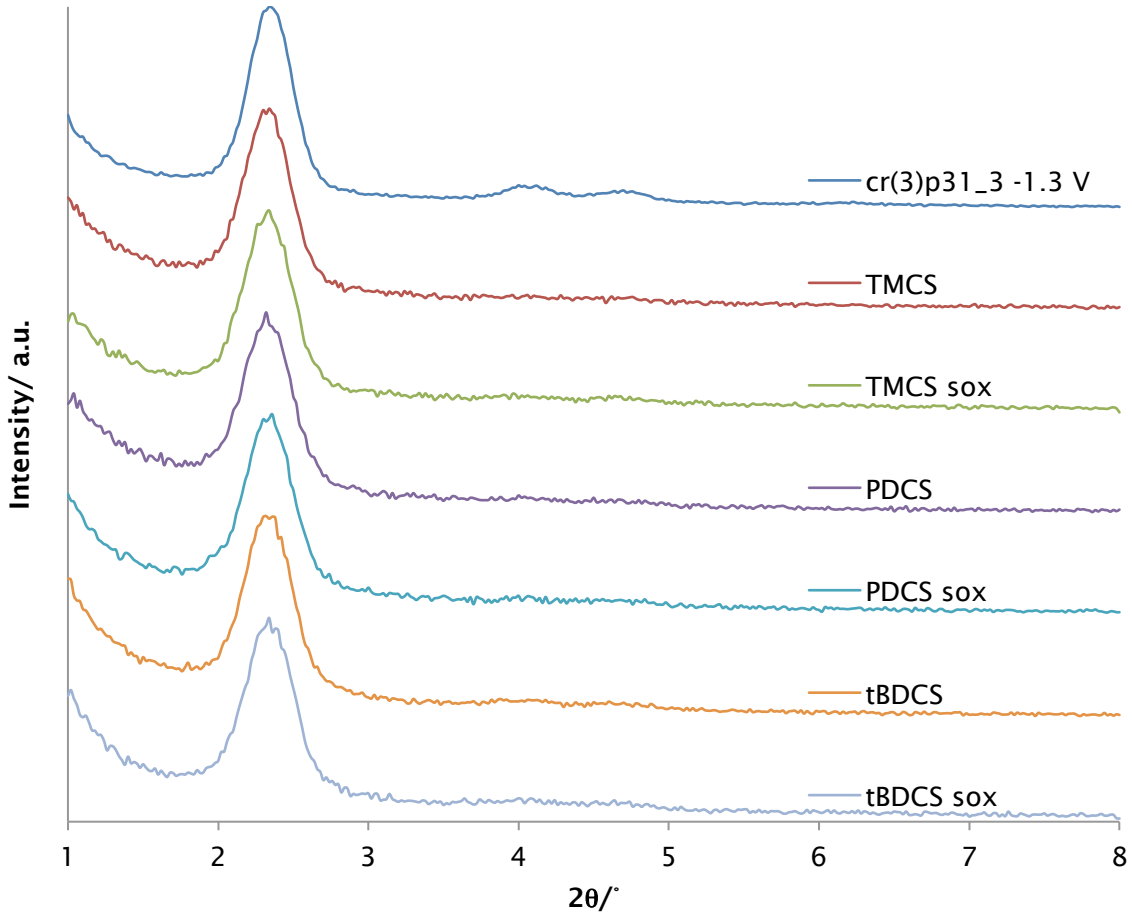

Figure 87 - In-plane GISAXS pattern comparing the original EASA film with grafted and Soxhlet washed films

5.4.6.1 Ellipsometric porosimetry of grafted EASA films

The ellipsometric porosimetry of the untreated Si-Mat EASA films has shown them to have a porosity of 40.3 % with toluene solvent (see section 4.7). The addition of the grafting agent to the walls of the films was expected to decrease the porosity, as well as reduce the pore diameter. Different responses are expected for each of the solvents based on their interaction with the pore wall. For example, as the pores are made more hydrophobic would lower the chance of water condensing within them.

5.4.6.2 Trimethylchlorosilane

It was established with grafting of mesoporous silica powder that TMCS reduced the PSD by 0.2 nm using BET. The resulting porosity from each of the solvents indicated that the TMCS has successfully attached to the pore walls of the sample. The resulting isotherms are aligned with Type I for toluene, Type II the other organic solvents, whereas it is Type III for water (see Fig. 88). The organic solvents showed relatively constant porosity results of around 30 %, whereas the water only reached 7.7 % (see Table 43). This implies that the water is struggling to enter the pore structure and change the density of the film. The three organic solvents are able to enter and condense in the pore structure. When compared against the ungrafted sample, the porosity has dropped by ~10 %. Again this suggests that the grafting agent reduces the pore diameter of the films. The PSD of toluene and IPA result in slight decrease in the pore diameter when compared against the untreated sample using DR method. Modified Kelvin equation produced a pore radius significantly larger than expected by almost two-fold. This can be attributed to an increase in the affinity of the solvent with the film. As a result, larger amounts of organic molecules collect within the pores of the film. This increases the density of the pores, resulting in a larger than expected pore radius.

Table 43 - Summary of data acquired from ellipsometric porosimetry from TMCS grafted films

Solvent	Porosity (%)	Mod. Kelvin Eq radius (nm)	DR radius (nm)
Toluene	30.4	$1.57_{abs}/1.57_{des}$	$0.77_{abs}/0.76_{des}$
Water	7.7	/	/
IPA	30.7	$1.43_{abs}/1.42_{des}$	$0.65_{abs}/0.68_{des}$
Methanol	29.26	/	/

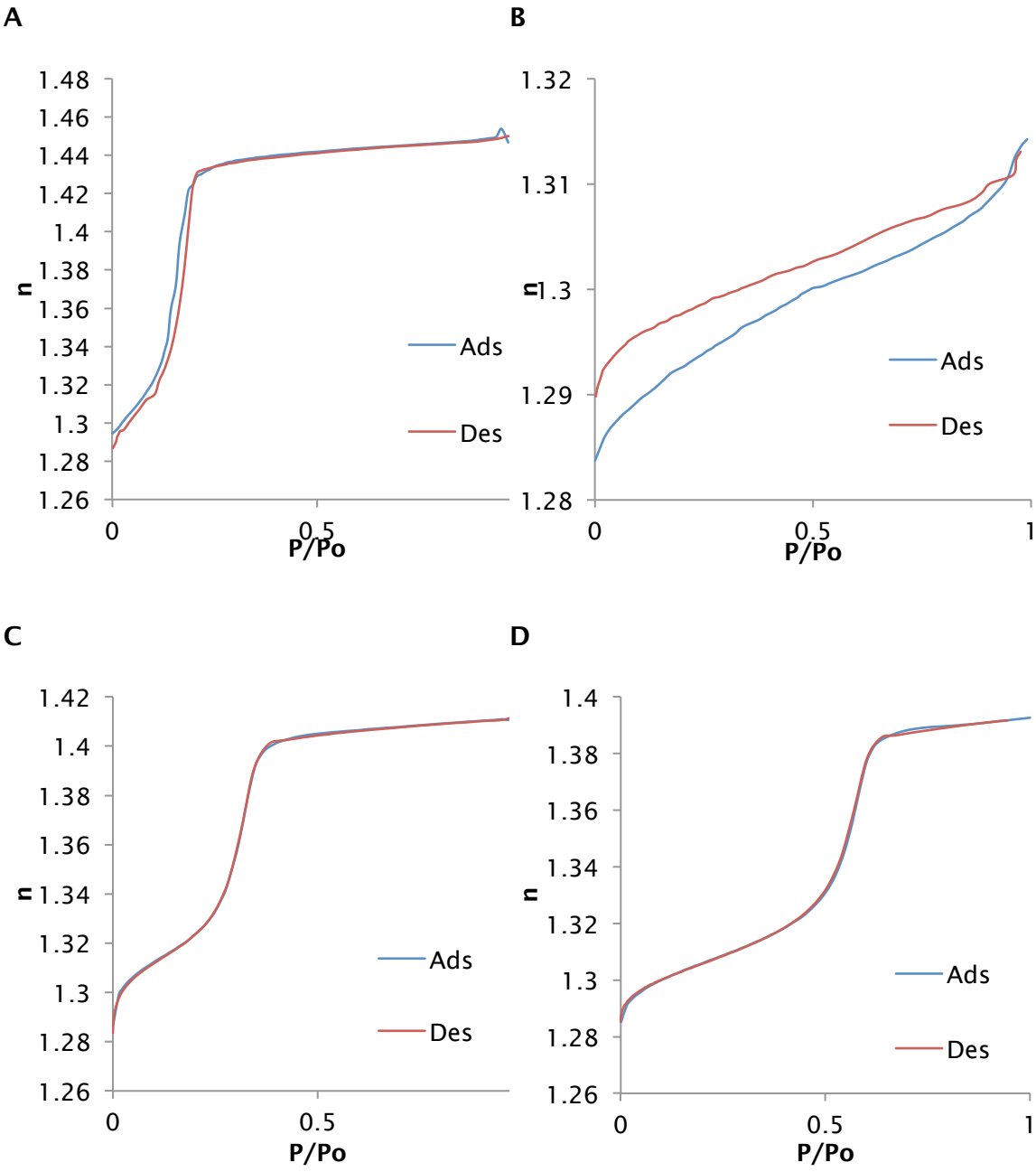

Figure 88 – EP adsorption-desorption isotherms of TMCS grafted films (A) Toluene (B) Water, (C) IPA, (D) Methanol (n, reflective index)

5.4.6.3 Phenyldimethylchlorosilane (PDCS)

PDCS is expected to decrease the pore size further than TMCS as seen in the work on mesoporous silica powders. This increase in volume of the grafting agent may also find it harder to diffuse down the pores of the film and react with the walls. The behaviour of the water isotherm differs from the organic solvents. It's behaviour is that of a Type III isotherm, indicating the existence

of macropores (see Fig. 89B). However, the porosity of the sample shows that water is entering the pore structure, as it has increased to 18.8 % and the organic solvents are still at ~29 % (see Table 44). Combining all these results it appears that PDCS is only partially functionalising the walls of the film. This was concluded based on the hysteresis loop present in the Type IV isotherms with the organic solvents (Fig 89A,C and D), which signifies the occurrence of bottlenecking of the pore. As a result, it appears the PDCS is only functionalising the entrance of the pore. To back this up further, an extra peak in the desorption curves was witnessed in the PSD when analysed using the modified Kelvin equation for the organic solvents. This is also seen in the contact angle study, which showed the agent has made the film's surface more hydrophobic. Therefore a number of partially grafted pores were present within the film.

Table 44 - Summary of data acquired from ellipsometric porosimetry from PDCS grafted films

Solvent	Porosity (%)	Mod. Kelvin Eq. radius (nm)	DR radius (nm)
Toluene	29.0	1.25_{ads} /1.22_{des}	0.84_{abs}/0.88_{des}
Water	18.8	/	/
IPA	28.4	1.16_{ads} /1.15_{des}	0.68_{abs}/0.69_{des}
Methanol	/	/	/

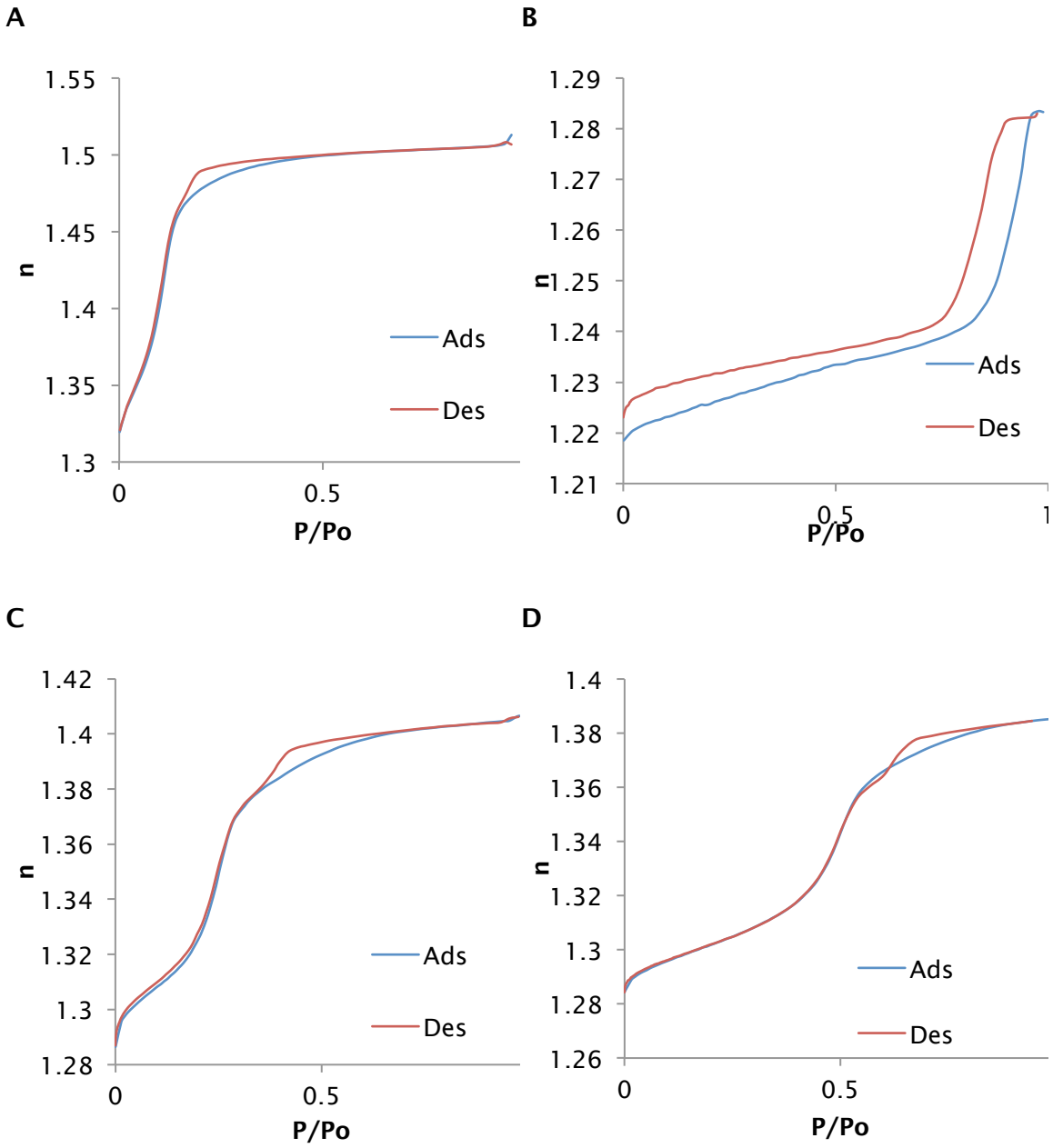

Figure 89 - EP adsorption-desorption isotherms of PDCS grafted films (A) Toluene (B) Water, (C) IPA, (D) Methanol (n, reflective index)

5.4.6.4 tert-Butyldimethylchlorosilane (tBDCS)

Comparing results obtained from the sample grafted with tBDCS with the ungrafted film, little change in the isotherms was found (see Fig. 90). As a result, it can be concluded that tBDCS was unsuccessful at attaching to the pore walls. If the grafting had been effective with tBDCS, then a hydrophobic response to water would have been expected as seen with TMCS. However, a

hydrophilic response was observed similar to that of the ungrafted film based on the porosity of the film using water (see Table 45). The contact angle study showed that the sample had the most hydrophobic response to the water droplet, but that only takes into account the sample's surface (see section 5.4.5). This may have been the result of tBDCS struggling to diffuse down the pore channels, due to the grafting agent's steric bulk.

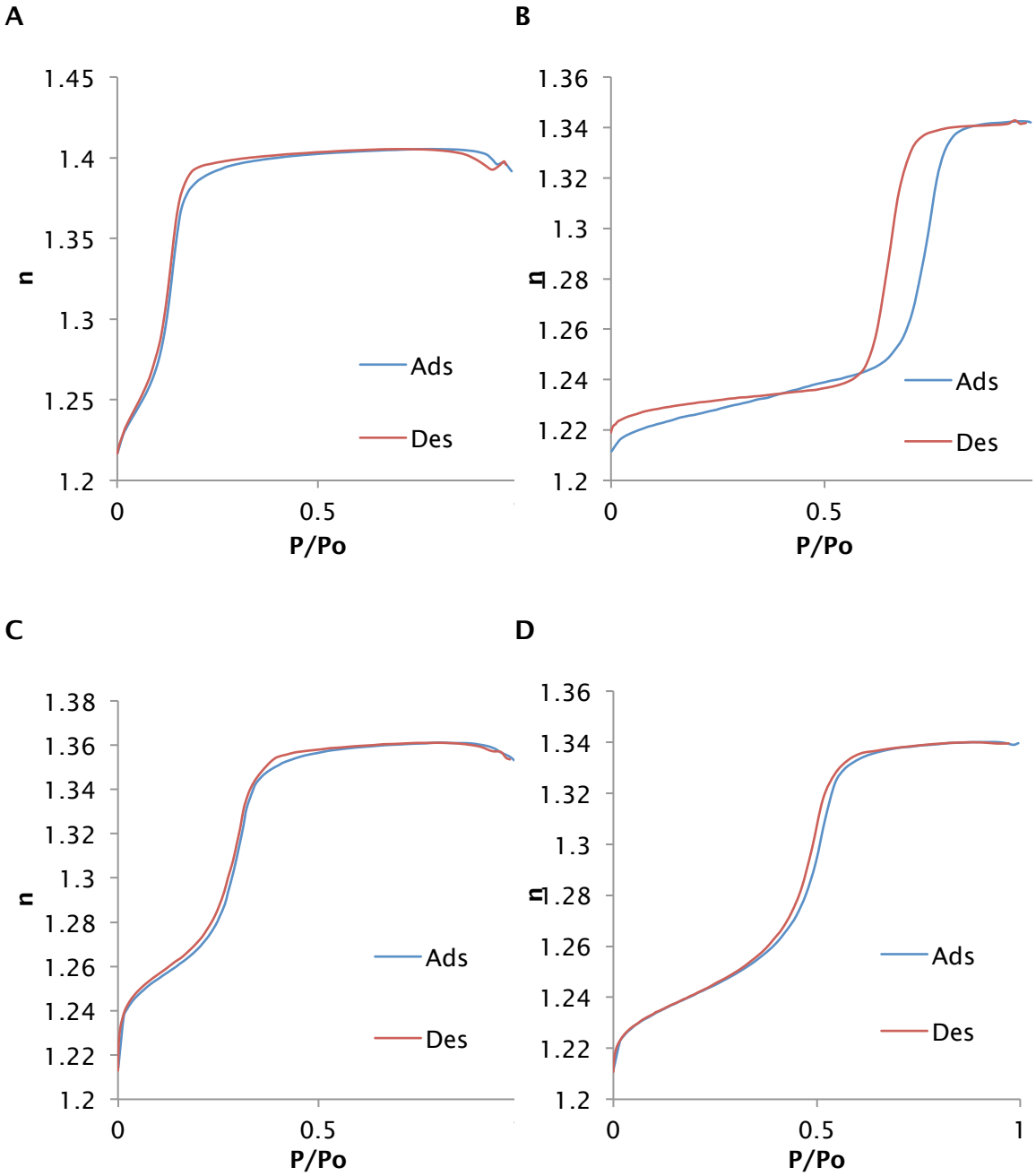

Figure 90 - EP adsorption-desorption isotherms of tBDCS grafted films (A) Toluene (B) Water, (C) IPA, (D) Methanol (n, reflective index)

Table 45 - Summary of data acquired from ellipsometric porosimetry from tBDCS grafted films

Solvent	Porosity (%)	Mod. Kelvin Eq. radius (nm)	DR radius (nm)
Toluene	37.3	1.38_{ads} /1.33_{des}	0.75_{ads} /0.77_{des}
Water	35.8	77.5_{ads} /69_{des}	/
IPA	38.7	1.33_{ads} /1.31_{des}	0.51_{ads} /0.56_{des}
Methanol	36.8	/	/

5.5 Summary

In this chapter two different methods for modifying the pore diameter and chemical properties have been applied to both mesoporous silica films and powders have been demonstrated. Initially the mesoporous silica powders were used to establish an efficient method of functionalising the pore walls. It was concluded that refluxing in dry THF was the best method for attaching monochlorosilane molecules. This was confirmed using nitrogen sorption and XRD showed that the pore structure endured the process. Extra silicon environments were observed in the ^{29}Si NMR, signifying that the functionalised silane molecules remained within the pore structure of the sample.

This method was then transferred onto the EASA silica films. In-plane GISAXS patterns of the grafted samples confirmed that the pore structure had survived the grafting process. Transferring the EASA films onto TiN had enabled the porosity of the samples to be determined using EP. TMCS and PDCS molecules have been attached to the surface of an EASA film based on an increase in hydrophobic response to water. TMCS provide to be the most successful grafting agent, most likely due to its smaller steric bulk, enabling the molecule to readily diffuse down the 1.6 nm pore channels. As a result, no porosity was observed in the film when water was used. This indicates that the walls of the pores had been successfully made hydrophobic due to the presence of methyl group. The organic solvents were still however able to enter the film, indicating that the pore structure was intact. A reduction in the porosity of the films also was witnessed; further confirming the grafting agent reduced the size of the pore. The pore diameter of the films remains inconclusive as the addition of organic groups to the walls of the pores lead to PSD results larger than the ungrafted sample. Both the Kelvin equation and DR had been converted to suit EP, but they do not fully account for the attraction between the solvent and the functionalised pore. PDCS showed partial functionalisation of the pore walls and it is believed that its steric bulk prevented it from fully diffusing down the pore channels. Whereas, tBDCS showed no sign of functionalisation as its isotherms were similar to that of the ungrafted EASA film.

A possible next step for this work might be the addition of different metal oxides to the surface of the film. For example, the addition of aluminium oxide to the surface of MCM 41 has shown to dramatically increase the stability of silica in steam.[65] Further investigations into using EP to examine changes in pore expansion caused by swelling agents would be of great interest. Post-synthesis grafting of these films may indicate that increasing the pore diameter may result in improved functionalisation when using larger silane molecules.

Chapter 6 – Conclusion and future work

The goal of this project was the synthesis of nanoporous templates with vertically aligned pore channels to be used in the growth of nanowires via SCFED. This was achieved using a Stöber-derived hydrothermal route and EASA electrochemical route. Both techniques required negatively charged surfaces for the films to remain well adhered to their supports. The silica films were successfully grown on TiN for the first time. Growing the films directly onto the reflective surface of TiN enabled the porosity of EASA samples using ellipsometric porosimetry. The 1.6 nm pore size closely matched that observed by TEM. This was also the first time He-ion microscopy was used to image these types of silica film, which confirmed that both methods produced open pore structures.

The Stöber-derived films had strong vertically aligned pores structure, as witnessed in both the in-plane GISAXS patterns and cross-sectional TEM imaging. Pore size (2.6 nm) was increased with the addition of swelling agents TMB and TIPB and reduced by decreasing the Alky tail length of the surfactant. A relationship was found between the bases used in the fabrication of the Stöber films and the uptake of swelling agent. In the case of TMB, ammonia was found to increase the effect of the swelling agent. Et_3N restricts it the uptake of TMB presumably as it dissolves in a similar position within the micelle, which agrees with Sayari *et al*.[59] This was reversed with the addition of TIPB. Addition of sodium bicarbonate to the Stöber sol resulted in a dramatic over three-fold increase in film thickness.

In the case of the Stöber-derived method, improvement in the pore ordering might be achievable using Gemini surfactants. Ma *et al* achieved highly ordered vertically aligned pore channels on silicon using a Gemini surfactant in an evaporation induced surfactant assembly (EISA) process.[135] The higher charge density on the polar head may encourage stricter tubular micelle alignment. Recent work by Kao *et al* demonstrated that the addition of decane improved the ordering of the Stöber films.[60] They achieved hexagonally

ordered pores with diameters as large as 5.7 nm, which could be grown on different substrates.

Urea was shown to be an effective catalyst for the fabrication of Stöber-derived films due to the slow release of ammonia. This steady adjustment to the pH has enabled the formation of inorganic oxide nanoparticles with uniform sizes[108] and the synthesis of mesoporous titania/silica powders.[136] As a result, it would be of interest to see if the Stöber method can incorporate aluminium or titanium into its framework. The addition of aluminium into mesoporous silica to form aluminosilicates has shown to dramatically increase the stability of the framework.[65,137,138]

A higher degree of hexagonal pore ordering was achieved in the EASA synthesis of porous silica on ITO, TiN and Au. Altering the orientation of the support during the growth from horizontal to vertical resulted in a reduction the silica particulates on the surface of the films relative to that reported by Walcarius *et al*.[78] Like the Stöber film, the pore size of the template could be altered by the addition of swelling agents and changing the surfactant tail length. Mesoporous silica powders were used to establish a grafting method, which was applied to the EASA films. This was based on the addition of functionalised monochlorosilane molecules in the presence of THF, which could accept protons from the silanol groups present at the films surface. EP could be performed on the samples to establish changes in porosity, which was only possible with films that had been grown on TiN. TMCS was found to be the most successful grafting agent based on the size of the molecule, which enabled it to diffuse more readily down the 1.6 nm pore channels. Larger grafting agents led to incomplete coverage of the pore walls. An interesting follow up study would be to graft into films that have had swelling agents added as the pore diameter was increased to ~2.4 nm. Increasing the pore size as shown with TMB may enable larger grafting agents to access to the pore channel. Tatsuda *et al* found that $Ti(O^{i}Pr)_4$ in $scCO_2$ could penetrate pores diameter as low as 2.3 to 2.7 nm, whereas in liquid IPA it could not enter channels less than 3.5 nm.[139] Utilising expertise available from this project, supercritical solvents could improve surface coverage of the grafting agents.

Also supercritical fluids have been shown to be more effective than liquid solvents at removing surfactant from the high-aspect ratio pores and avoid oxidising the TiN's surface.[140,141]

The deposition of Sn into the EASA film was attempted via SCFED. The electrochemistry and EDX mapping of the film's cross-section indicated the presence of tin within the template, though no nanowires in the TEM. It was concluded that the growth of the nanowires was occurring within a very small number of pores with in any specific region of the film, which would restrict the growth of surrounding nanowires based on reduced diffusion length. Further work is needed to optimise the deposition process, which should include pulsed electrodeposition. This has been shown to improve the quality of nanowires when depositing into high-aspect ratio pores with slow diffusion rates.[142]

Using the conditions established with silica sols led to films with no observable porosity when TEOS was replaced with titania precursors. This was attributed the positive charge that developed at the metal centre opposed to silica which has a negative charge. This meant that titania could not coordinate with CTAB, instead resulting in the bulk precipitation during electrodeposition. Though anionic surfactant SDS was used instead of CTAB, instead of forming discrete micelle in solution it reacted with the titanate species (H_2O^+-Ti-O-S(O)$_3C_{12}H_{25}$). However this positive charge could to utilised in a similar manner to CTAB.

The fabrication of EASA films on graphene would be of particular interest in the development of electrical and optical devices. Its great strength and high electrical conductivity would allow for the creation of ultra thin devices. Mesoporous silica films have been shown to grown on graphene oxide with vertically aligned pore channels.[51] The addition of insulating mesoporous scaffolding to perovskite solar cells have been shown to increase the power-conversion efficiency.[143] Utilising both of these methods to build multi-layered devices may be to further maximise the perovskite power-conversion efficiency by tailoring the film thicknesses to the wavelength of light. This would be of

great interest in the creation of cheap and effective solar cells. It utilises the silica templates fabricated in this thesis and the technique (SCFED) they were created to test.

Bibliography

1. C. Acikgoz, M. A. Hempenius, J. Huskens, and G. J. Vancso, *Eur. Polym. J.*, 2011, **47**, 2033

2. O. Vazquez-Mena, L. Gross, S. Xie, L. G. Villanueva, and J. Brugger, *Microelec. Eng.*, 2015, **132**, 236–254

3. J. M. Blackburn, D. P. Long, A. Cabanas, and J. J. Watkins, *Science*, 2001, **294**, 141

4. V. Cauda, B. Torre, A. Falqui, G. Canavese, S. Stassi, T. Bein, and M. Pizzi, *Chem. Mater.*, 2012, **24**, 4215

5. X. Wu, J. S. Kulkarni, G. Collins, N. Petkov, J. J. Boland, D. Erts, and J. D. Holmes, *Chem. Mater.*, 2008, **20**, 5954

6. J. a. Darr and M. Poliakoff, *Chem. Rev.*, 1999, **99**, 495

7. R. A. Williams and S. Naiditch, *Phys. Chem. Liq.*, 1970, **8**, 67

8. H. Yoshida, M. Sone, H. Wakabayashi, H. Yan, K. Abe, X. T. Tao, A. Mizushima, S. Ichihara, and S. Miyata, *Thin Solid Films*, 2004, **446**, 194

9. H. Yan, M. Sone, N. Sato, S. Ichihara, and S. Miyata, *Surf. Coat. Technol.*, 2004, **182**, 329

10. M. M. Rahman, M. Sone, H. Uchiyama, M. Sakurai, S. Miyata, T. Nagai, Y. Higo, and H. Kameyama, *Surf. Coatings Technol.*, 2007, **201**, 7513

11. J. Ke, W. Su, S. M. Howdle, M. W. George, D. Cook, M. Perdjon-Abel, P. N. Bartlett, W. Zhang, F. Cheng, W. Levason, G. Reid, J. Hyde, J. Wilson, D. C. Smith, K. Mallik, and P. Sazio, *PNAS*, 2009, **106**, 14768

12. J. Ke, P. N. Bartlett, D. Cook, T. L. Easun, M. W. George, W. Levason, G. Reid, D. Smith, W. Su, and W. Zhang, *Phys. Chem. Chem. Phys.*, 2012, **14**, 1517

13. J. A. Branch, D. A. Cook, and P. N. Bartlett, *Phys. Chem. Chem. Phys.*, 2015, **17**, 261

14. D. Cook, P. N. Bartlett, W. Zhang, W. Levason, G. Reid, J. Ke, W. Su, M. W. George, J. Wilson, D. Smith, K. Mallik, E. Barrett, and P. Sazio, *Phys. Chem. Chem. Phys.*, 2010, **12**, 11744

15. P. N. Bartlett, M. Perdjon-Abel, D. Cook, G. Reid, W. Levason, F. Cheng, W. Zhang, M. W. George, J. Ke, R. Beanland, and J. Sloan, *Chem. Electro. Chem*, 2014, **1**, 187

16. M. Skerget, Z. Knez, and M. Knez-Hrncic, *J. Chem. Eng. Data*, 2011, **56**, 694

17. N. R. B. Coleman, K. M. Ryan, T. R. Spalding, J. D. Holmes, and M. A. Morris, *Chem. Phys. Lett.*, 2001, **343**, 2

18. N. R. Coleman, M. a Morris, T. R. Spalding, and J. D. Holmes, *J. Am. Chem. Soc.*, 2001, **123**, 187

19. J. Yang, J. R. Hyde, J. W. Wilson, K. Mallik, P. J. Sazio, P. O'Brien, M. a. Malik, M. Afzaal, C. Q. Nguyen, M. W. George, S. M. Howdle, and D. C. Smith, *Adv. Mater.*, 2009, **21**, 4115

20. G. Aksomaityte, F. Cheng, A. L. Hector, J. R. Hyde, W. Levason, G. Reid, D. C. Smith, J. W. Wilson, and W. Zhang, *Chem. Mater.*, 2010, **22**, 4246

21. B. Finney and M. Jacobs, *Wikipedia*, 2010, https://en.wikipedia.org/wiki/Supercritical_fluid#.

22. A. Cabañas, X. Shan, and J. J. Watkins*, *Chem. Mater.*, 2003, **15**, 2910

23. B. D. Wang, W. L. Zhou, B. F. Mccaughy, J. E. Hampsey, X. Ji, Y. Jiang, H. Xu, J. Tang, R. H. Schmehl, C. O. Connor, C. J. Brinker, and Y. Lu, *Adv. Mater.*, 2003, **15**, 130

24. A. Keilbach, J. Moses, R. Köhn, M. Döblinger, and T. Bein, *Chem. Mater.*, 2010, **22**, 5430

25. H.-J. Wang, C.-W. Zou, B. Yang, H.-B. Lu, C.-X. Tian, H.-J. Yang, M. Li, C.-S. Liu, D.-J. Fu, and J.-R. Liu, *Electrochem. Commun.*, 2009, **11**, 2019

26. C. Xu, M. Li, X. Zhang, K.-N. Tu, and Y. Xie, *Electrochim. Acta*, 2007, **52**, 3901

27. G. S. Attard, P. N. Bartlett, N. R. B. Coleman, J. M. Elliott, J. R. Owen, and J. H. Wang, *Science.*, 1997, **278**, 838

28. D. H. Everett, *Pure Appl. Chem*, 1972, **31**, 577–638

29. B. Platschek, A. Keilbach, and T. Bein, *Adv. Mater.*, 2011, **23**, 2395

30. A. M. Md Jani, D. Losic, and N. H. Voelcker, *Prog. Mater. Sci.*, 2013, **58**, 636

31. W. Lee, R. Ji, U. Gösele, and K. Nielsch, *Nature. Mater.*, 2006, **5**, 741

32. S. Alami-younssi, C. Kiefer, A. Larbot, M. Persin, and J. Sarrazin, *J. Membr. Sci.*, 1998, **143**, 27

33. J. Randon, P. Blanc, and R. Paterson, *J. Memb. Sci.*, 1995, **98**, 119

34. A. Mutalib Md Jani, I. M. Kempson, D. Losic, and N. H. Voelcker, *Angew. Chem. Int. Ed.*, 2010, **49**, 7933

35. A. Mutalib Md Jani, E. J. Anglin, S. J. P. McInnes, D. Losic, J. G. Shapter, and N. H. Voelcker, *Chem. Commun.*, 2009, 3062

36. A. L. Hector, *Chem. Soc. Rev.*, 2007, **36**, 1745

37. C. T. Kresge, M. E. Leonowicz, W. J. Roth, J. C. Vartuli, and J. S. Beck, *Nature*, 1992, **359**, 710

38. G. S. Attard, J. C. Glyde, and C. G. Goltner, *Nature*, 1995, **378**, 366

39. N. R. . Coleman and G. S. Attard, *Micro. Meso. Mater.*, 2001, **44-45**, 73

40. J. M. Elliott, G. S. Attard, P. N. Bartlett, N. R. B. Coleman, D. A. S. Merckel, and J. R. Owen, *Chem. Mater.*, 1999, 3602

41. I. Nandhakumar, J. M. Elliott, and G. S. Attard, *Chem. Mater*, 2001, **13**, 3840

42. T. Gabriel, I. S. Nandhakumar, and G. S. Attard, *Electrochem. Commun.*, 2002, **4**, 610

43. X. Li, I. S. Nandhakumar, T. Gabriel, G. S. Attard, M. L. Markham, D. C. Smith, J. J. Baumberg, K. Govender, P. O'Brien, and D. Smyth-Boyle, *J. Mater. Chem.*, 2006, **16**, 3207

44. G. J. D. a a Soler-Illia, C. Sanchez, B. Lebeau, and J. Patarin, *Chem. Rev.*, 2002, **102**, 4093

45. A. Monnier, F. Schüth, Q. Huo, D. Kumar, D. Margolese, R. S. Maxwell, G. D. Stucky, M. Krishnamurty, P. Petroff, A. Firouzi, M. Janicke, and B. F. Chmelka, *Science.*, 1993, **261**, 1299

46. H. Yang, A. Kuperman, N. Coombs, S. Mamiche-Afara, and A. Ozin, G, *Nature*, 1996, **379**, 703

47. C. J. Brinker, Y. Lu, A. Sellinger, and H. Fan, *Adv. Mater.*, 1999, **11**, 579

48. E. K. Richman, T. Brezesinski, and S. H. Tolbert, *Nature. Mat*, 2008, **7**, 712

49. Z. Teng, G. Zheng, Y. Dou, W. Li, C.-Y. Mou, X. Zhang, A. M. Asiri, and D. Zhao, *Angew. Chem. Int. Ed.*, 2012, **51**, 2173

50. W. Stöber, A. Fink, and E. Bohn, *J. Colloid. Interf. Sci*, 1968, **26**, 62

51. Z.-M. Wang, W. Wang, N. Coombs, N. Soheilnia, and G. A. Ozin, *ACS Nano*, 2010, **4**, 7437

52. A. Walcarius, E. Sibottier, M. Etienne, and J. Ghanbaja, *Nature. Mat*, 2007, **6**, 602

53. G. H. A. Therese and P. V. Kamath, *Chem. Mater.*, 2000, **12**, 1195

54. Z. Yang, Z. Niu, X. Cao, Z. Yang, Y. Lu, Z. Hu, and C. C. Han, *Angew. Chem. Int. Ed.*, 2003, **42**, 4201

55. B. Platschek, N. Petkov, and T. Bein, *Angew. Chem. Int. Ed.*, 2006, **118**, 1152

56. B. Platschek, N. Petkov, D. Himsl, S. Zimdars, Z. Li, R. Köhn, and T. Bein, *J. Am. Chem. Soc.*, 2008, **130**, 17362

57. A. Fukuoka, I. Kikkawa, Y. Sasaki, A. Shimojima, and T. Okubo, *Langmuir*, 2009, **25**, 10992

58. T. Sakai, H. Yano, H. Shibata, T. Endo, K. Sakamoto, H. Fukui, N. Koshikawa, H. Sakai, and M. Abe, *Colliods. Surf. A*, 2010, **371**, 29

59. A. Sayari, Y. Yang, M. Kruk, and M. Jaroniec, *J. Phys. Chem. B*, 1999, **103**, 3651

60. K.-C. Kao, C.-H. Lin, T.-Y. Chen, Y.-H. Liu, and C.-Y. Mou, *J. Am. Chem. Soc.*, 2015, **137**, 3779

61. S. Goubert-Renaudin, F. Gaslain, C. Marichal, B. Lebeau, R. Schneider, and A. Walcarius, *New J. Chem.*, 2009, **33**, 528

62. M. M. Mekawy, A. Yamaguchi, S. a El-Safty, T. Itoh, and N. Teramae, *J. Colloid. Interf. Sci*, 2011, **355**, 348

63. J. S. Beck, J. C. Vartuli, W. J. Roth, M. E. Leonowicz, C. T. Kresge, K. D. Schmitt, C. T.-W. Chu, E. W. Olson, E. W. Sheppard, S. B. McCullen, J. B. Higgins, and J. L. Schlenkert, *J. Am. Chem. Soc.*, 1992, **114**, 10834

64. M. Schoeffel, N. Brodie-Linder, F. Audonnet, and C. Alba-Simionesco, *J. Mater. Chem.*, 2012, **22**, 557

65. J. T. Tompkins and R. Mokaya, *ACS Appl. Mater. Interfaces*, 2014, **6**, 1902

66. M. D. Jones, R. Raja, J. M. Thomas, B. F. G. Johnson, D. W. Lewis, J. Rouzaud, and K. D. M. Harris, *Angew. Chem. Int. Ed.*, 2003, **42**, 4326

67. D. J. Macquarrie, *Chem. Commun.*, 1996, **2**, 1961

68. M. H. Lim, C. F. Blanford, and A. Stein, *J. Am. Chem. Soc*, 1997, **119**, 4090

69. S. L. Burkett, S. D. Sims, and S. Mann, *Chem. Commun.*, 1996, 1367

70. G. Herzog, E. Sibottier, M. Etienne, and A. Walcarius, *Faraday Discuss.*, 2013, **164**, 259

71. M. Etienne and A. Walcarius, *Electrochem. Commun.*, 2005, **7**, 1449

72. P. Bernado, E. Mylonas, M. V Petoukhov, M. Blackledge, and D. I. Svergun, *J. Am. Chem. Soc*, 2007, **129**, 5656

73. A. Sasaki, *Rigaku J.*, 2005, **22**, 31

74. K. Omote, Y. Ito, and S. Kawamura, *Appl. Phys. Lett.*, 2003, **82**, 544

75. Y. Ito, *Rigaku J.*, 2009, **25**, 1

76. A. Ogi and K. Inaba, *Rigaku J.*, 2011, **27**, 1

77. Smilgies, *Wikipedia*, 2008, https://commons.wikimedia.org/wiki/File:GISAXS.png

78. A. Goux, M. Etienne, E. Aubert, C. Lecomte, J. Ghanbaja, and A. Walcarius, *Chem. Mater.*, 2009, **21**, 731

79. Y. Guillemin, J. Ghanbaja, E. Aubert, M. Etienne, and A. Walcarius, *Chem. Mater.*, 2014, **26**, 1848

80. M. Mouanga, M. Puiggali, B. Tribollet, V. Vivier, N. Pébère, and O. Devos, *Electrochim. Acta*, 2013, **88**, 6

81. S. Rodrigues, N. Munichandraiah, and A. K. Shukla, *J. Power Sources*, 2000, **87**, 12

82. S. J. Lenhart, D. D. Macdonald, and B. G. Pound, *J. Electrochem. Soc.*, 1988, **135**, 1063

83. D. C. Joy and C. S. Joyt, *Micron*, 1996, **27**, 247

84. A. M. Donald, *Nature. Mat.*, 2003, **2**, 511

85. J. C. Meyer, C. O. Girit, M. F. Crommie, and A. Zettl, *Nature*, 2008, **454**, 319

86. T. Ishitani, H. Tsuboi, T. Yaguchi, and F. Koike, *J. Electron. Microsc*, 1994, **43**, 322

87. G. Hlawacek, I. Ahmad, M. a. Smithers, and E. S. Kooij, *Ultramicroscopy*, 2013, **135**, 89

88. A. S. Terpstra, K. E. Shopsowitz, C. F. Gregory, A. P. Manning, C. a Michal, W. Y. Hamad, J. Yang, and M. J. MacLachlan, *Chem. Commun.*, 2013, **49**, 1645

89. R. Hill and F. H. M. Faridur Rahman, *Nucl. Instrum. Methods Phys. Res., Sect. A*, 2011, **645**, 96

90. I. Langmuir, *J. Am. Chem. Soc*, 1918, **40**, 1361

91. E. P. Barrett, L. G. Joyner, and P. P. Halenda, *J. Am. Chem. Soc.*, 1951, **73**, 373

92. K. S. W. Sing, D. H. Everett, R. A. W. Haul, L. Moscou, R. A. Pierotti, J. Rouquerol, and T. Siemieniewska, *Pure Appl. Chem.*, 1985, **57**, 603

93. M. R. Baklanov, K. P. Mogilnikov, V. G. Polovinkin, and F. N. Dultsev, *J. Vac. Sci. Technol. B*, 2000, **18**, 1385

94. R. Simonutti, A. Comotti, S. Bracco, and P. Sozzani, *Chem. Mater.*, 2001, **13**, 771

95. X. S. Zhao and G. Q. Lu, *J. Phys. Chem. B*, 1998, **102**, 1556

96. B. Avasarala and P. Haldar, *Electrochim. Acta*, 2010, **55**, 9024

97. C. Robertson, R. Beanland, S. A. Boden, A. L. Hector, R. J. Kashtiban, J. Sloan, D. C. Smith, and A. Walcarius, *Phys. Chem. Chem. Phys.*, 2015, **17**, 4763

98. B. Ward, J. A. Notte, N. P. Economou, A. Business, and C. Zeiss, *Photonic Spectra*, 2007

99. T.-C. Wei and H. W. Hillhouse, *Langmuir*, 2007, **23**, 5689

100. R. I. Nooney, D. Thirunavukkarasu, Y. Chen, R. Josephs, and A. E. Ostafin, *Chem. Mater.*, 2002, **14**, 4721

101. P. C. A. Alberius, K. L. Frindell, R. C. Hayward, E. J. Kramer, G. D. Stucky, and B. F. Chmelka, *Chem. Mater*, 2002, **14**, 3284

102. E. Leontidis, *Curr. Opin. Colloid Interface Sci.*, 2002, **7**, 81–91.

103. R. Ryoo and S. Jun, *J. Phys. Chem. B*, 1997, **101**, 317

104. H. Lin and C. Mou, *Microporous Mesoporous. Mater.*, 2002, **55**, 69

105. H. Lin, C. Kao, and C. Mou, *Microporous Mesoporous. Mater.*, 2001, **48**, 135

106. B. Echchahed, M. Morin, S. Blais, A.-R. Badiei, G. Berhault, and L. Bonneviot, *Microporous Mesoporous. Mater.*, 2001, **44-45**, 53

107. G. J. de A. A. Soler-Illia, A. Louis, C. Sanchez, and M. Curie, *Chem. Mater.*, 2002, **14**, 750

108. J. Šubrt, V. Štengl, S. Bakardjieva, and L. Szatmary, *Powder Technol.*, 2006, **169**, 33

109. K. Chang and Y. Kang, *Mater. Lett.*, 2000, **42**, 283

110. L. Sicard, P. . Llewellyn, J. Patarin, and F. Kolenda, *Microporous Mesoporous Mater.*, 2001, **44-45**, 195

111. A. Caragheorgheopol, H. Caldararu, M. Vasilescu, A. Khan, D. Angelescu, N. Žilková, and J. Čejka, *J. Phys. Chem. B*, 2004, **108**, 7735

112. C. Shao, G. Zhou, Z. Li, Y. Wu, D. Xu, and B. Sun, *Chem. Eng. J.*, 2013, **230**, 227

113. D. Janssen, R. De Palma, S. Verlaak, P. Heremans, and W. Dehaen, *Thin Solid Films*, 2006, **515**, 1433

114. C. Boissiere, D. Grosso, S. Lepoutre, L. Nicole, A. B. Bruneau, and C. Sanchez, *Langmuir*, 2005, **21**, 12362

115. C. Lastoskie, K. E. Gubbins, and N. Quirkeft, *J. Phys. Chem.*, 1993, **97**, 4786

116. M. Thommes, *Chemie Ing. Tech.*, 2010, **82**, 1059

117. A. Fujishima and X. Zhang, *C. R. Chim.*, 2006, **9**, 750

118. L. Liu and X. Chen, *Chem. Rev.*, 2014, **114**, 9890

119. D. M. Antonelli and J. Y. Ying, *Angew. Chem. Int. Ed.*, 1995, **334**, 2014

120. K. Wang, B. Yao, M. A. Morris, J. D. Holmes, R. V April, V. Re, M. Recei, and V. July, *Chem. Mater.*, 2005, **17**, 4825

121. Y. Matsumoto, Y. Ishikawa, M. Nishida, and S. Ii, *J. Phys. Chem. B*, 2000, **104**, 4204

122. S. Karuppuchamy, K. Nonomura, T. Yoshida, T. Sugiura, and H. Minoura, *Solid State Ionics*, 2002, **151**, 19

123. H. Luo, J. Zhang, and Y. Yan, *Chem. Mater.*, 2003, **15**, 3769–3773.

124. N. Arconada, Y. Castro, and A. Durán, *Appl. Catal. A Gen.*, 2010, **385**, 101

125. M. Ogawa, K. Ikeue, and M. Anpo, *Chem. Mater*, 2001, **13**, 2900

126. N. Husing and B. Launay, *Chem. Mater.*, 2002, **14**, 2429

127. M. D. Chadwick, J. W. Goodwin, E. J. Lawson, P. D. a Mills, and B. Vincent, *Colliods. Surf. A*, 2002, **203**, 229

128. D. J. Macquarrie, *Green Chem.*, 1999, **1**, 195

129. X. Feng, G. E. Fryxell, l.-Q. Wang, A. Y. Kim, J. . Liu, and K. M. Kemner, *Science.*, 1997, **276**, 923

130. T. Deschner, Y. Liang, R. Anwander, and E. K. Universita, *J. Phys. Chem. C*, 2010, **114**, 22603

131. J. Landers, G. Y. Gor, and A. V. Neimark, *Colloids Surfaces A Physicochem. Eng. Asp.*, 2013, **437**, 3

132. L. J. Brown, R. C. D. Brown, and R. Raja, *RSC Adv.*, 2013, **3**, 843

133. P. Sutra, D. Brunel, P. Lentz, G. Daelen, and B. Nagy, *Colloids Surfaces A Physicochem. Eng. Asp.*, 1999, **158**, 21

134. N. Fukaya, H. Haga, T. Tsuchimoto, S. Y. Onozawa, T. Sakakura, and H. Yasuda, *J. Organomet. Chem.*, 2010, **695**, 2540

135. L. Han, Z. Jiang, Z. Huang, J. Feng, Y. Yao, and S. Che, *Chem. Mater*, 2011, **23**, 3583

136. X. Zhang, H. Yang, F. Zhang, and K.-Y. Chan, *Mater. Lett.*, 2007, **61**, 2231

137. Y. Liu, W. Zhang, and T. J. Pinnavaia, *J. Am. Chem. Soc.*, 2000, **122**, 8791

138. D. R. Dunphy, S. Singer, A. W. Cook, B. Smarsly, D. A. Doshi, and C. J. Brinker, *Langmuir*, 2003, **19**, 10403

139. N. Tatsuda, Y. Fukushima, and H. Wakayama, *Chem. Mater.*, 2004, **16**, 1799

140. S. Kawi and M. W. Lai, *Chem. Commun.*, 1998, 1407

141. R. Van Grieken, G. Calleja, G. D. Stucky, J. a. Melero, R. a. García, and J. Iglesias, *Langmuir*, 2003, **19**, 3966

142. K. Kim, M. Kim, and S. M. Cho, *Mater. Chem. Phys.*, 2006, **96**, 278

143. J. M. Ball, M. M. Lee, A. Hey, and H. J. Snaith, *Energy Environ. Sci.*, 2013, **6**, 1739